Slope Stability of the Rangamati Hilly Area Due to Earthquake Load Using PLAXIS 2D

Afia Nawar

Jannatun Nyeem Oyshee

Mustakim Ur Rashid

DEPARTMENT OF CIVIL AND ENVIRONMENTAL ENGINEERING

ISLAMIC UNIVERSITY OF TECHNOLOGY (IUT)

BOARD BAZAR, GAZIPUR-1704

DHAKA, BANGLADESH

JUNE, 2023

Slope Stability of the Rangamati Hilly Area Due to Earthquake Load Using PLAXIS 2D

Afia Nawar (180051141)

Jannatun Nyeem Oyshee (180051213)

Mustakim Ur Rashid (180051244)

A THESIS SUBMITTED

FOR THE DEGREE OF BACHELOR OF SCIENCE IN CIVIL ENGINEERING

DEPARTMENT OF CIVIL AND ENVIRONMENTAL ENGINEERING

ISLAMIC UNIVERSITY OF TECHNOLOGY

May, 2023

PROJECT REPORT APPROVAL

The title of our thesis is " Slope Stability of the Rangamati Hilly Area Due to Earthquake Load Using PLAXIS 2D" and the explanatory title is Slope Stability using Pseudo-static Method due to Earthquake Load using PLAXIS 2D Software at Rangamati" by Afia Nawar, Jannatun Nyeem Oyshee, Mustakim Ur Rashid Student No. 180051141, 180051213, 180051244 respectively, have been found as satisfactory and accepted as partial fulfillment of the requirements for the Degree Bachelor of Science in Civil and Environmental Engineering.

SUPERVISOR

Prof. Dr. Hossain MD. Shahin

Head of Department
Department of Civil and Environmental Engineering (CEE)
Islamic University of Technology (IUT),
Board Bazar, Gazipur, Bangladesh.

DECLARATION OF CANDIDATE

We hereby declare that the undergraduate research work described in this thesis was performed by us under the supervision of Professor Dr. Hossain Md. Shahin and that it has not been submitted elsewhere for any reason (except for publication).

Dr. Hossain Md. Shahin
Professor,
Department of Civil and
Environmental Engineering (CEE)
Islamic University of Technology (IUT)
Board Bazar, Gazipur, Bangladesh

Afia Nawar
Student No: 180051141
Academic Year: 2021-2022
Date:

Jannatun Nyeem Oyshee
Student No: 180051213
Academic Year: 2021-2022
Date:

Mustakim Ur Rashid
Student No: 180051244
Academic Year: 2021-2022
Date:

DEDICATION

We would like to extend our dedication of this thesis to our cherished family members and a select group of close friends who have consistently stood by our side, providing unwavering support whenever we needed it. The immeasurable love and encouragement from our parents, as well as the guidance from Prof. Dr. Hossain Md. Shahin, have been invaluable to our journey.

This is a humble expression of appreciation to all those who assisted us along the way, serving as a source of inspiration that motivated us to persevere until the very end. Furthermore, we commit our thesis work to the pursuit of advancing the well-being of humanity.

ACKNOWLEDGEMENTS

"*In the name of Allah, Most Gracious, Most Merciful*."

All the praises to Almighty Allah Subhanahu wa'tala for blessing us with the opportunity and always being kind.

We would like to express our deepest gratitude and appreciation to all those who have supported us throughout the completion of this thesis. We are immensely grateful to our thesis advisor, Professor Dr. Hossain Md. Shahin for his invaluable guidance, expertise, and continuous encouragement. His insightful feedback and unwavering support have been instrumental in shaping this research project. We are truly fortunate to have had the opportunity to work under his supervision. We are grateful to the faculty members of the CEE Department for their dedication to educational quality and for presenting us with a dynamic academic environment. Their expertise and enthusiasm for their various disciplines have served as a continual source of inspiration. We are also grateful to PROSOIL for helping us with the data we needed throughout our research. We would also like to express our gratitude to our family for their unwavering love, understanding, and support. Their belief in our abilities and their encouragement during challenging times has been the driving force behind our accomplishments. We would like to thank all the individuals who participated in this study as providers of data and information. Without their contributions, this research would not have been possible.

We would also want to express our deepest gratitude to everyone who has contributed, directly or indirectly, to our endeavor. We are grateful for the assistance we have received during our endeavor.

ABSTRACT

Keywords: Slope stability, Earthquake, PLAXIS- 2D, Pseudo static method, Mohr-coulomb model, Seismic Coefficient, Soil Parameter, Displacement, Factor of Safety, Finite Element Method.

Slope stability is one of the most important aspects of geotechnical engineering. Slope failure can cause significant economic and human losses. Earthquake loads are among the most critical factors affecting slope stability. The pseudo-static approach is used to analyze seismic slope stability. This thesis paper aims to evaluate the slope stability due to earthquake loads using PLAXIS 2D software, determine the factor of safety due to different pseudo-static coefficients, and determine the stress development in the slope.

Contents

Figures:

List of Tables:

List of Graphs:

Chapter 1 Introduction

1.1 General

Slope stability is a crucial aspect of geotechnical engineering, playing a vital role in ensuring the safety of infrastructure, property, and human lives in hilly regions. When subjected to earthquakes, slopes may experience various types of failure, including rotational, translational, and compound, leading to landslides and significant damages. Seismic slope stability analysis is essential for evaluating the performance of slopes under seismic loading conditions and mitigating the risks associated with these failures, particularly in regions prone to earthquakes.

Betchari Bazar, located on Rangamati Road in Mohalchari, Khagrachari, is a hilly area in Bangladesh that is susceptible to seismic activity due to its proximity to the tectonically active Indo-Burman Ranges. The complex geology and diverse soil types in the region further exacerbate the risk of slope failures and landslides triggered by earthquakes. Therefore, a comprehensive understanding of the factors affecting the stability of slopes in Betchari Bazar under earthquake loading conditions is critical for developing effective prevention and mitigation strategies.

The pseudo-static method is a widely-used approach to analyze slope stability during seismic events. By incorporating seismic forces as equivalent static forces, the pseudo-static method provides a simplified means to account for the effects of earthquakes on slopes, making it a valuable tool for preliminary analysis and design. The Plaxis 2D software, a powerful geotechnical analysis tool, employs the finite element method to simulate the behavior of slopes under various loading conditions, including earthquakes. With its advanced capabilities, Plaxis 2D can provide a more detailed analysis of slope stability, accounting for complex interactions between soil, groundwater, and seismic forces.

This thesis focuses on the assessment of slope stability in the Betchari Bazar area under earthquake loading using the pseudo-static method and Plaxis 2D software. The study also considers the geological and geotechnical characteristics of the area, incorporating field investigations and laboratory testing to develop a comprehensive understanding of the local soil conditions and their impact on slope stability. Additionally, the research explores the potential benefits of ground improvement techniques for enhancing slope stability in the context of earthquake loading.

The findings of this research will contribute to the understanding of seismic slope stability in the Betchari Bazar area and provide valuable information for future slope stability analyses and mitigation efforts in similar regions. Furthermore, the results will help inform the development of appropriate design guidelines and policies to enhance the resilience of infrastructure and communities in earthquake-prone hilly areas.

1.2 Objectives of the Study

The main objective of this study is to evaluate the slope stability in the Betchari Bazar area under earthquake loading using the pseudo-static method and Plaxis 2D software. To accomplish this objective, the following specific aims have been identified:

1. To review the literature on seismic slope stability, the pseudo-static method, and relevant studies in earthquake-prone hilly areas.

2. To obtain geological and geotechnical data of the Betchari Bazar area from a reliable organization.

3. To analyze the geotechnical properties of the soils in the study area using the provided data.

4. To develop a numerical model using Plaxis 2D software to simulate slope behavior in the Betchari Bazar area under earthquake loading.

5. To apply the pseudo-static method with three different coefficients for assessing seismic slope stability and evaluating the numerical model's performance.

6. To compare the results of the pseudo-static method and Plaxis 2D analysis for both before and after earthquake conditions.

7. To identify key factors affecting seismic slope stability in the Betchari Bazar area and provide recommendations for future analyses and mitigation efforts in similar regions.

1.3 Scopes of the Study

The main objective of this study is to evaluate the slope stability in the Betchari Bazar area under earthquake loading using the pseudo-static method and Plaxis 2D software. To accomplish this objective, the following specific aims have been identified:

1. To review the literature on seismic slope stability, the pseudo-static method, and relevant studies in earthquake-prone hilly areas.

2. To obtain geological and geotechnical data of the Betchari Bazar area from a reliable organization.

3. To analyze the geotechnical properties of the soils in the study area using the provided data.

4. To develop a numerical model using Plaxis 2D software to simulate slope behavior in the Betchari Bazar area under earthquake loading.

5. To apply the pseudo-static method with three different coefficients for assessing seismic slope stability and evaluating the numerical model's performance.

6. To compare the results of the pseudo-static method and Plaxis 2D analysis for both before and after earthquake conditions.
7. To identify key factors affecting seismic slope stability in the Betchari Bazar area and provide recommendations for future analyses and mitigation efforts in similar regions.

Chapter 2 Literature Review

2.1 General

The study of seismic slope stability is a critical aspect of geotechnical earthquake engineering, as it helps to assess the safety and resilience of infrastructure and communities in earthquake-prone regions. This chapter presents a review of the relevant literature on seismic slope stability, with a focus on studies that have used the pseudo-static method and Plaxis 2D software for slope stability analysis under various conditions. The literature review aims to provide a comprehensive understanding of the current state of knowledge in the field, identify research gaps, and establish the context for the present study.

Several studies have used Plaxis 2D for analyzing seismic slope stability in various contexts, demonstrating the effectiveness of Plaxis 2D in capturing the complex behavior of slopes during earthquakes and providing valuable insights for the design and assessment of slope stability:

- Ndoudy Noël (2022) used PLAXIS 2D to evaluate slope stability under saturated conditions and completely drained slopes for earthquake accelerations of 0.2g and 0.4g.
- Kallimath (2019) determined the factor of safety and slip surface of earthen slopes using Plaxis software for various slopes and compared the results with practical implementations.
- Ghosh (n.d.) used PLAXIS to analyze the deformation pattern, acceleration at various areas and stresses that emerge in earth dams in response to earthquake ground shaking, considering variables such as water level, foundation material properties, and soil mass's Young's modulus.
- Zardari et al. (2017) conducted a finite element analysis to evaluate liquefaction potential, permanent deformations, and the post-seismic stability of a dam under both a regular and a more severe earthquake using PLAXIS 2D and the UBCSAND constitutive model.
- Carlton et al. (2016) discussed the impacts of slope angle, soil sensitivity, ground motion orientation, and multidirectional shaking on seismic slope stability, highlighting the importance of permanent shear strains in calculating permanent displacements from earthquake-induced landslide hazard studies.

2.2 Seismic slope stability

Seismic slope stability is a critical concern in earthquake-prone regions, as slope failures induced by earthquakes can cause severe damage to infrastructure and communities. Earthquakes pose a significant threat to the long-term stability of slopes, and damage from landslides and other ground failures often exceeds the damage directly related to strong shaking and fault rupture. Seismically triggered landslides can destroy homes, structures, roads, pipelines, and block stream drainages, resulting in substantial economic and social impacts (Kramer, 1996).

The acceleration produced by ground motions during earthquakes induces cyclically varying forces on slopes, embankments, and dams, and can cause degradation in the soil's shear strength.

However, the increase in instant shear strength for clay soils due to strain rate effects can offset the reduction in shear strength associated with soil strain, making it reasonable to neglect degradation in some cases (Kramer, 1996).

Four primary methods are commonly used to assess slope stability under earthquake loading: the pseudo-static analysis approach, the dynamic stress-deformation analysis approach, the Newmark sliding-block approach, and various testing methods (Kramer, 1996).

1. The pseudo-static analysis approach is the simplest method, involving the addition of a permanent body force representing earthquake shaking to a static limit-equilibrium analysis. This approach is suitable for preliminary analyses and screening procedures.
2. The dynamic stress-deformation analysis approach involves more complex modeling of slopes using numerical methods, such as the finite element method, finite difference method, boundary element method, and discrete element method. This method provides reliable predictions of failure modes but requires more detailed soil data input and computational effort. It is applicable for critical infrastructure like dams, embankments, or slopes adjacent to vital lifelines or structures.
3. The Newmark sliding-block approach is more convenient than the stress-deformation analysis, providing more useful information than the pseudo-static analysis while being slightly more complex. Modifications to the sliding-block analysis have made it applicable to a wider range of landslide types.
4. Various testing methods can identify weak geological features, damage mechanisms, and stability states of slopes, providing more realistic assessments of slope stability.

Depending on the chosen method, tools for analyzing slope stability may include simple equations, charts, spreadsheet software, and slope stability analysis codes. In many cases, multiple tools are used to evaluate a particular slope's stability.

It is essential to note that both the pseudo-static analysis approach and the Newmark sliding-block approach are suitable for analyzing the inertial instability of slopes. However, if shear strength reduction occurs due to factors like pore-water pressure generations, different approaches must be adopted to assess weakening instabilities. Additionally, post-earthquake slope instabilities caused by reduced shear strength under cyclic loading should be assessed by accounting for the effects of pore-water pressure development in soils (Kramer, 1996).

2.3 Plaxis 2D Software for slope stability analysis

Plaxis 2D is a finite element software primarily used by geotechnical engineers for the analysis of rock and soil. The software was developed in 1987 by the Technical University of Delft to address the soft soil conditions prevalent in the lowlands of Holland. Over time, Plaxis expanded to encompass various aspects and applications of geotechnical engineering, providing a user-friendly interface combined with the power of finite element analysis. The first commercial version of Plaxis was made available in 1998.

The software consists of a range of soil models incorporated within it, as well as a versatile library of structural elements. The creation of models in Plaxis 2D is straightforward, and the software generates meshes using 6-node and 15-node triangular elements. Plaxis 2D is composed of four main subroutines: Plaxis Input, Plaxis Output, Plaxis Calculation, and Plaxis Curves. These subroutines allow for easy input of data, visualization of results, execution of calculations, and analysis of various curves related to slope stability.

One of the key advantages of Plaxis 2D in slope stability analysis is its ability to model complex soil and rock behavior accurately. The software allows engineers to assess the impact of various factors, such as earthquake loading, on slope stability. By incorporating advanced numerical methods and built-in soil models that account for different soil types and behaviors, Plaxis 2D can effectively simulate seismic slope stability scenarios. This enables geotechnical engineers to evaluate the safety and performance of slopes, embankments, and other geotechnical structures under seismic loading.

In the context of earthquake-induced slope stability, Plaxis 2D allows engineers to perform pseudo-static analysis, taking into account the effects of earthquake acceleration on the slope. By using various pseudo-static coefficients, engineers can simulate different levels of seismic activity and compare the results to evaluate the overall stability of the slope under different earthquake scenarios.

Overall, Plaxis 2D is an essential tool for geotechnical engineers working on slope stability analysis, particularly in seismic-prone regions. The software's user-friendly interface, advanced numerical methods, and comprehensive library of soil and structural models enable accurate and reliable assessments of slope stability under varying conditions, including seismic loading.

2.4 Summary

The literature review emphasizes the importance of understanding earthquake-induced slope instability and the various methods used in assessing seismic slope stability. Several approaches have been discussed, including the pseudo-static analysis, dynamic stress-deformation analysis, and Newmark sliding-block approach. Among these, the pseudo-static analysis is commonly employed for preliminary analyses, while the more sophisticated dynamic stress-deformation analysis is better suited for critical infrastructures and complex scenarios.

Plaxis 2D, a widely-used finite element software in geotechnical engineering, offers a user-friendly interface, advanced numerical methods, and a comprehensive library of soil and structural models. The software enables accurate assessments of slope stability under seismic loading and allows for the simulation of different seismic scenarios. In summary, employing advanced numerical tools and methods like Plaxis 2D is crucial for assessing slope stability in earthquake-prone regions

Chapter 3 Methodology

3.1 General

In this chapter, the methodology employed for the study of slope stability under seismic conditions is presented. The chapter provides an overview of the steps involved in the process, from the initial assessment of the study area and site conditions to the numerical analysis using Plaxis 2D software. This includes field investigations, material collection, laboratory tests, and the application of various methods to assess seismic slope stability. The methodology is designed to provide a comprehensive understanding of the factors influencing slope stability and to develop appropriate solutions for improving the stability of slopes in the study area under seismic loading.

3.2 Study Area

For this study, three different locations around Chittagong Hilly Regions were chosen. The locations were:

Location-01: Betchari Bazar, Rangamati Road, Mohalchari, Khagrachari

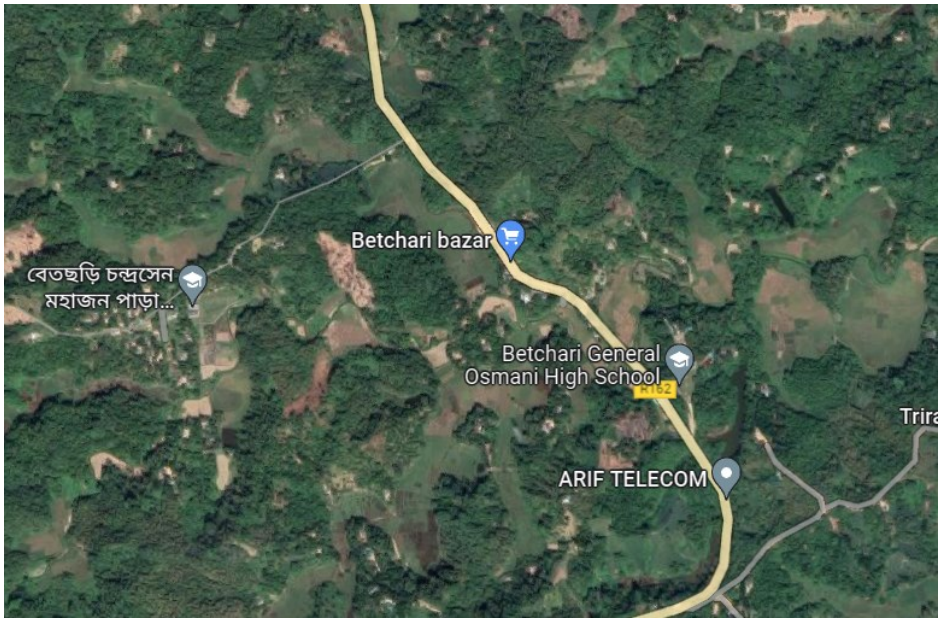

Figure 3.1 Betchari Bazar, Rangamati Road, Mohalchari, Khagrachari

Location-02: Lemuchari, Mohalchari, Khagrachari

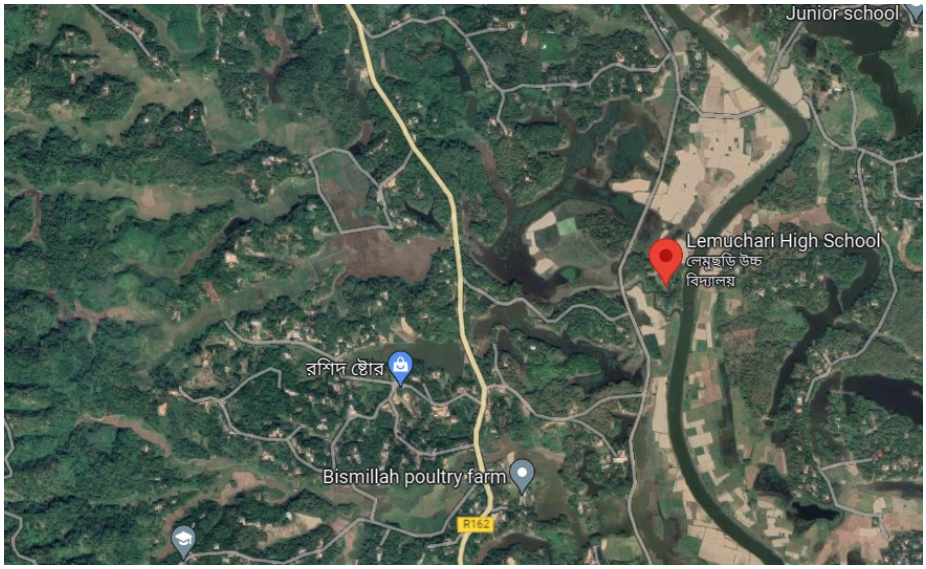

Figure 3.2 Lemuchari, Mohalchari, Khagrachari

Location-03: Baghaihat, Rangmati, 14 Beer Baghaihat Army Camp

Figure 3.3 Baghaihat, Rangmati, 14 Beer Baghaihat Army Camp

These regions are known for its hilly terrain and susceptibility to slope failures. This region is also within an earthquake-prone zone, which makes the analysis of slope stability under seismic conditions crucial for the safety of the inhabitants and infrastructure in the area. In this section, several images and figures will be incorporated to provide a visual representation of the study area, illustrating its geographical features, soil composition, and slope characteristics. The images and

figures will aid in understanding the unique challenges posed by the study area, and help in devising appropriate methodologies for slope stability analysis under seismic conditions.

3.3 Site Conditions

This section provides an overview of the soil conditions encountered at the study site. Detailed information about the soil conditions can be found in the borehole logs provided in the appendices. These logs offer a comprehensive account of the subsurface conditions at each specific boring location.

It is essential to note that the summary of borehole data is represented as a generalized subsoil profile, which is an interpolation between the boreholes. While this profile offers valuable information about the site conditions, it may not precisely represent the true conditions on site due to the interpolation process. Therefore, the generalized subsoil profile should be used as a guide for understanding the overall soil conditions in the area, while keeping in mind the possible variations in the actual site conditions.

3.3.1 Description of subsoil condition

The study site is located at Betchari Bazar, Rangamati Road, Mohalchari, Khagrachari, and is intended for the construction of a telecommunication tower. Three boreholes (BH-1, BH-2, and BH-3) were drilled to investigate the subsoil conditions. The subsoil within the vicinity of the boreholes consists mainly of the following strata:

1. A thick layer of topsoil composed of silt is found at BH-1, BH-2, and BH-3.

2. The bottom layer of soil is fine sand at BH-1, BH-2, and BH-3.

3. Intermediate layers of fine sand and silty sand are present at BH-1, BH-2, and BH-3.

The water table was too deep to measure from the existing ground level at BH-1, BH-2, and BH3. Each borehole was terminated at a depth of 15.0m (BH1, BH2, and BH3). Details on thickness, depth, distribution, Standard Penetration Test (SPT) blow counts, and depth are shown in the borehole log.

3.4 Methods to Assess Seismic Slope Stability

3.4.1 Pseudo-static Analysis

The pseudo-static method, first introduced by Terzaghi in 1950, is a foundational technique used to evaluate seismic slope stability. It defines a seismic coefficient (k). It is a result of the gravitational acceleration and the highest horizontal acceleration caused by an earthquake. The pseudo-static study of slopes relies heavily on this seismic coefficient. By combining the weight of the sliding mass with the seismic coefficient, this technique treats the complex dynamic load brought on by an earthquake as a single, unidirectional static force. Terzaghi advised that this force be delivered near the center of gravity of the slices even if the precise application location was not specified.

Once the pseudo-static horizontal force is determined, a standard static slope stability analysis can be performed using limit equilibrium methods, leading to a factor of safety calculation. The factor of safety for an infinite slope can be computed using the following equation:

$$F_s = \frac{\mathrm{C} + (\gamma z \cos^2\beta - k\gamma z \cos\beta \sin\beta)\tan\phi}{(\gamma z \cos\beta \sin\beta + k\gamma z \cos^2\beta)} \dots\dots\dots (1)$$

β is the inclination angle, and W is the weight of the slice.

Various formulae and recommendations for determining the seismic coefficient exist in the literature, with general values ranging from 0.05 to 0.25. Approaches to this determination include using half of the peak ground acceleration, or a range of values based on the severity of the seismic event. Other complex expressions for determining k are provided by Bray and Travasarou (2009), as follows:

$$K = \frac{exp[-\mathrm{a} + \sqrt{\mathrm{b}}]}{0.665} \dots\dots\dots (2)$$

$$a = 2.83 - 0.566 ln(S_a) \dots\dots\dots (3)$$

$$b = a^2 - 1.33\left[ln(D_a) + 1.10 - 3.04 ln(S_a) + 0.244\left(ln\,(S_a)\right)^2 - 1.5T_s - 0.278(M-7) - \varepsilon\right] \dots\dots\dots (4)$$

Here, an is a function of the initial fundamental period (Da), the initial spectral acceleration of 5% (Sa), and b is a function of the seismic displacement (Da), which the engineer will determine.

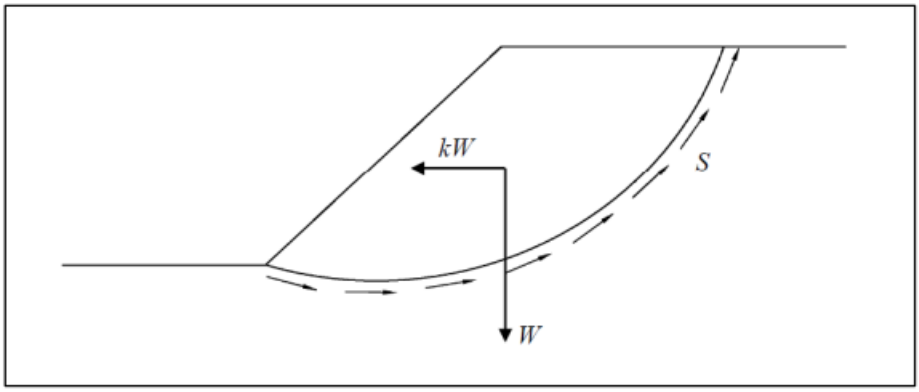

Figure 3.4 A simplified sketch of Pseudo-static slope stability analysis

(T_s), the moment magnitude of the earthquake (M), and the normally distributed random variable (ε).

An advantage of the pseudo-static method is its simplicity, enabling the straightforward implementation of a seismic load in the slope stability analysis. However, this simplicity also brings drawbacks. As the dynamic load is simplified, the method can often be overly conservative. Furthermore, it maintains the typical limitations of limit equilibrium methods, such as assumptions

about the location and shape of failure surfaces, and a constant shear strength across the surface. Lastly, the pseudo-static method provides limited post-failure analysis, which could be important for evaluating the serviceability of a structure post-earthquake. Therefore, while the pseudo-static method is a good starting point for seismic slope stability analysis, it should be supplemented with other, more comprehensive methods for more critical evaluations.

3.4.2 Sliding Block Analysis

Although the pseudo-static analysis approach offers helpful information, it doesn't cover the slope's performance in seismic circumstances. As a result, Newmark (1965) developed the rigid-block analysis, also known as the sliding block analysis, to determine the permanent displacements caused by seismic activity on dams and embankments. This method combines the ground motion as an acceleration time history and handles the sliding mass as a rigid body on an inclined surface. The yield acceleration (A_y) is calculated as the sum of the yield coefficient (k_y) and the acceleration of gravity (A_g). This coefficient has a safety factor of one and is identical to the seismic coefficient (k).

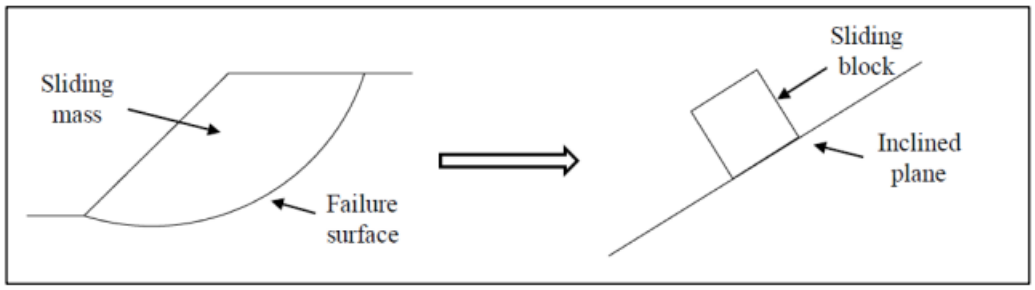

Figure 3.5 Demonstration of Newmark's sliding block analysis

Once the acceleration a (t) surpasses A_y, the block begins to slide. It halts when the velocity of the block and the velocity of the underlying mass become equal. The accelerations exceeding A_y are integrated once to find the system's velocity and twice to find a permanent displacement.

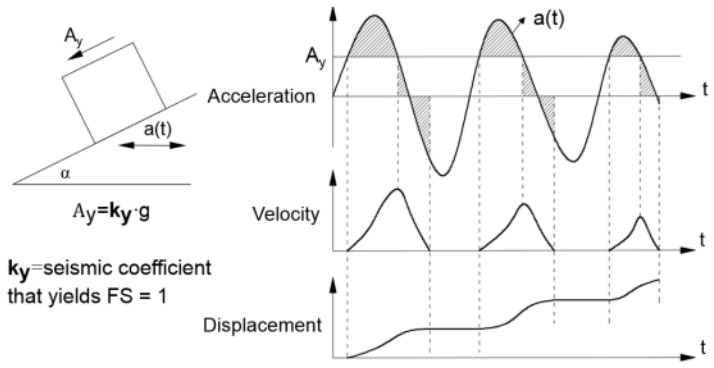

Figure 3.6 Sliding block analysis

The yield coefficient (k_y), which depends on the geometry (such as height and inclination) of the slope as well as the materials shear qualities (such as friction angle and cohesiveness), indicates the slope's dynamic resistance. Three slip surfaces must be examined in order to calculate k_y: the slip surface that produces the lowest static factor of safety, the slip surface that produces the lowest k_y, and the slip surface that reflects the distribution of accelerations throughout the soil mass.

The yield acceleration A_y is also referred to as critical acceleration A_c by Jibson (2010), which can be calculated using the following equation:

$$A_c = A_y = (FS - 1)g \sin \alpha \dots \dots \dots (1)$$

In order to forecast displacements brought on by 'slides' kind of motions, such as rotational and translational landslides, sliding block techniques are typically used. The permitted permanent displacement is the factor that is examined to gauge the effectiveness and stability of the slope. The slope may fail if the ultimate displacement is more than the permitted permanent displacement.

More complex techniques, referred to as decoupled and fully coupled approaches, have been developed to get around some of the drawbacks of the rigid block analysis. Decoupled techniques compute the constant displacements using the corresponding input motion in the rigid block method while estimating the average acceleration time response. A simultaneous study of the deformations brought on by the dynamic response and the sliding response, taking into consideration plastic deformations, is achieved using fully coupled techniques. However, compared to rigid block and decoupled techniques, these methods need more processing.

3.4.3 Stress-Deformation Analysis

Theoretical representations of material mechanics and boundary conditions can be used to describe geotechnical issues like sloping earthworks. However, as they are frequently represented by intricate sets of differential equations, it is frequently necessary to simplify the boundary conditions and material behavior of the model in order to find solutions. Therefore, due to the shortcomings or misrepresentations of analytical solutions, numerical techniques are often required.

The category of stress-deformation analysis for evaluating seismic slope stability is quite new. This approach uses a variety of numerical approaches to roughly solve boundary value issues. The governing equations are solved for a limited set of points while the problem domain is discretized into smaller chunks. Complex constitutive models and seismic loads can be used to describe the acceleration or stress time-history of soil behavior. Stress-deformation studies are computationally intensive despite the fact that they provide accurate representations of characteristics and geometry.

A more modern method for evaluating seismic slope stability is stress-deformation analysis. A variety of numerical approaches are used in this approach to roughly solve boundary value issues. The governing equations are solved for a finite set of points throughout this procedure, which discretizes the problem domain into smaller parts. Complex constitutive models and seismic loads

in terms of acceleration or stress time-history can be used to describe soil behavior. Stress-deformation studies may depict characteristics and geometry realistically, but they need a lot of processing power.

The most popular approaches are mesh-based ones, including the Finite Element Method (FEM) or the Finite Differences Method (FDM). To reference the material characteristics, they use a deformable mesh. These techniques are appropriate for cases where mesh distortions do not jeopardize the convergence condition since they can struggle with mesh tangling when substantial deformations are present.

They use a deformable mesh as a point of reference for the material characteristics. When there are significant deformations, these approaches can encounter mesh tangling issues, making them suited for cases where the convergence condition is not jeopardized by mesh distortions.

3.4.4 Summary

We've explored several methodologies in this study that tackle the issue of slope stability in the presence of dynamic loads. The most familiar of these methods, and the first to be established, was the pseudo-static analysis. This technique, initially proposed by Terzaghi, operates by introducing a horizontal load equivalent to the weight of the sliding mass or block multiplied by the seismic coefficient ks. Following the introduction of this horizontal load, a conventional static slope stability analysis is performed to determine a factor of safety.

Another approach that has gained popularity in engineering practice is the sliding-block analysis, developed by Newmark. This method necessitates two levels of integration: the first involves integrating the acceleration time record that exceeds the yield acceleration (Ay) – this being the seismic coefficient that would lead to a safety factor of 1, and the second integration is performed to calculate the permanent displacements.

The most prevalent methodologies include mesh-based approaches like the Finite Element Method (FEM) or the Finite Differences Method (FDM). For the purpose of referencing the material characteristics, they use a deformable mesh. These approaches are suitable for cases when mesh distortions do not jeopardize the convergence condition, but they can encounter problems with mesh tangling when substantial deformations are involved.

While sliding-block methods can be effective for predicting deformations resulting from slides, including rotational and translational landslides, they are limited when large deformations are involved. In scenarios involving significant deformations, like lateral spreads and flows, particle-based numerical techniques become necessary.

Through this study, we have successfully identified how these different methodologies evaluate the onset of failure (stability analysis) and their respective applicability's in predicting post-failure deformations and final run-outs (post-failure analysis). The findings are summarized in Table 1.

Table 3-1 A summary of the approaches' application to a) stability and b) post-failure analysis.

Analysis Method	Stability Analysis	Post-failure Analysis (Risk Analysis)
Pseudo-static	Factor of Safety FS > 1	Not applicable
Sliding Block	Allowable permanent displacements	Constrained to small deformations
Stress Deformation	Strength Reduction Factor SRF > 1	Applicable (Large run-outs only particle-based methods)

These investigations will contribute significantly to our understanding of slope stability under seismic loading and guide the further course of our study.

3.5 Material Collection

The material collection process for this particular project was handled by our experienced team who were accountable for executing the Standard Penetration Test (SPT) and gathering both disturbed and undisturbed subsurface soil samples.

3.5.1 Field Exploration

Field exploration is a crucial initial step in our geotechnical investigations, as it provides firsthand data and insights about the site's subsurface conditions. For this project, our dedicated team performed a thorough field exploration that involved drilling three boreholes, labeled BH1, BH2, and BH3.

These boreholes were drilled up to a depth of 15.0 meters below the existing ground level, in strategic locations as shown in the Appendix-A1 Borehole Location Plan. This enabled us to delve deeper into the earth's strata, understand the subsurface geology, and collect pertinent data.

During the drilling process, the team also retrieved both disturbed and undisturbed soil samples. The careful and meticulous execution of the field exploration process is fundamental to the subsequent seismic slope stability analysis, as it provides critical input data that influence the reliability of the study's outcome.

3.5.2 Standard Penetration Test (SPT)

The Standard Penetration Test (SPT) is a dynamic, in-situ testing method extensively employed in geotechnical engineering to determine key soil properties. It's one of the oldest and most frequently used methods for soil exploration due to its simplicity in terms of equipment use and procedure.

SPT has a fundamental role in geotechnical earthquake engineering where it is used for seismic site characterization, site-response studies, and liquefaction assessments, contributing significantly

to seismic micro-zonation. Its popularity is largely attributable to its ease of use, cost-effectiveness, and adaptability of SPT equipment, which can be rapidly integrated with virtually any type of drilling rig. These advantages maintain its status as the most widely used field test method despite its limitations and the need for numerous corrections.

The test involves driving a 50mm O.D. x 600mm long thick-walled split sampler tube into undisturbed soil using a 63.5kg sliding hammer dropped from a height of 760mm. The penetration resistance, or 'N' value, is the number of hammer blows needed to drive the sampler an additional 300mm into the soil following an initial penetration of 150mm to bypass any disturbed materials at the borehole's bottom.

For a more accurate representation of the soil's behavior, we utilize the normalized N-value, or (N1)60. This parameter accounts for the energy efficiency of the SPT hammer and corrects the measured N-value for overburden pressure, making it a more reliable indicator of soil strength properties.

It's important to note that correlations between N-values and soil properties are generally most reliable for cohesion-less soils. In gravelly soils, particles can obstruct the sampler, leading to inflated blow counts and overestimations of friction angles. Similarly, caution is advised when interpreting N-values in silts or clays due to the dynamic nature of the test, which can cause rapid pore pressure changes and soil disturbance. For these more challenging soil types, the Becker Hammer Penetration Test (BPT) can offer a more reliable alternative.

The bearing capacity of the soil can be estimated from SPT results. We use a simple rule of thumb: multiplying the 'N' value by 10 to yield an approximate bearing capacity in kilo-newtons per square meter (kN/m^2). This method offers a preliminary indication of the soil's load-bearing potential.

3.5.3 Collection of Undisturbed Soil Samples

The acquisition of undisturbed soil samples was a critical component of the field exploration procedure, accomplished under the direct guidance of the site engineer and adapted to specific site conditions.

To collect these samples, we utilized a 75mm O.D. thin-walled Undisturbed (UD) sampler. The sampler was driven into the ground by a drilling machine employing a donut hammer, ensuring that the applied force did not cause an uplift of the drilling machine. Once the sampler was removed from the borehole, we meticulously measured and recorded the length of the recovered samples, from which we calculated the recovery ratio.

During the sampling process, special care was taken when operating beneath the water table or in conditions where water was used to clean the casing. In such scenarios, the water level was maintained at the top of the casing until the sampler was safely removed, ensuring the samples' integrity and reliability.

To isolate individual soil samples for further analysis, up to 50mm of undisturbed material was removed from both the top and the bottom of the tube. This material was subsequently preserved in jars for both the upper and lower portions. Following sample preparation, both ends of the sample were coated with a non-shrinking wax to establish an airtight seal, preserving the sample in its true, undisturbed state for subsequent laboratory analysis.

In addition to undisturbed samples, disturbed samples were also collected. These samples, gathered from the continuation of the sampling process and split barrel sample during the penetration resistance test, serve primarily for laboratory soil classification purposes, allowing us to gain comprehensive insights into the site's subsurface characteristics.

3.6 Methods of Field Investigation

To gain comprehensive insights into the geotechnical properties of the subsurface soil in the study area, we performed several tests and analyses. The field investigation process was critical for understanding the site's conditions and predicting how these might influence the stability of the slope under seismic loading. The methodologies of the key field tests performed, including sieve analysis, specific gravity, and direct shear, are detailed below.

3.6.1 Sieve Analysis

The sieve analysis was conducted to understand the particle size distribution of the soil, which directly impacts the soil's mechanical behavior. The procedure was as follows:

1. First, soil samples collected from the site were oven-dried at a temperature range of 105110 degrees Celsius until their weight remained constant, ensuring that all moisture content was effectively removed.

2. The initial weight of the oven-dried soil was then recorded.

3. The soil was sieved using a series of sieves arranged in descending order of size, from the largest sieve on top to the smallest sieve at the bottom.

4. After the sieving process, the weight of the soil retained on each sieve was determined and recorded.

5. Using this data, the percentage of soil retained on each sieve, as well as the cumulative percentage passing through each sieve, was calculated. The results were then plotted on a graph to obtain the particle size distribution curve.

3.6.2 Specific Gravity

The specific gravity of soil is an essential property that influences the soil's behavior under various conditions. This test was performed following the standard test method as per ASTM D854. The procedure involved:

1. Taking a small, oven-dried soil sample and placing it in a specific gravity flask.

2. The flask was then filled with a known volume of distilled water, and the flask was weighed.

3. The soil was allowed to soak, and the flask was agitated to remove air bubbles.

4. After soaking, the flask was filled to its calibration mark with distilled water, and the final weight was taken.

5. The specific gravity was calculated using the known volume of water, the weight of the oven-dry soil, and the weight of the water displaced by the soil.

3.6.3 Direct Shear

The direct shear test provided us with critical information about the soil's shear strength parameters, particularly the angle of internal friction and cohesion. The test was conducted as per ASTM D3080 standard. The procedure involved:

1. Placing a compacted or undisturbed soil sample in the direct shear box.

2. Applying a normal load to the sample and then applying a horizontal load until failure.

3. The shear stress at failure and the corresponding normal stress were recorded.

4. The test was repeated for different normal loads, and the peak shear stresses for each normal load were plotted against the normal stresses to obtain the shear strength parameters.

These methodologies provided us with essential geotechnical properties of the soil, which were then used in subsequent stability analyses and numerical modeling.

3.7 Numerical Analysis

Numerical analysis plays a pivotal role in comprehending and solving complex geotechnical problems. It involves the use of computational algorithms and methods that enable the quantification and evaluation of complex scenarios, allowing for more informed decision-making.

In the context of geotechnical engineering, numerical analysis, such as the Finite Element Method (FEM), allows for the effective modelling and simulation of geotechnical structures and their

response to various loading conditions. This section explores the implementation of FEM in software like Plaxis 2D, which is widely used for slope stability analysis. It further delves into the procedures involved, the significance of the constitutive soil model in Plaxis, specifically the Mohr-Coulomb model, and the importance of mesh quality in the finite element analysis.

3.7.1 Finite Element Method

The Finite Element Method (FEM) is a powerful numerical tool used in solving boundary value problems in various fields, including geotechnical engineering. It is particularly useful in the analysis of soil-structure interaction problems, slope stability analysis, and seismic analysis, among others.

The method works by dividing a complex structure or region into a finite number of smaller, simpler, interconnected units, or 'elements.' These elements are interconnected at nodes and collectively form a 'mesh' that approximates the geometry of the structure or region.

Each element is assumed to behave according to certain mathematical relationships or 'element equations' that describe its mechanical behavior. These equations are based on the chosen constitutive model, such as the Mohr-Coulomb model for soils.

The equations for all elements are assembled into a system of equations that represents the behavior of the entire structure or region. This system of equations can then be solved to determine the unknowns, such as displacements at the nodes. From these displacements, strains and stresses within each element can be calculated, providing a detailed picture of the mechanical behavior of the structure or region under the given loading conditions.

One of the strengths of the FEM is its flexibility. It can handle complex geometries, different types of boundary conditions, and a variety of material behaviors, making it a versatile tool in geotechnical analysis. However, the accuracy of the results depends significantly on the quality of the mesh and the chosen constitutive model. These topics are explored further in the following sections.

3.7.2 Procedure of FEM

The implementation of the Finite Element Method involves a series of steps that can be generally classified into three phases: preprocessing, processing, and post processing.

Preprocessing Phase:

1. Problem Definition: Define the problem, including the geometry of the structure or region, material properties, boundary conditions, and loadings.

2. Discretization: Divide the structure or region into a finite number of elements interconnected at nodes to form a mesh. This is an important step as the quality of the mesh affects the accuracy of the results.

3. Selection of Element Type: Choose the type of element to be used (e.g., linear, quadratic, triangular, quadrilateral, tetrahedral, etc.). The choice of element type depends on the nature of the problem and the geometry of the structure or region.

4. Formulation of Element Equations: Formulate the element equations that describe the mechanical behavior of each element. The equations are usually formulated in terms of displacements and are based on the chosen constitutive model.

Processing Phase:

1. Assembly: Assemble the element equations into a global system of equations that represents the behavior of the entire structure or region. This involves adding together the contributions from all elements that share a common node.

2. Application of Boundary Conditions: Apply the boundary conditions to the system of equations. This involves setting the displacements at the boundary nodes to their known values and modifying the system of equations accordingly.
3. Solution of the System of Equations: Solve the system of equations to find the unknown displacements at the nodes. This typically involves the use of numerical methods such as direct or iterative solvers.

Post Processing Phase:

1. Calculation of Strains and Stresses: Calculate the strains and stresses within each element based on the obtained displacements.

2. Interpretation of Results: Interpret the results in the context of the problem. This might involve evaluating the safety of a structure, assessing the stability of a slope, or predicting the deformation of a region under specified loading conditions.

The system of equations in FEM is generally in the following form:

$$[K]\{u\} = \{f\}$$

Where:

- $[K]$ is the global stiffness matrix,
- $\{u\}$ is the vector of unknown displacements at the nodes,
- $\{f\}$ is the vector of external forces.

Each element contributes to the global stiffness matrix $[K]$ and the force vector $\{f\}$ based on its geometry, material properties, and the applied loads. The boundary conditions modify this system of equations to reflect the constraints on the displacements at the boundary nodes. After solving this system of equations, the strains and stresses in each element can be calculated from the displacements using the relationships defined by the constitutive model.

3.7.3 Background of the Finite Element Method (FEM)

The Finite Element Method (FEM) is a powerful numerical technique for solving partial differential equations (PDEs) over complex geometries. The method is based on the concept of dividing a complex problem into smaller, simpler parts (known as elements) that are interconnected at points called nodes. The method provides a way to convert the differential equations, which are continuous in nature, into a system of algebraic equations which can be solved using numerical methods.

The origins of the FEM date back to the early 20th century, but the method was not fully developed until the 1960s with the advent of digital computers. One of the earliest uses of the method was in the field of structural engineering to analyze the stresses and deformations in complex structures.

Today, the FEM is used in a wide variety of fields, from geotechnical and civil engineering to fluid dynamics, heat transfer, electromagnetics, and even in the field of finance for option pricing.

The underlying principle of the FEM is the vibrational methods, which seek to find the minimum or maximum of a function. This method gives the FEM a strong mathematical foundation, making it a robust and reliable numerical method.

In the FEM, the original complex problem is approximated by a simpler one on a subdivided geometry. In other words, a complex structure is replaced by an assembly of simple elements interconnected at nodes. The behavior of each element is expressed in terms of its nodal values, leading to a system of algebraic equations that can be solved using standard numerical methods.

The method allows for the analysis of physical structures of arbitrary complexity, and the flexibility of the FEM is further enhanced by the use of a variety of element types, such as linear or quadratic elements, triangular, quadrilateral, or brick elements, etc.

The FEM has proven to be particularly effective in the field of structural and geotechnical engineering, where it has been used for the analysis of stresses and deformations in soils, rocks, and various types of structures. The FEM provides a systematic way to account for the geometrical complexity, material heterogeneity, and complex boundary and loading conditions that are often encountered in these problems.

3.8 Slope Stability in Plaxis 2D

Plaxis 2D is a powerful tool for the numerical analysis of geotechnical stability and deformation. It provides a sophisticated platform for modeling complex geotechnical problems, including slope stability analysis. Plaxis 2D employs the Finite Element Method (FEM), making it possible to analyze the stability of slopes under various loading and soil conditions.

To evaluate the stability of a slope in Plaxis 2D, the following general steps are often followed:

1. Geometry Setup: The first step in a Plaxis 2D analysis is to set up the geometry of the problem. This involves inputting the dimensions and shape of the slope, along with any relevant structures or features.

2. Material Properties: Once the geometry is set up, the properties of the soil or other materials that make up the slope must be defined. This includes parameters such as the unit weight, cohesion, friction angle, and any other relevant material properties.

3. Boundary and Initial Conditions: The boundary conditions (such as loadings or support conditions) and the initial conditions (such as initial stresses or displacements) must then be specified.

4. Mesh Generation: The geometry is then discretized into a mesh of finite elements. The mesh size and element type can have a significant impact on the accuracy and efficiency of the analysis, so careful attention must be paid to this step.

5. Analysis: Once the problem is fully defined, the analysis can be run. Plaxis 2D offers several types of analysis, including deformation analysis, stability analysis, and consolidation analysis. For slope stability problems, a stability analysis is typically used to calculate the Factor of Safety (FOS).
6. Post-Processing: After the analysis is complete, the results can be reviewed and interpreted. Plaxis 2D provides a range of tools for visualizing and examining the results, including contour plots, deformation plots, and plots of the variation of quantities such as stress or strain along a line.

Through this process, Plaxis 2D allows for a comprehensive and detailed analysis of slope stability, providing valuable insights into the behavior of slopes under different conditions and allowing for the design and analysis of effective slope stabilization measures.

3.8.1 Finite Element Method in Plaxis 2D

In the field of geotechnical engineering, achieving exact solutions to problems can often be complex and challenging. Nevertheless, approximate solutions can be obtained through the use of numerical modeling techniques. One such technique is the Finite Element Method (FEM), which divides the problem geometry into smaller, manageable elements (or meshes) to derive finite element matrices at the nodes, consequently approaching the desired solution.

Under specific conditions, such as when plane-strain conditions are valid, the problem can be modeled in two dimensions (2D). In this study, we're using the PLAXIS 2D software to analyze the problem of permanent slope displacement under seismic loading within a 2D plane-strain context.

A critical aspect of this approach is the selection of an appropriate soil model capable of accurately simulating the real-life behavior of the site. Equally important is the choice of element type. To

enhance accuracy within the PLAXIS 2D software, we employed 15-noded triangular elements, which consist of 12 stress points and 15 nodes for calculations.

Additionally, this study utilizes both phi/c reduction (safety) analysis and dynamic analysis options within PLAXIS 2D. The former is used to calculate static safety factor values for slopes, while the latter is employed to compute earthquake-induced displacements. The selection of a suitable material model for these analyses is crucial, as it enables us to emulate complex, non-linear soil behavior.

3.8.2 Constitutive Soil Model in Plaxis

3.8.2.1 Linear Elastic Model

This is the most basic model, which assumes that the soil behaves elastically and linearly. It is often used for preliminary analyses where the soil is not expected to yield or undergo plastic deformations.

3.8.2.2 Mohr-Coulomb Model

This model is also relatively simple and assumes that soil failure occurs when the shear stress on a plane reaches a certain value that depends on the normal stress on that plane and the soil's cohesion and internal friction angle. This model is often used for general geotechnical problems but has limitations when it comes to accurately predict the behavior of over consolidated clays and sands at strains beyond the elastic range.

3.8.2.3 Hardening Soil Model

This model is more advanced and takes into account the non-linear elastic deformation and plastic yielding of soils under different stress states. It is suitable for predicting the behavior of soils undergoing substantial deformations.

3.8.2.4 Hoek-Brown Model (HB)

This model was originally developed for rock mechanics but has since been extended to soils. It is particularly useful for predicting the behavior of jointed rock masses and heavily over consolidated clays.

3.8.2.5 Soft Soil Model (SS)

This model represents the time-independent behavior of soft soils, such as clays, and includes the effects of creep (time-dependent deformation). It can capture the non-linear consolidation and creep behavior of these types of soils.

3.8.2.6 Soft Soil Creep Model (SSC)

This is an extension of the Soft Soil Model and includes the effects of both primary and secondary consolidation (creep). This model is suitable for situations where substantial long-term deformations are expected.

3.8.3 Mohr-Coulomb Model

The PLAXIS 2D software includes the Mohr-Coulomb material model, a constitutive model that is frequently used in geotechnical engineering. The behavior of soils under both drained and undrained situations, including the results of soil dilatation and failure, is simulated using this model.

In the Mohr-Coulomb model, the shear strength of soil is defined by the Mohr-Coulomb failure criterion, which relates the shear stress τ to the normal stress σ through the equation:

$\tau = c + \sigma tan(\varphi)$; Where $tan(\varphi)$ is the Mohr-Coulomb envelope's slope, is the friction angle, and c is the cohesion intercept. The Mohr-Coulomb model makes the assumption that the soil's shear strength is unaffected by the rate of strain and the direction of the stress.

To use the Mohr-Coulomb model in PLAXIS 2D, the values of the model parameters, including the cohesion intercept, friction angle, and dilation angle must be specified. The dilation angle is an additional parameter that accounts for the rise in soil volume throughout shearing and is defined by the equation:

$$tan\ (\delta) = \frac{(1 - sin\ (\varphi))}{(1\ +\ sin\ (\varphi))}$$

Where δ is the dilation angle.

The Mohr-Coulomb model can be used in PLAXIS 2D to simulate both drained and undrained soil dynamics. The model presupposes that the soil deforms as a granular material in drained conditions and that pore water pressure is released during this process. The model assumes that the soil behaves as a cohesive medium in undrained conditions and that the pore water pressure does not vary during deformation.

The Mohr-Coulomb model has a number of benefits over other models in some circumstances, despite the fact that each model has strengths and drawbacks of its own.

The Mohr-Coulomb model has a number of benefits over other material models in PLAXIS 2D, including:

1. Simplicity: The Mohr-Coulomb model is a commonly used constitutive model that accurately simulates the behavior of a variety of soils. It is quite basic. When compared to more complex models, its simplicity makes it simple to implement and calibrate for particular soil conditions, which can save time and resources.

2. Versatility: The Mohr-Coulomb model is applicable to a wide range of soil types, including sand, gravel, and clay, and may be used to predict the behavior of both drained and undrained soils. It is a useful tool for many geotechnical engineering applications because of its adaptability.

3. Calibration: The Mohr-Coulomb model has a relatively small number of parameters that need to be calibrated, including the cohesion intercept, friction angle, and dilation angle. The calibration procedure can be made simpler and more accurate results can be obtained by determining these parameters by laboratory, field, or empirical correlations.

4. Failure criteria: The Mohr-Coulomb model makes use of a well-known and extensively used failure criterion in geotechnical engineering. This criterion accurately predicts soil failure under a variety of stress scenarios by correlating the shear strength of the soil to the normal stress.

5. Compatibility: In PLAXIS 2D, the Mohr-Coulomb model is compatible with a wide range of other models and analysis methods, such as the analysis of soil-structure interactions and finite elements. It can therefore be used as a tool to model how soil structures and geotechnical issues will behave under various loads and boundary conditions.

3.8.4 Nodes and Element

In PLAXIS 2D, the 6-noded and 15-noded triangular elements are frequently employed. While the 15-noded element has three additional nodes at the midpoints of each edge, the 6-noded element has three nodes at each corner of the triangle.

For our simulation 15 nodded element was used because the 15-noded element's principal benefit is its improved ability to record curved borders and gradients. This is crucial for modeling complex geometries, where there are considerable fluctuations in the soil qualities or when the borders are not straight lines. The 15-noded element's extra nodes give it more degrees of freedom, enabling a better estimate of the solution and a more precise depiction of the behavior of the soil.

Additionally, localized phenomena like failure zones, shear bands, and stress concentrations can be better simulated using the 15-noded element. It can produce more realistic findings since it can more properly capture these occurrences. Due to its simpler design and fewer nodes, the 6-noded element would not be able to adequately reflect these events.

3.8.5 Mesh

To execute finite element computations, the geometry must be broken down into finite elements when the geometry model is fully established. A mesh is a collection of finite elements. In the Mesh mode, the mesh is produced.

The mesh needs to be fine enough to produce accurate numerical values. On the other side, very fine meshes ought to be avoided because they'll make calculations take too long. The creation of finite element meshes is completely automatic with the PLAXIS 2D application. A reliable triangulation method is used to generate the mesh. The soil stratigraphy is taken into account during the mesh creation process together with other structural elements, loads, and boundary conditions.

The desired element dimension, represented by the global meshing parameter le, is needed by the mesh generator. This parameter in PLAXIS 2D is determined by the outside geometrical dimensions (x_{min}, x_{max}, y_{min}, y_{max}). The target element dimension is calculated using the equation below:

$$l_{e=} r_e \times 0.06 \times \sqrt{(x_{max} - x_{min})^2 + (y_{max} - y_{min})^2}$$

Where the Relative element size factor (re) is derived from the Element distribution. Five worldwide levels are present.

The option re (Element distribution)'s default values are:

Table 3-2 Element Distribution

Element Distribution	Re
Very coarse	2.00 (30 - 70 elements)
Course	1.33 (50 - 200 elements)
Medium	1.00 (90 - 350 elements)
Fine	0.67 (250 - 700 elements)
Very Fine	0.50 (500 - 1250 elements)

Among the five global levels, we used “Medium” based on our desired level of accuracy and technological resources. It is also preferable for us as it strikes a balance between providing accurate results while keeping computational time and memory requirements manageable.

Chapter 4 Material and Model Consideration

4.1 Construction Method

- PLAXIS 2D Software
- 15 nodded element
- Plane strain condition
- Drained Condition
- Consideration of Pseudo static Coefficient
- Materials are modeled with Mohr-Coulomb Model
- Microsoft Excel for calculation of parameters, generating tables and graphs
- AutoCAD 2020 for drawing figures.

4.2 Slope Section Geometry

Table 4-1 Slope Section Geometry

Location	Length	Depth	Slope
1	15	30	2:1
2	21	42	2:1
3	15	30	2:1

4.3 Soil Parameter

The soil sample data collected from Prosoil Foundation Consultant contains information from three diverse locations, referred to as Location 1, Location 2, and Location 3. These locations were designated as representative sites for the study. The collected data aids as the basic design input for the model being developed.

The parameters considered for the model are derived from the Unified Soil Classification System (USCS), Standard Penetration Test (SPT) values, and various correlations. These correlations are mathematical relationships that link certain soil properties to other computable variables. By employing these correlations, the report offers perceptions of the soil's behavior and helps in making informed design decisions.

Table 4-2 Soil Parameters

Location	Layer	Depth (m)	Classification of Soil (USCS)	Avg SPT	Cohesion, C (Kpa)	Friction Angle, ϕ (˚)	Poisson's Ratio (v)	Dialatancy angle, ψ (˚)	Modulus of elasticity, E (KN/m²)
Betchari bazar, Rangamati road, Mohalchari, Khagrachari.	1	3	ML	17	5	39	0.35	9	25000
	2	1.5	SM	25	1	38	0.35	8	22000
	3	3	SM	24.5	1.2	36	0.35	6	24000
	4	7.5	SM	31.4	2	37	0.35	7	20000
Lemuchari 41m land, Mohalchari, Khagrachari	1	6	ML	11.8	5	30.62	0.35	0	18000
	2	4.5	SM	21.7	1	33.44	0.35	3.44	20000
	3	10.5	SM	31.4	1.5	40.26	0.35	10.26	32000
Baghaihat, Rangamati, 14 beer Baghaihat army camp	1	2	ML	7.5	2	29.47	0.35	0	12000
	2	5	ML	22	3	35.77	0.35	5.77	26000
	3	3.5	SM	30.5	1	39.15	0.35	9.15	30000
	4	4.5	SM	32.5	1	40.75	0.35	10.75	28000

4.4 Soil Profile

In this research work three different location were studied under earthquake load. Each location was analyzed in Plaxis 2D Software.

4.4.1 Location 01

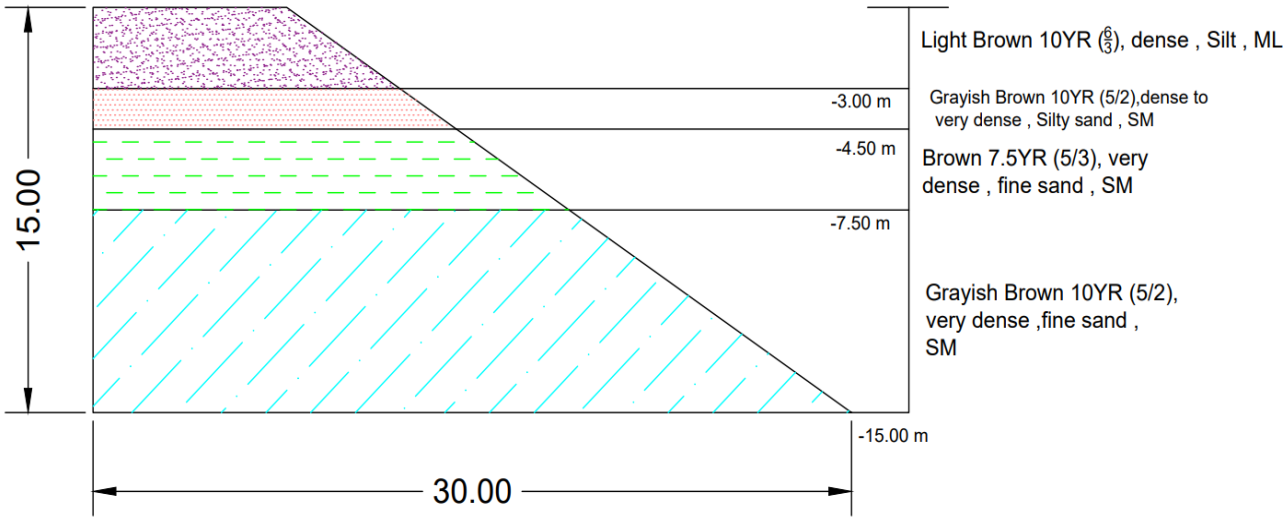

Figure 4.1 Location 01-Soil profile

4.4.2 Location 02

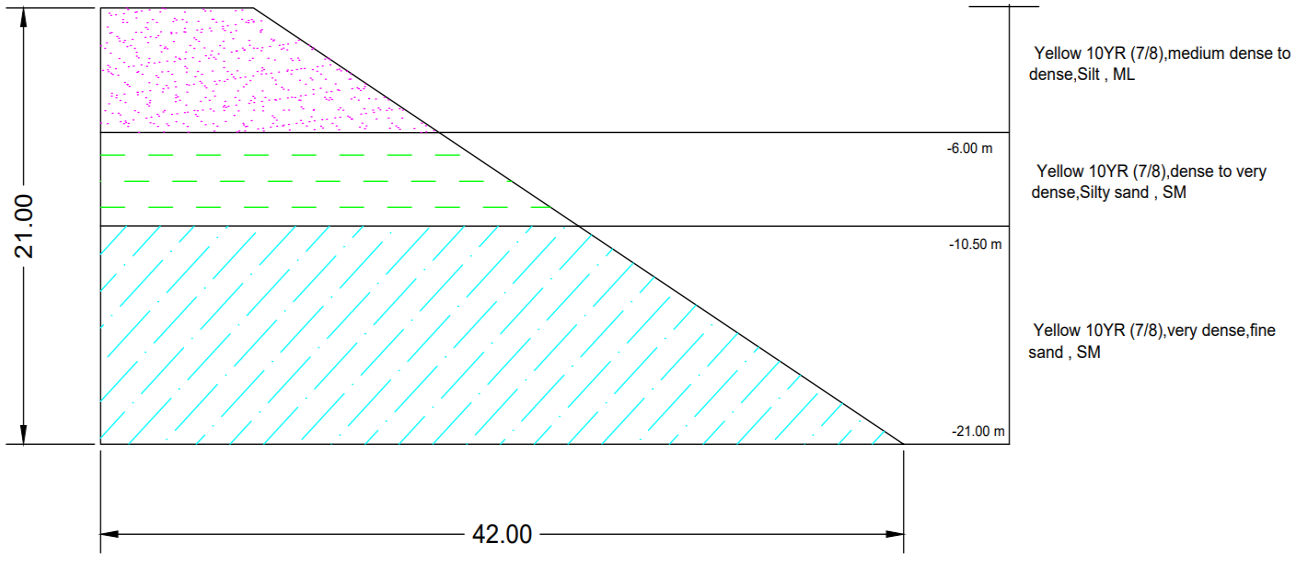

Figure 4.2 Location 02-Soil profile

4.4.3 Location 03

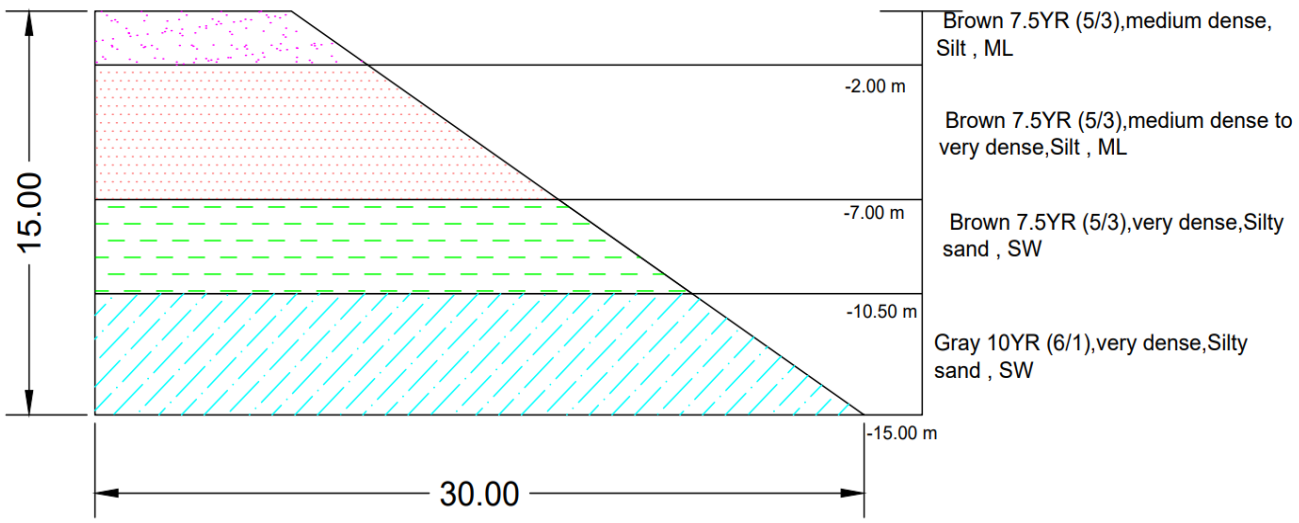

Figure 4.3 Location 03-Soil profile

4.5 Selection of Pseudo-static Coefficient

For this study each location was analyzed for four different pseudo static coefficients. The pseudo static coefficients are chosen according to Terzaghi's recommendation and Rangamati district to analyze the effect of earthquake at several magnitudes.

Bangladesh is divided into four seismic zones as per the Seismic Zoning Map of BNBC 2020. Rangamati is situated in Seismic Zone 3 and has a corresponding Seismic Coefficient value of 0.28g. The Peak Ground Acceleration values in the study wards of Rangamati range between 0.33 and 0.39. So, for location based seismic coefficient 0.28g was selected.

Table 4-3 Selected Pseudo-Static Coefficient

	Coefficient	Specification
Terzaghi	0.1	Severe
	0.3	Violent
	0.5	Catastrophic
Location Based	0.28	Seismic Zone III

Chapter 5 Results and Discussions

This section presents the outcomes obtained from the Plaxis 2D analysis. The results encompass various components such as the deformed mesh, deformations observed in different phases, and graphs illustrating the factor of safety both prior to and following the application of earthquake loading at all locations. Additionally, a comparative analysis is conducted to assess the extent of damage caused by the earthquake. The findings are effectively represented through the utilization of graphs and tables.

5.1 Location 01

5.1.1 Before earthquake

Deformed Mesh:

In the pre-earthquake condition at location 1, the deformed mesh exhibited a uniform value of 0.01392 m at the true scale in phase 1. However, when a 50-times scaled-up scale was applied in phase 2, the maximum deformed mesh value reached 0.01392 m.

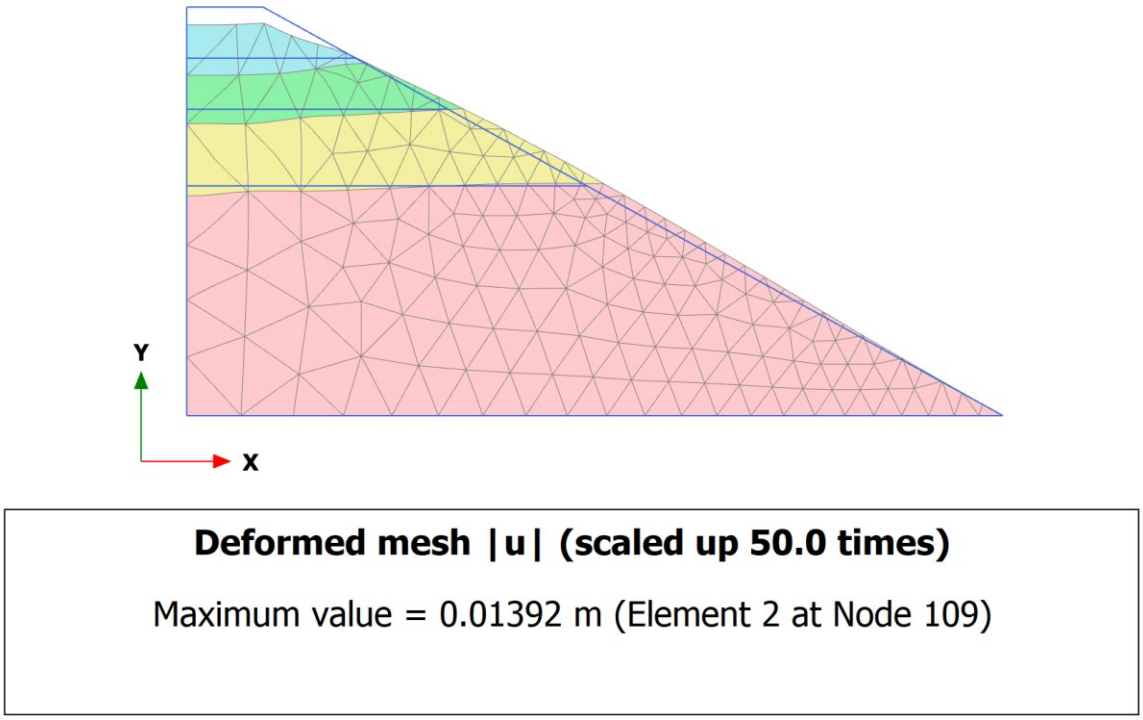

Figure 5.1 Location 01-Before earthquake, Deformed mash (Phase 01)

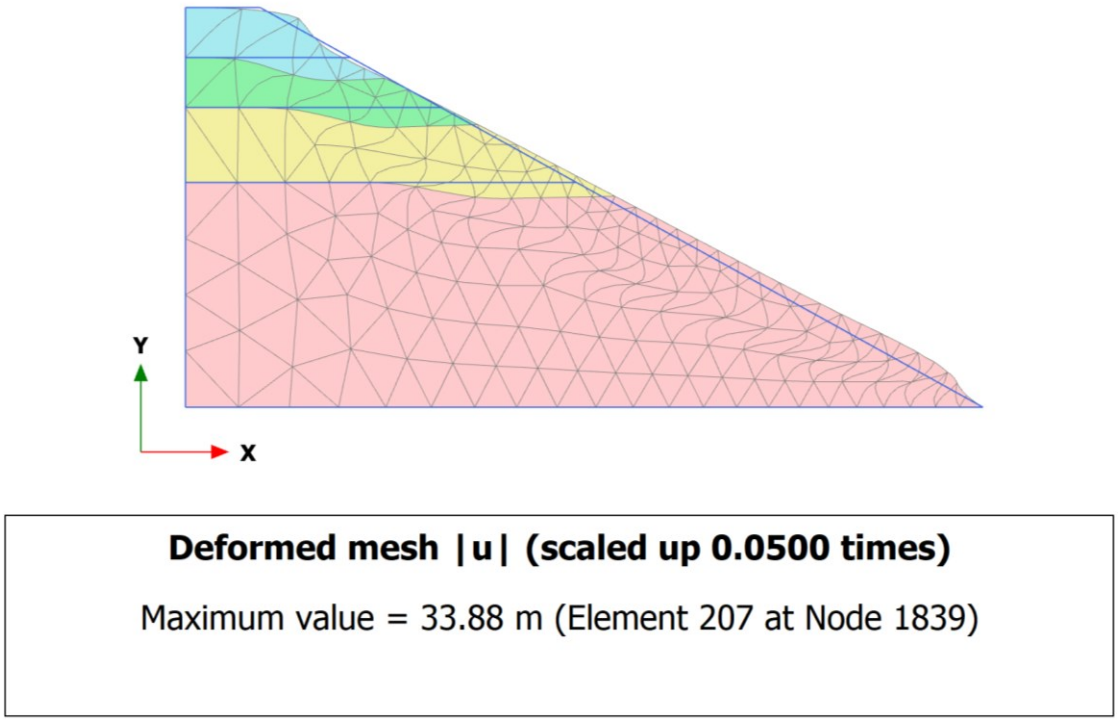

Figure 5.2 Location 01-Before earthquake, Deformed mash (Phase 02)

Displacement:

Considering the total displacements, the highest value recorded was 0.01392 m at a 50.0 times scaled-up scale in phase 01. Additionally, at a 0.0500 times scaled-up scale in phase 02, the maximum total displacement measured 33.88 m.

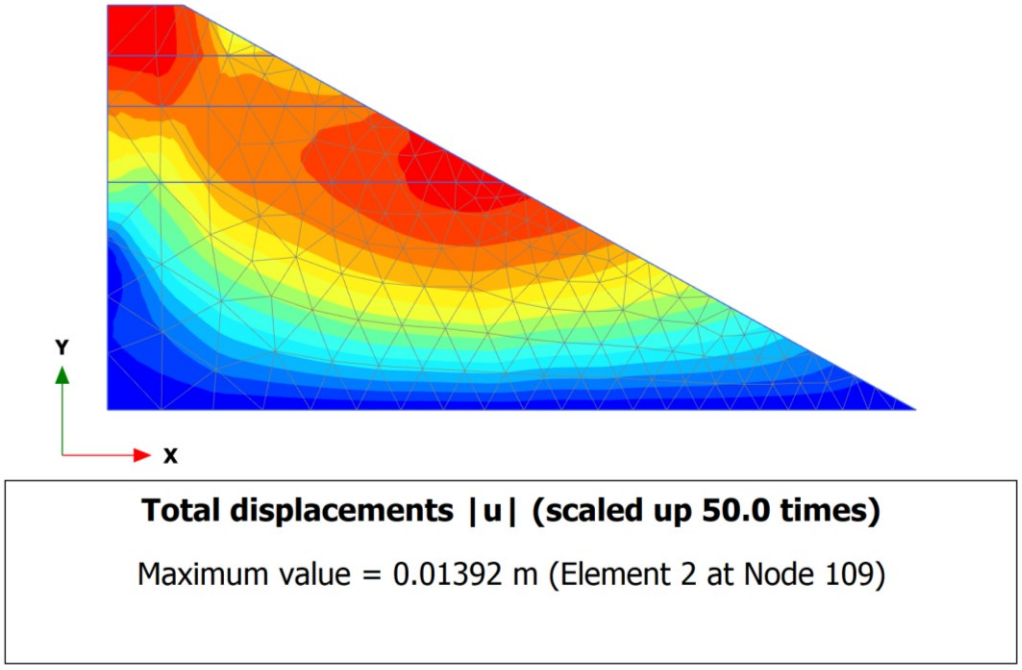

Figure 5.3 Location 01-Before earthquake, Displacement (Phase 01)

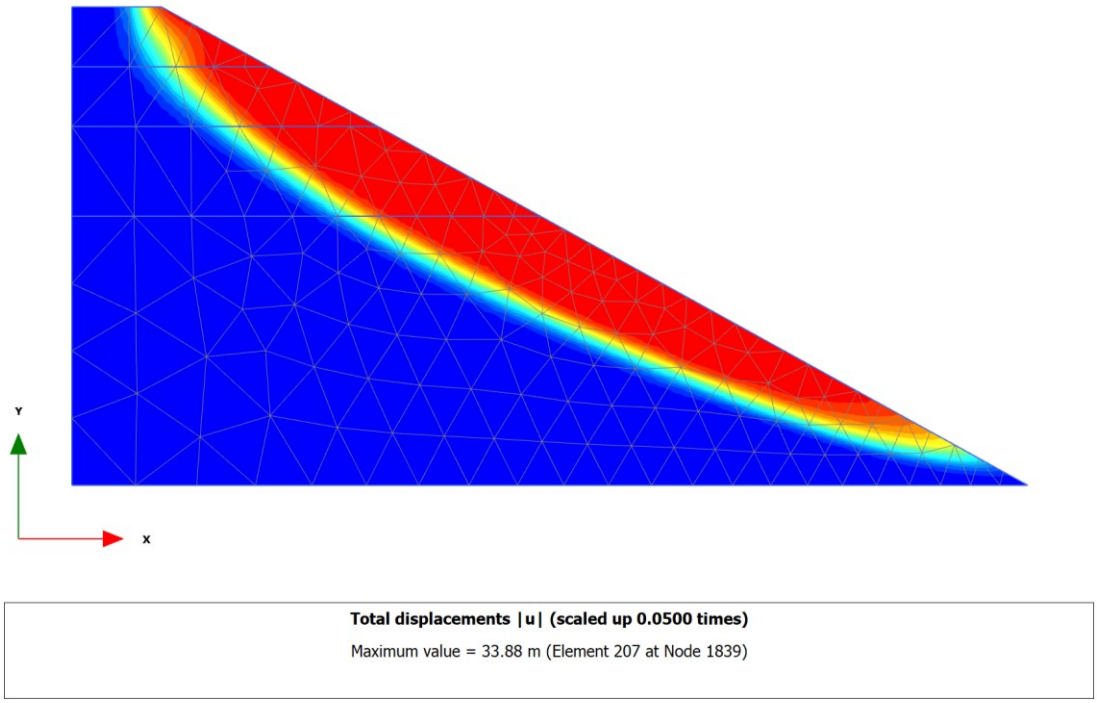

Figure 5.4 Location 01-Before earthquake, Displacement (Phase 02)

Factor of Safety:

Throughout these calculations, the factor of safety remained at 1.573.

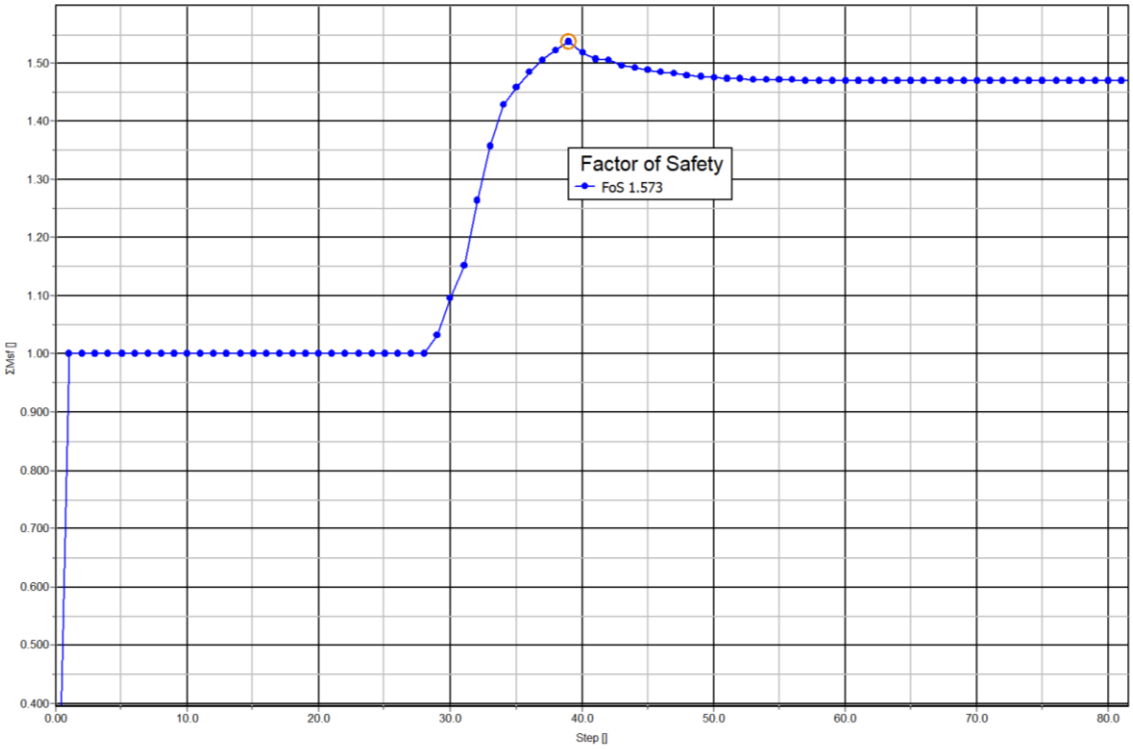

Figure 5.5 Location 01-Before earthquake, Factor of Safety

5.1.2 After earthquake

5.1.2.1 Seismic Coefficient 0.1

Deformed Mesh:

In the aftermath of the earthquake in location 1, various conditions and scaled-up scales were considered for analysis. Firstly, when a seismic coefficient of 0.1 was used at a 10.0 times scaled-up scale, the maximum deformed mesh values were found to be 0.09184 m in phase 01 and 0.08109 m in phase 02. Additionally, at a 0.0500 times scaled-up scale in phase 03, the maximum deformed mesh value was measured as 26.29 m.

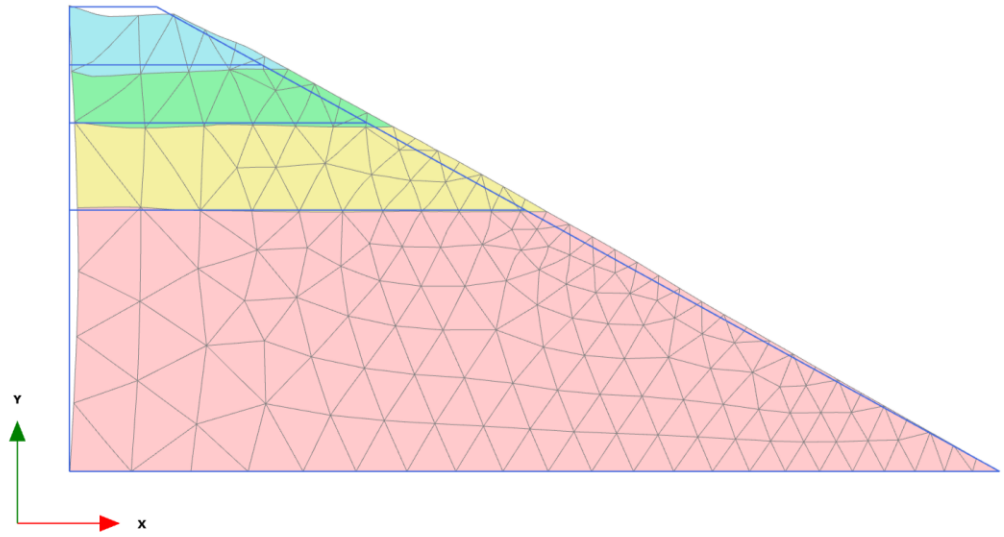

Deformed mesh |u| (scaled up 10.0 times) (Time 1.000 s)

Maximum value = 0.09184 m (Element 22 at Node 60)

Figure 5.6 Location 01-After earthquake, Deformed Mesh-Seismic Coefficient 0.1 (Phase 01)

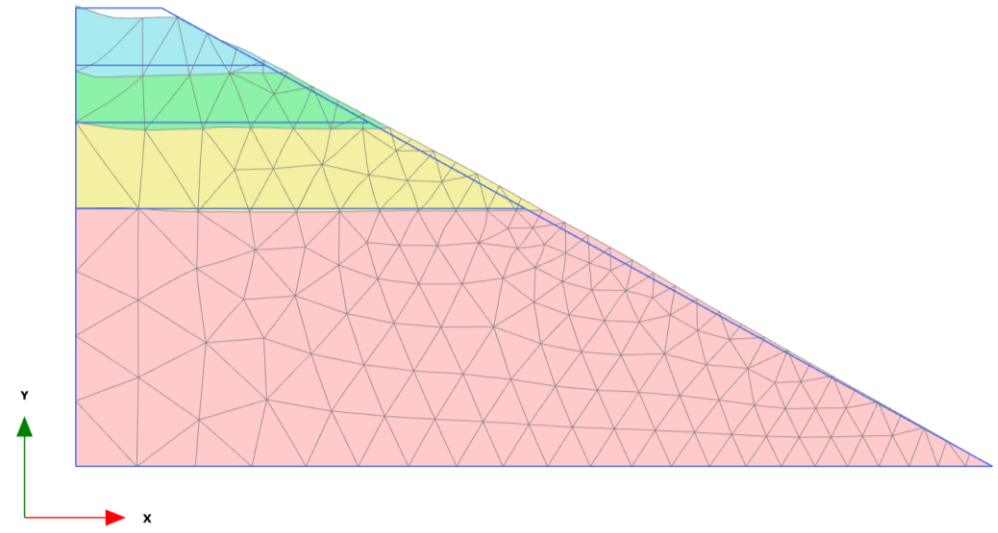

Deformed mesh |u| (scaled up 10.0 times)

Maximum value = 0.08109 m (Element 10 at Node 64)

Figure 5.7 Location 01-After earthquake, Deformed Mesh-Seismic Coefficient 0.1 (Phase 02)

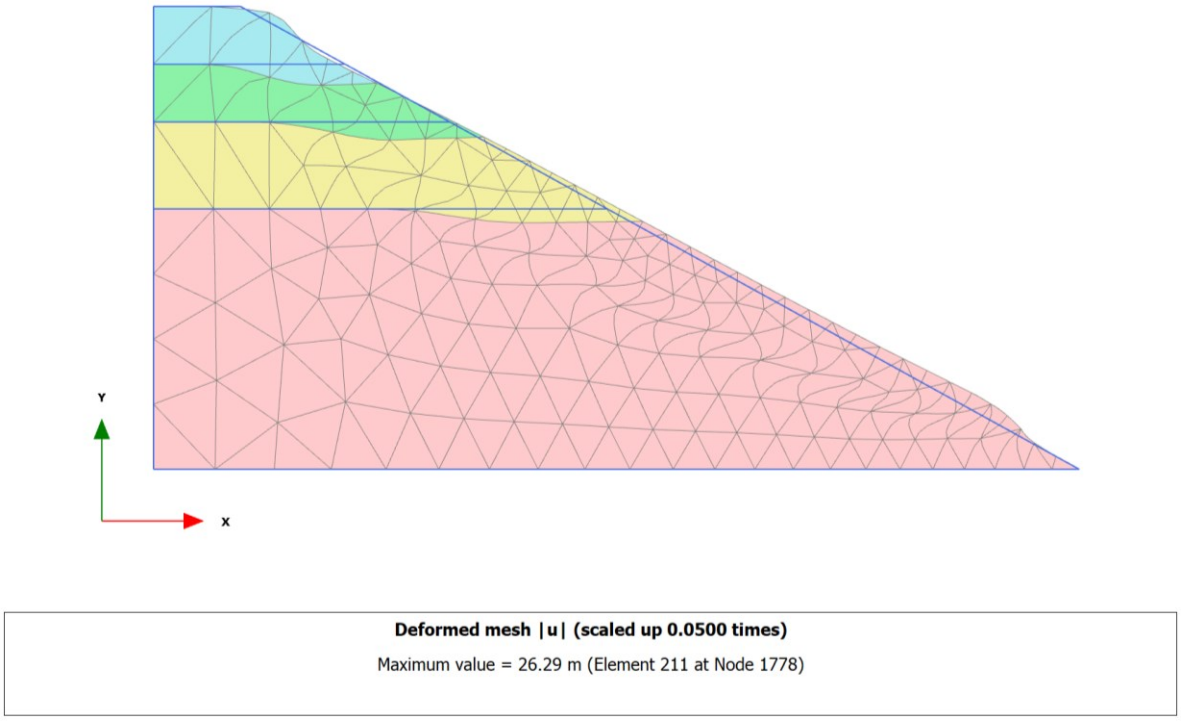

Figure 5.8 Location 01-After earthquake, Deformed Mesh-Seismic Coefficient 0.1 (Phase 3)

Displacement:

When examining the total displacements at the same 10.0 times scaled-up scale, the maximum values were recorded as 0.09184 m in phase 01 and 0.08109 m in phase 02. However, at a 0.0500 times scaled-up scale in phase 03, the maximum total displacement reached 26.29 m.

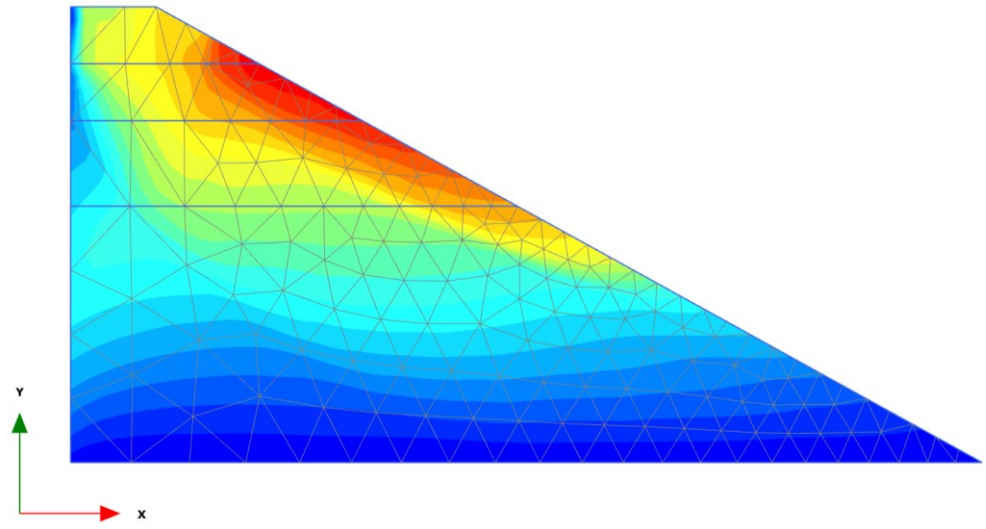

Total displacements |u| (scaled up 10.0 times) (Time 1.000 s)

Maximum value = 0.09184 m (Element 22 at Node 60)

Figure 5.9 Location 01-After earthquake, Displacement-Seismic Coefficient 0.1 (Phase 1)

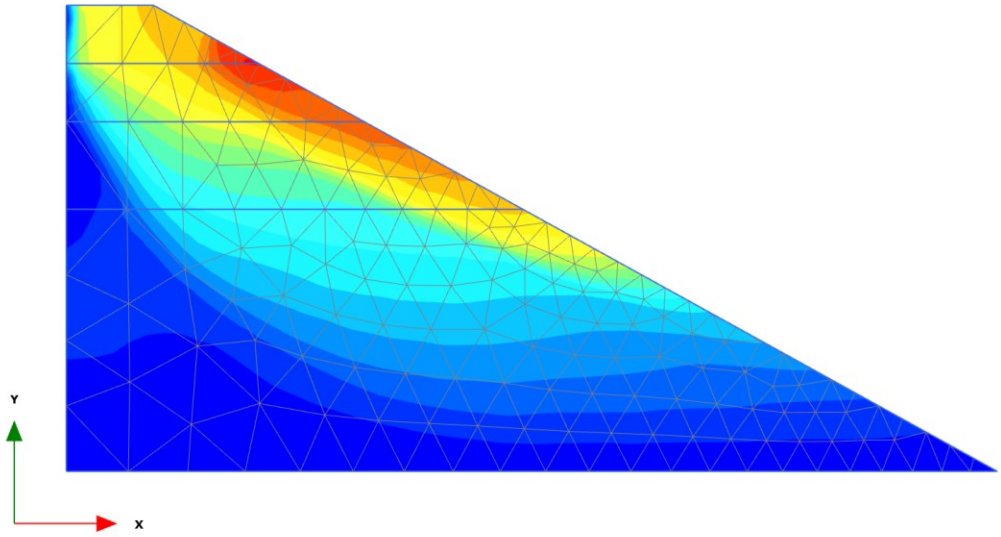

Total displacements |u| (scaled up 10.0 times)

Maximum value = 0.08109 m (Element 10 at Node 64)

Figure 5.10 Location 01-After earthquake, Displacement-Seismic Coefficient 0.1 (Phase 2)

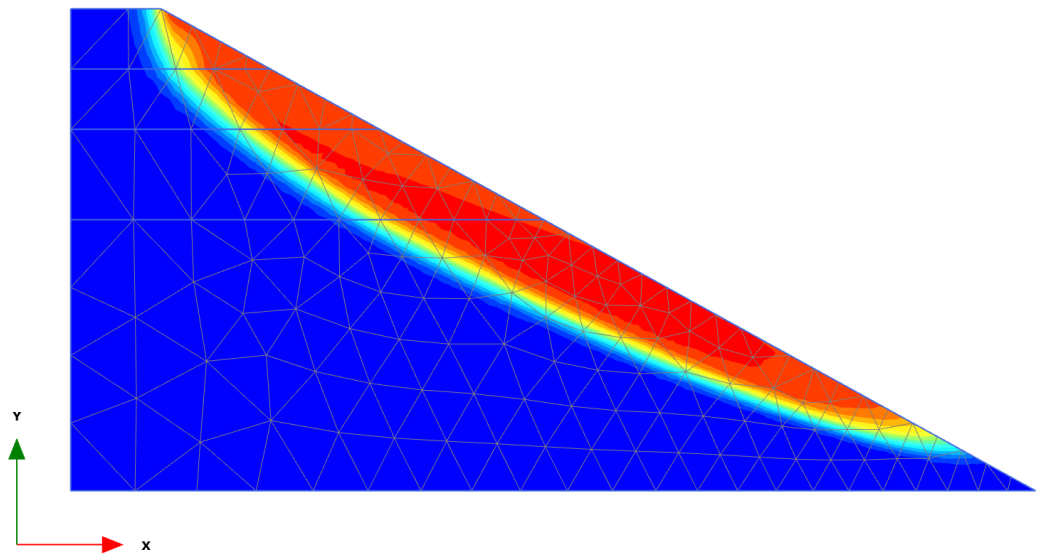

Total displacements |u| (scaled up 0.0500 times)

Maximum value = 26.29 m (Element 211 at Node 1778)

Figure 5.11 Location 01-After earthquake, Displacement-Seismic Coefficient 0.1 (Phase 3)

Factor of Safety:

In all these cases, the factor of safety was calculated as 1.473.

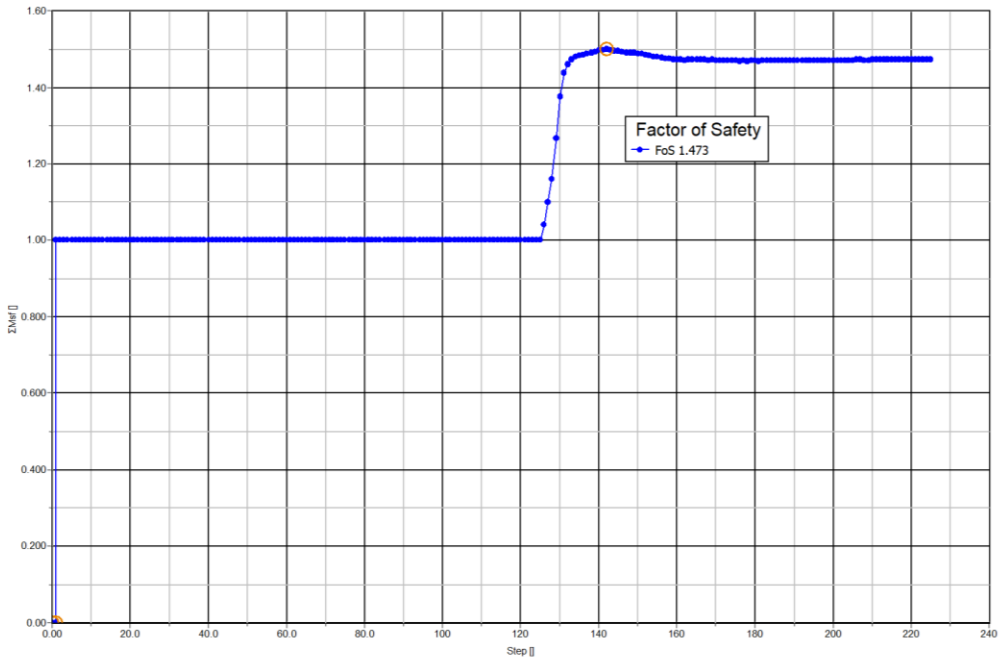

Figure 5.12 Location 01-After earthquake, Factor of Safety-Seismic Coefficient 0.1

5.1.2.2 Seismic Coefficient 0.28

Deformed Mesh:

Similarly, when the seismic coefficient was adjusted to 0.28 and a 5.0 times scaled-up scale was used, the maximum deformed mesh value was observed as 0.9139 m in phase 01. In phase 02, at a 50.0 times scaled-up scale, the maximum deformed mesh value decreased significantly to 0.01392 m. Furthermore, in phase 03 at a 0.0500 times scaled-up scale, the maximum deformed mesh value was measured as 33.88 m.

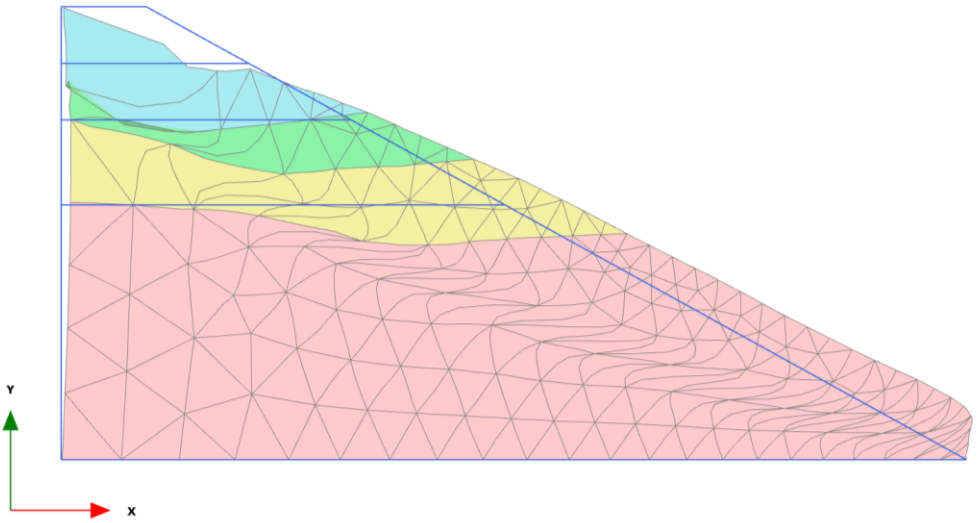

Deformed mesh |u| (scaled up 5.00 times) (Time 1.000 s)

Maximum value = 0.9139 m (Element 21 at Node 196)

Figure 5.13 Location 01-After earthquake, Deformed Mesh-Seismic Coefficient 0.28 (Phase 1)

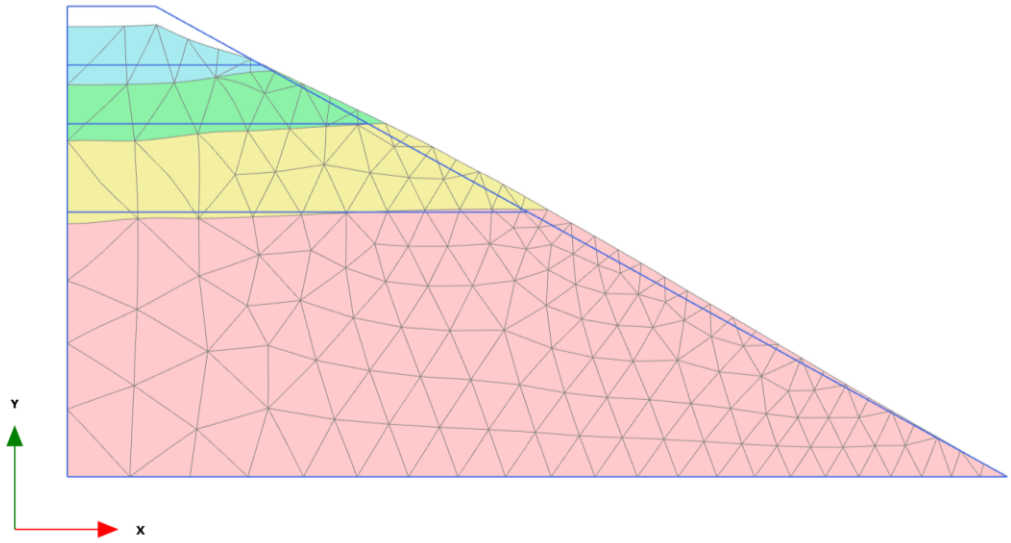

Deformed mesh |u| (scaled up 50.0 times)

Maximum value = 0.01392 m (Element 2 at Node 109)

Figure 5.14 Location 01-After earthquake, Deformed Mesh-Seismic Coefficient 0.28 (Phase-02)

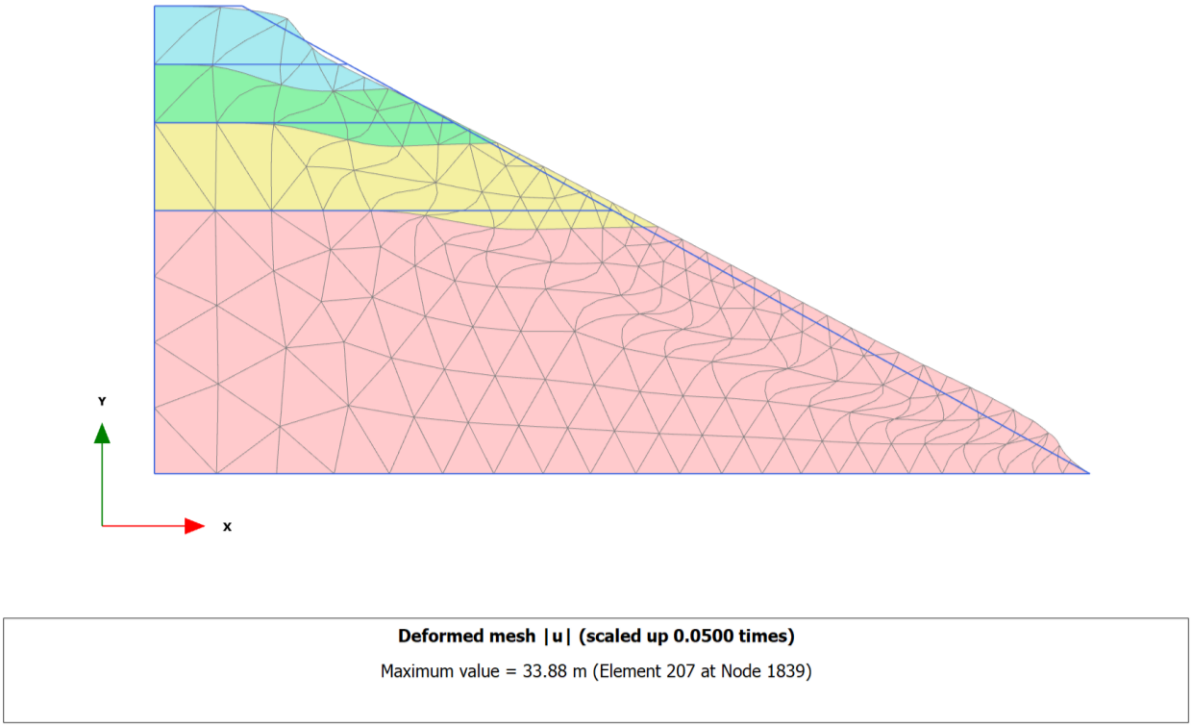

Figure 5.15 Location 01-After earthquake, Deformed Mesh-Seismic Coefficient 0.28 (Phase-03)

Displacement:

As for the total displacements, at the 5.0 times scaled-up scale in phase 01, the maximum value was found to be 0.9139 m. In phase 02, at a 50.0 times scaled-up scale, the maximum total displacement reduced to 0.01392 m.

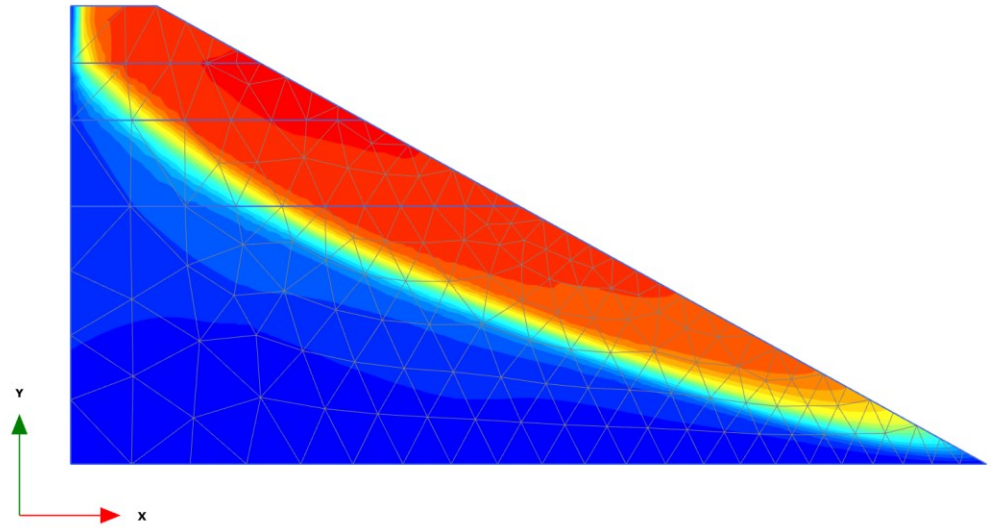

Total displacements |u| (scaled up 5.00 times) (Time 1.000 s)

Maximum value = 0.9139 m (Element 21 at Node 196)

Figure 5.16 Location 01-After earthquake, Displacement-Seismic Coefficient 0.28 (Phase-01)

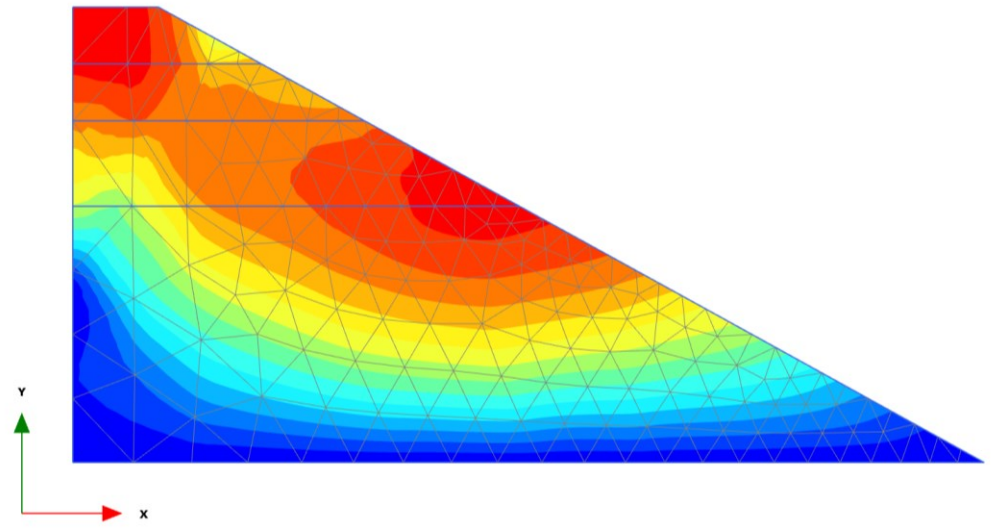

Total displacements |u| (scaled up 50.0 times)

Maximum value = 0.01392 m (Element 2 at Node 109)

Figure 5.17 Location 01-After earthquake, Displacement-Seismic Coefficient 0.28 (Phase-02)

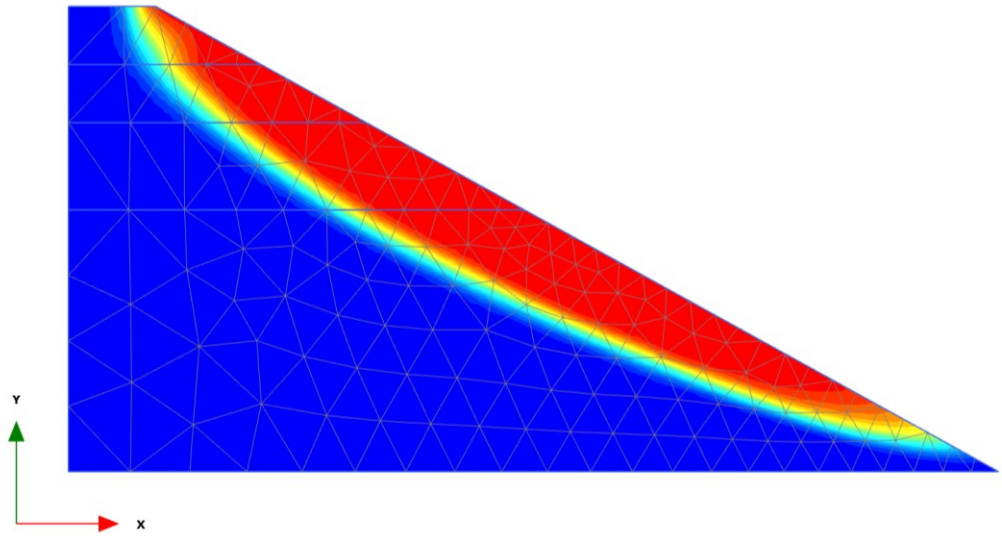

Total displacements |u| (scaled up 0.0500 times)

Maximum value = 33.88 m (Element 207 at Node 1839)

Figure 5.18 Location 01-After earthquake, Displacement-Seismic Coefficient 0.28 (Phase-03)

Factor of Safety:

In all these scenarios, the factor of safety remained at 1.462.

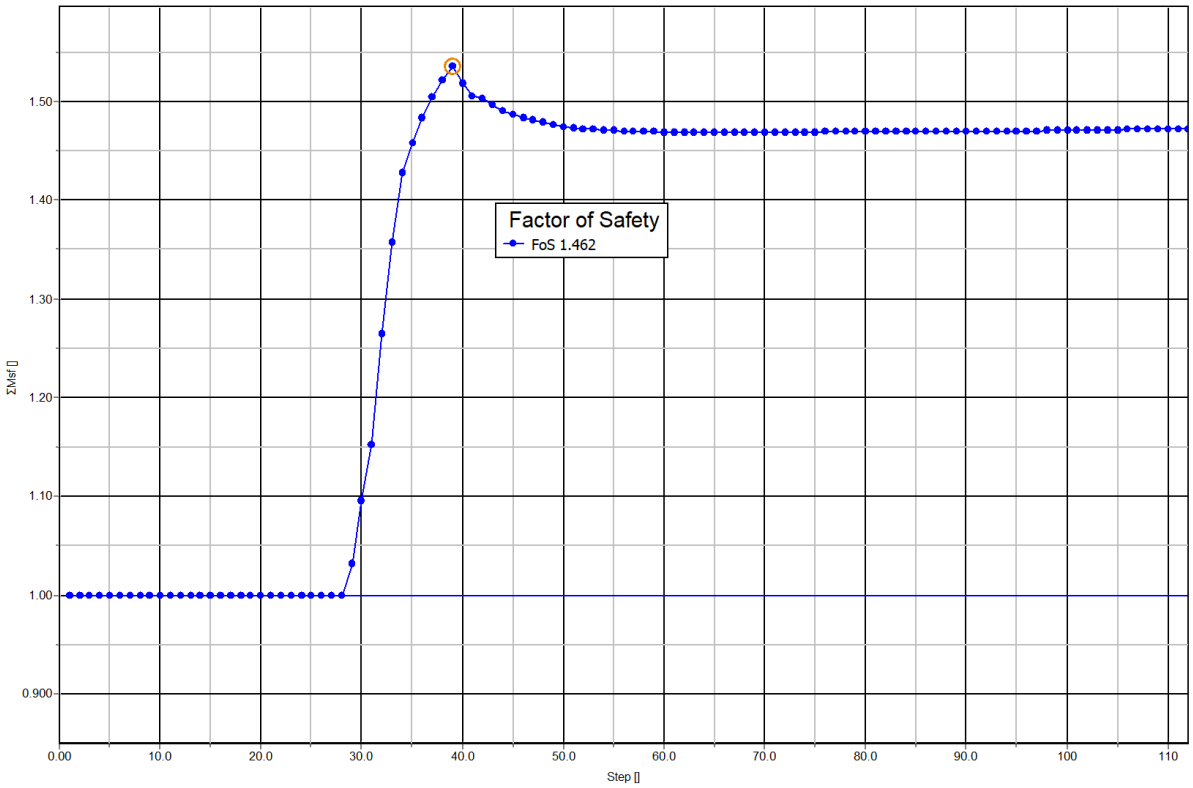

Figure 5.19 Location 01-After earthquake, Factor of Safety-Seismic Coefficient 0.28

5.1.2.3 Seismic Coefficient 0.3

Deformed Mesh:

Similarly, at a seismic coefficient of 0.3 and a 5.0 times scaled-up scale, the maximum deformed mesh value was calculated as 1.022 m in phase 01. In phase 02, at a 10.0 times scaled-up scale, the maximum deformed mesh value reduced to 0.08109 m. Additionally, in phase 03 at a 0.0500 times scaled-up scale, the maximum deformed mesh value reached 26.29 m.

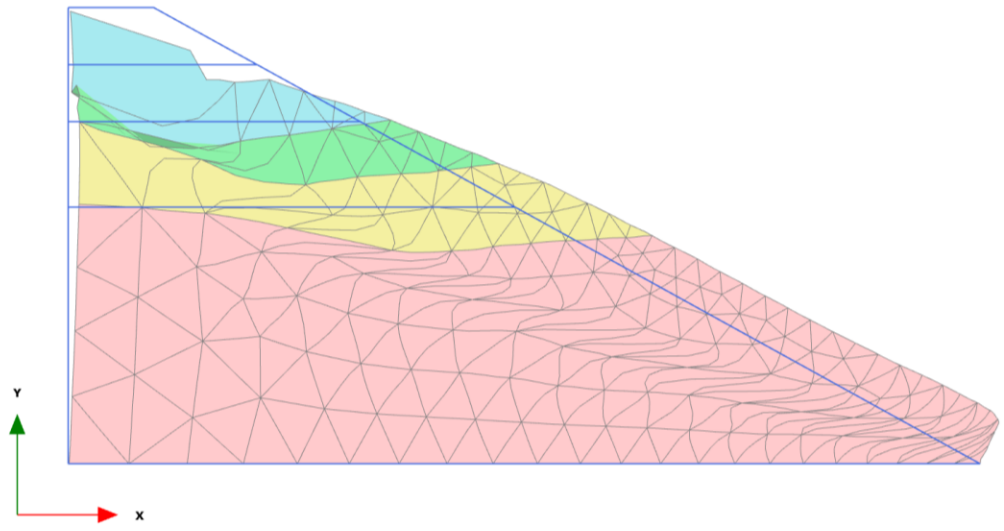

Deformed mesh |u| (scaled up 5.00 times) (Time 1.000 s)

Maximum value = 1.022 m (Element 21 at Node 196)

Figure 5.20 Location 01-After earthquake, Deformed Mesh-Seismic Coefficient 0.3(Phase-01)

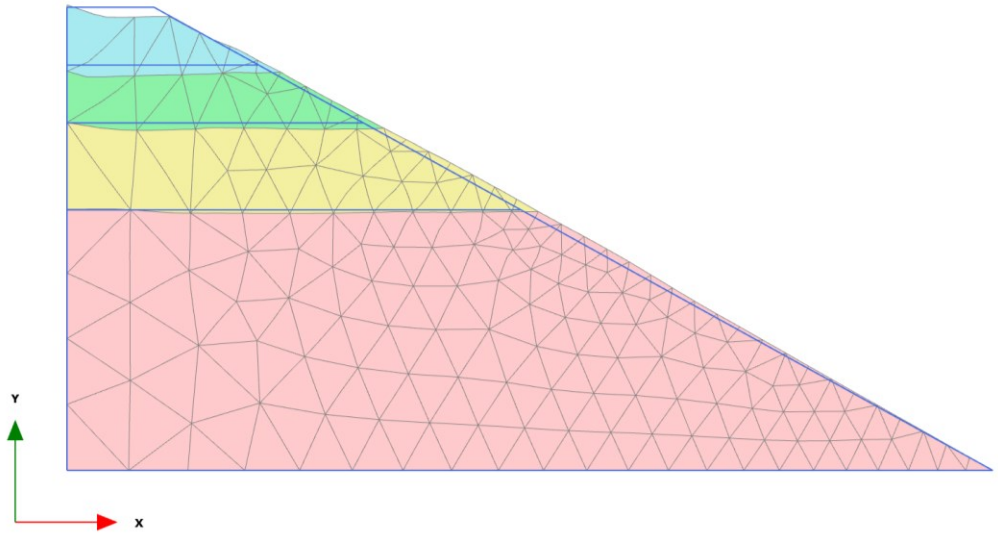

Deformed mesh |u| (scaled up 10.0 times)

Maximum value = 0.08109 m (Element 10 at Node 64)

Figure 5.21 Location 01-After earthquake, Deformed Mesh-Seismic Coefficient 0.3(Phase-02)

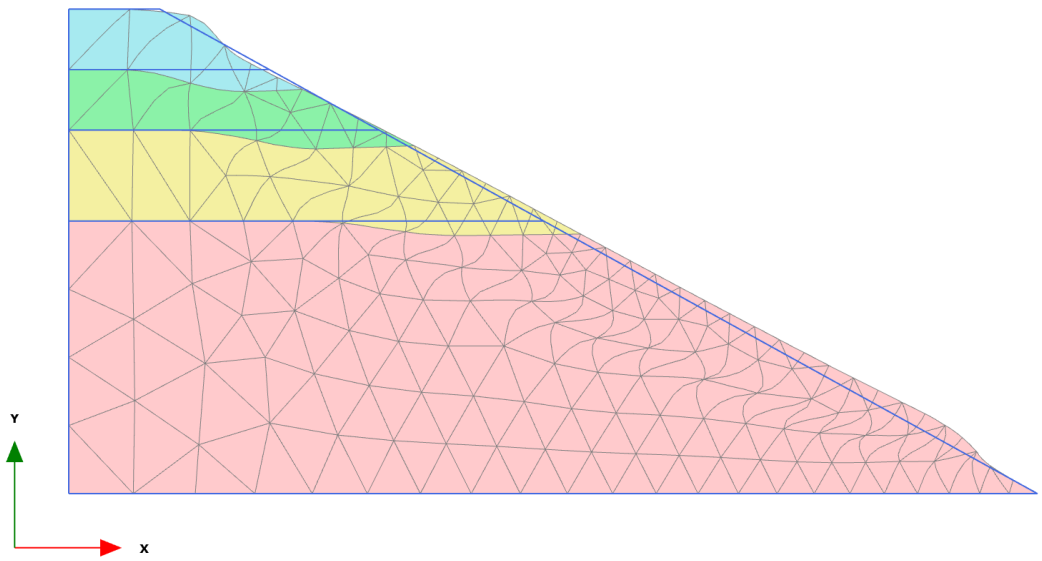

Deformed mesh |u| (scaled up 0.0500 times)

Maximum value = 26.29 m (Element 211 at Node 1778)

Figure 5.22 Location 01-After earthquake, Deformed Mesh-Seismic Coefficient 0.3(Phase-03)

Displacement:

Regarding total displacements, the highest value recorded was 1.022 m in phase 01 at a 5.0 times scaled-up scale. In phase 02, at a 10.0 times scaled-up scale, the maximum total displacement was 0.08109 m. Finally, in phase 03 at a 0.0500 times scaled-up scale, the maximum total displacement measured 26.29 m.

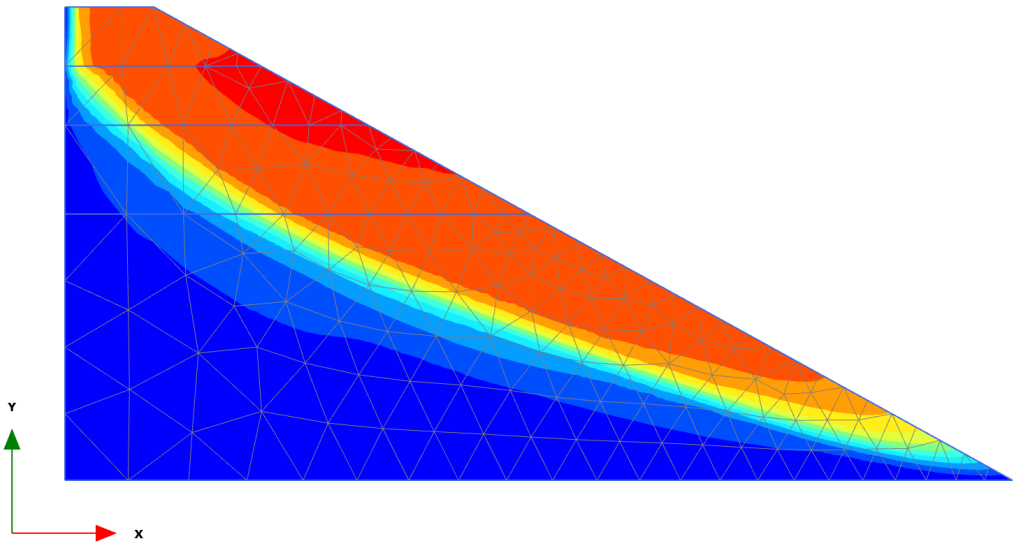

Total displacements |u| (scaled up 5.00 times) (Time 1.000 s)

Maximum value = 1.022 m (Element 21 at Node 196)

Figure 5.23 Location 01-After earthquake, Displacement-Seismic Coefficient 0.3(Phase-01)

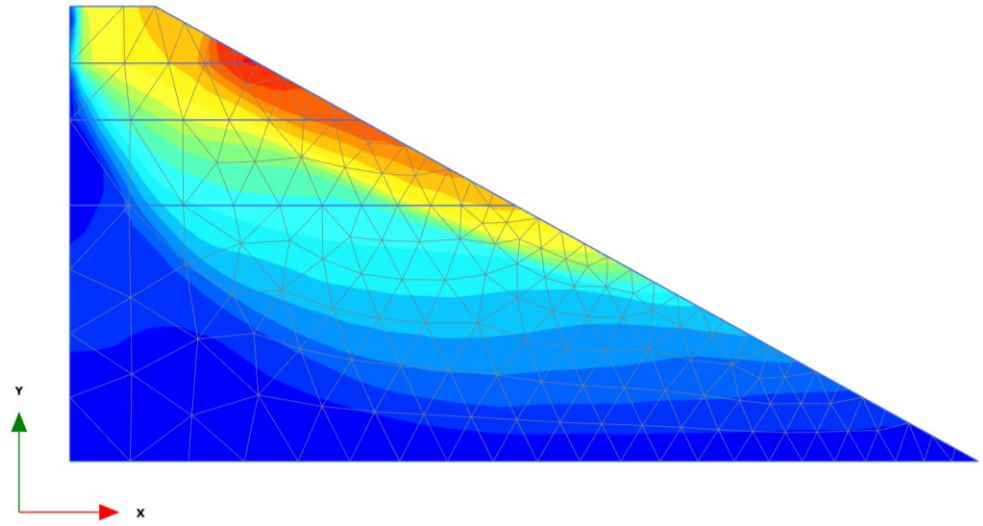

Total displacements |u| (scaled up 10.0 times)

Maximum value = 0.08109 m (Element 10 at Node 64)

Figure 5.24 Location 01-After earthquake, Displacement-Seismic Coefficient 0.3(Phase-02)

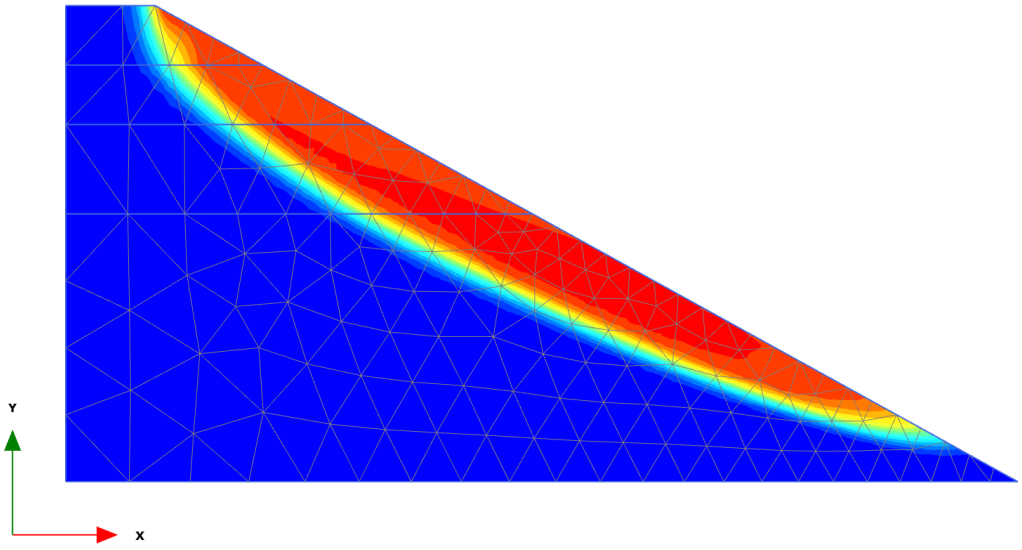

Total displacements |u| (scaled up 0.0500 times)

Maximum value = 26.29 m (Element 211 at Node 1778)

Figure 5.25 Location 01-After earthquake, Displacement-Seismic Coefficient 0.3(Phase-03)

Factor of Safety:

As before, the factor of safety remained at 1.420.

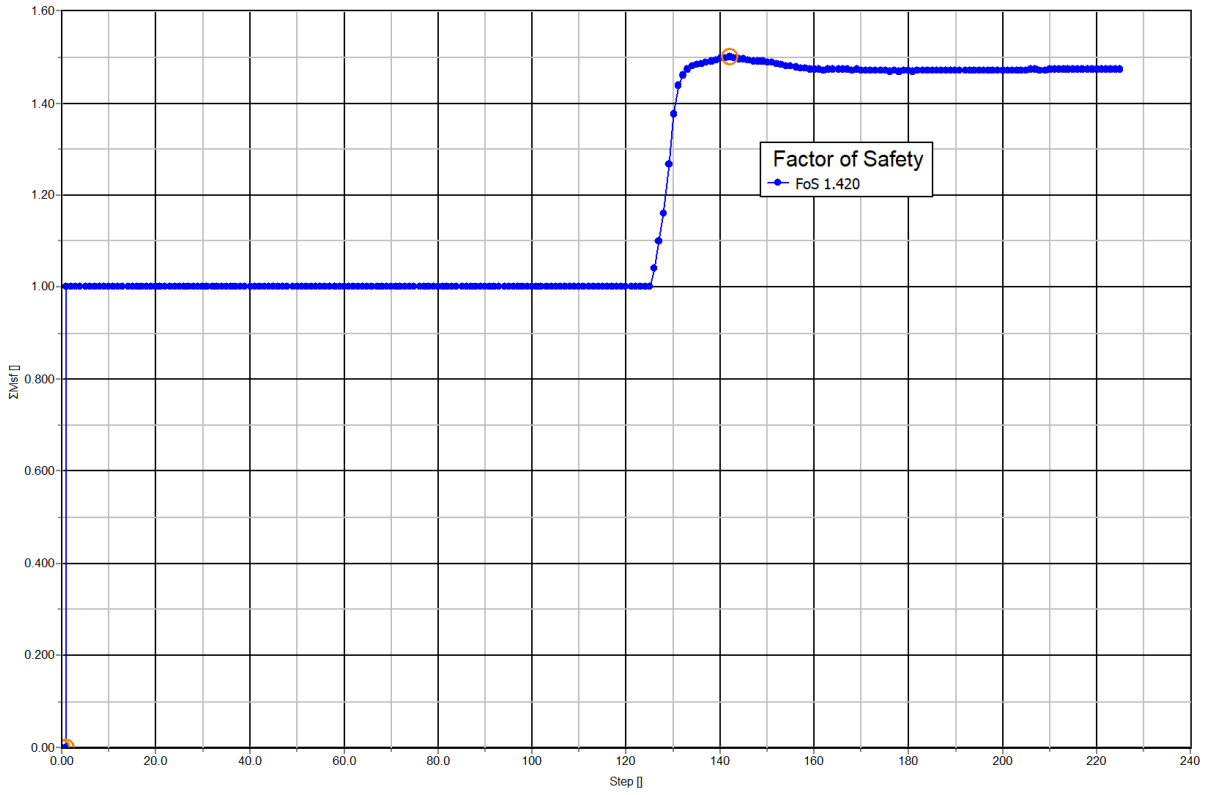

Figure 5.26 Location 01-After earthquake, Factor of Safety-Seismic Coefficient 0.3

5.1.2.4 Seismic Coefficient 0.5

Deformed Mesh:

Lastly, when utilizing a seismic coefficient of 0.5 and a 0.500 times scaled-up scale, the maximum deformed mesh value was determined to be 2.162 m in phase 01. In phase 02, at a 10.0 times scaled-up scale, the maximum deformed mesh value reduced to 0.08109 m. Similarly, in phase 03 at a 0.0500 times scaled-up scale, the maximum deformed mesh value measured 26.29 m.

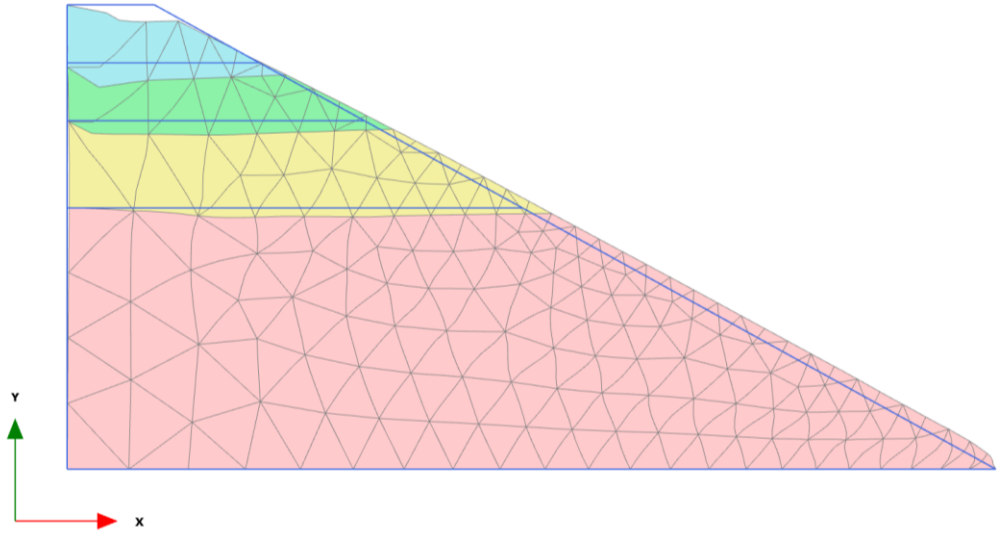

Deformed mesh |u| (scaled up 0.500 times) (Time 1.000 s)

Maximum value = 2.162 m (Element 1 at Node 222)

Figure 5.27 Location 01-After earthquake, Deformed Mesh-Seismic Coefficient 0.5(Phase-01)

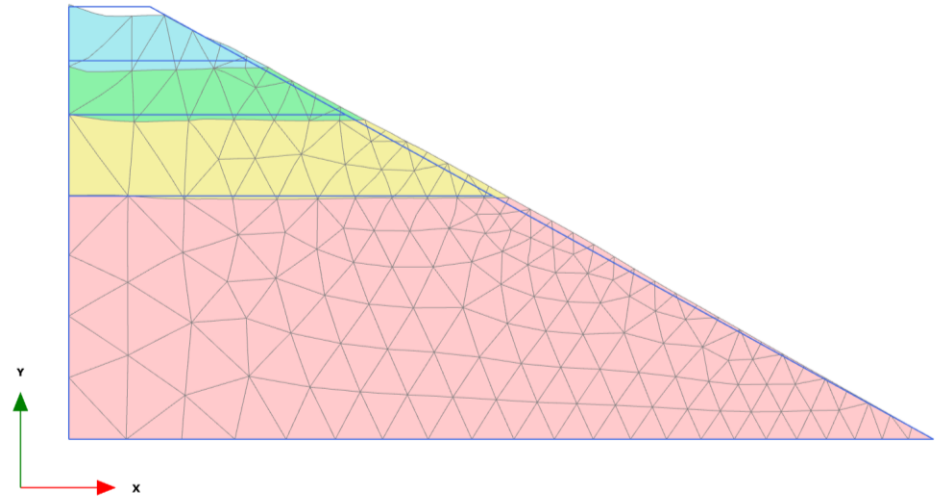

Deformed mesh |u| (scaled up 10.0 times)

Maximum value = 0.08109 m (Element 10 at Node 64)

Figure 5.28 Location 01-After earthquake, Deformed Mesh-Seismic Coefficient 0.5(Phase-02)

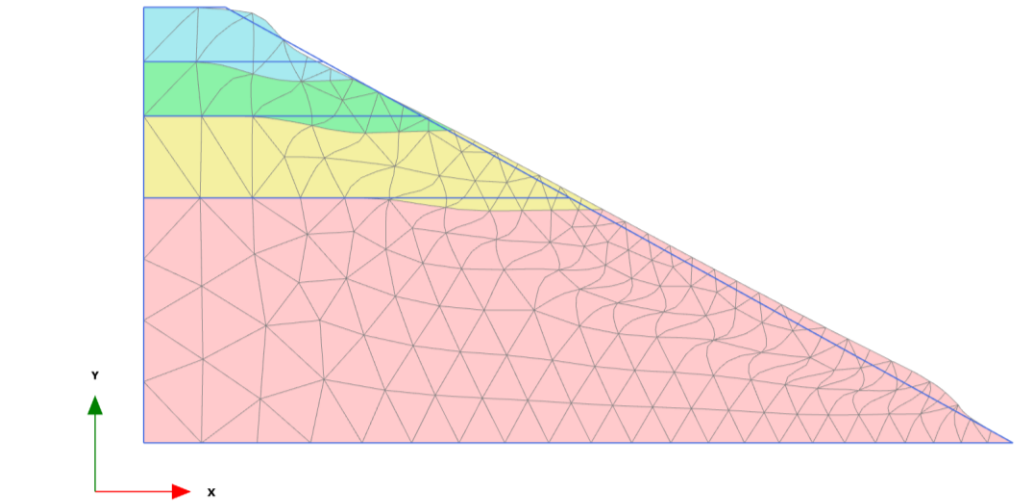

Figure 5.29 Location 01-After earthquake, Deformed Mesh-Seismic Coefficient 0.5(Phase-03)

Displacement:

Examining the total displacements, the highest value obtained was 2.162 m in phase 01 at a 0.500 times scaled-up scale.

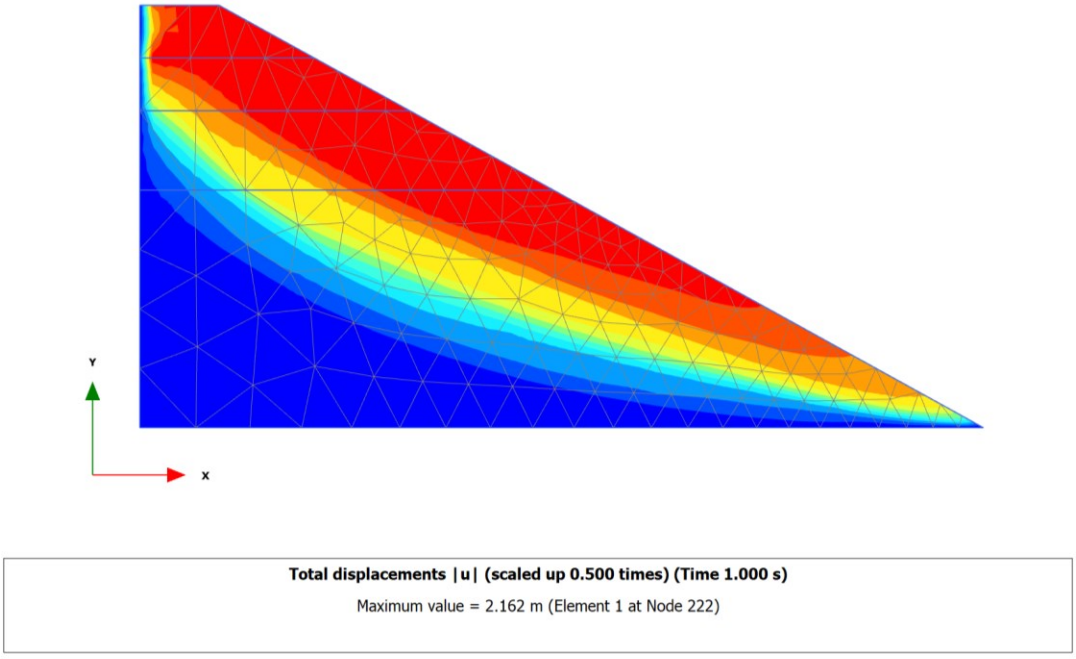

Figure 5.30 Location 01-After earthquake, Displacement-Seismic Coefficient 0.5(Phase-01)

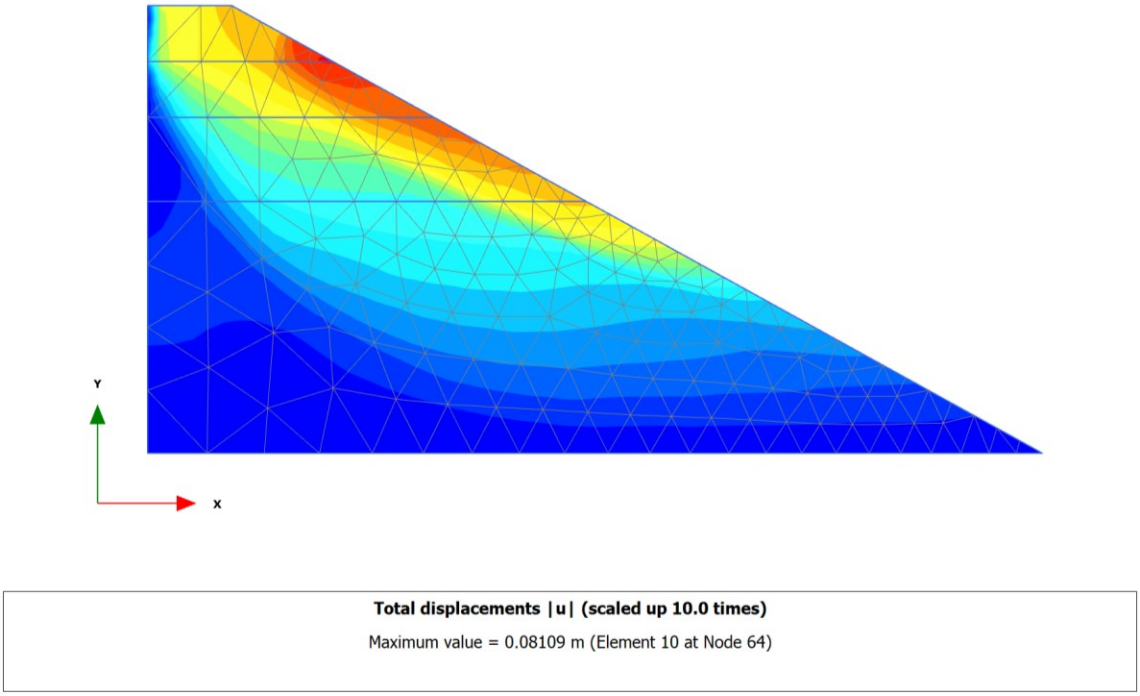

Figure 5.31 Location 01-After earthquake, Displacement-Seismic Coefficient 0.5(Phase-02)

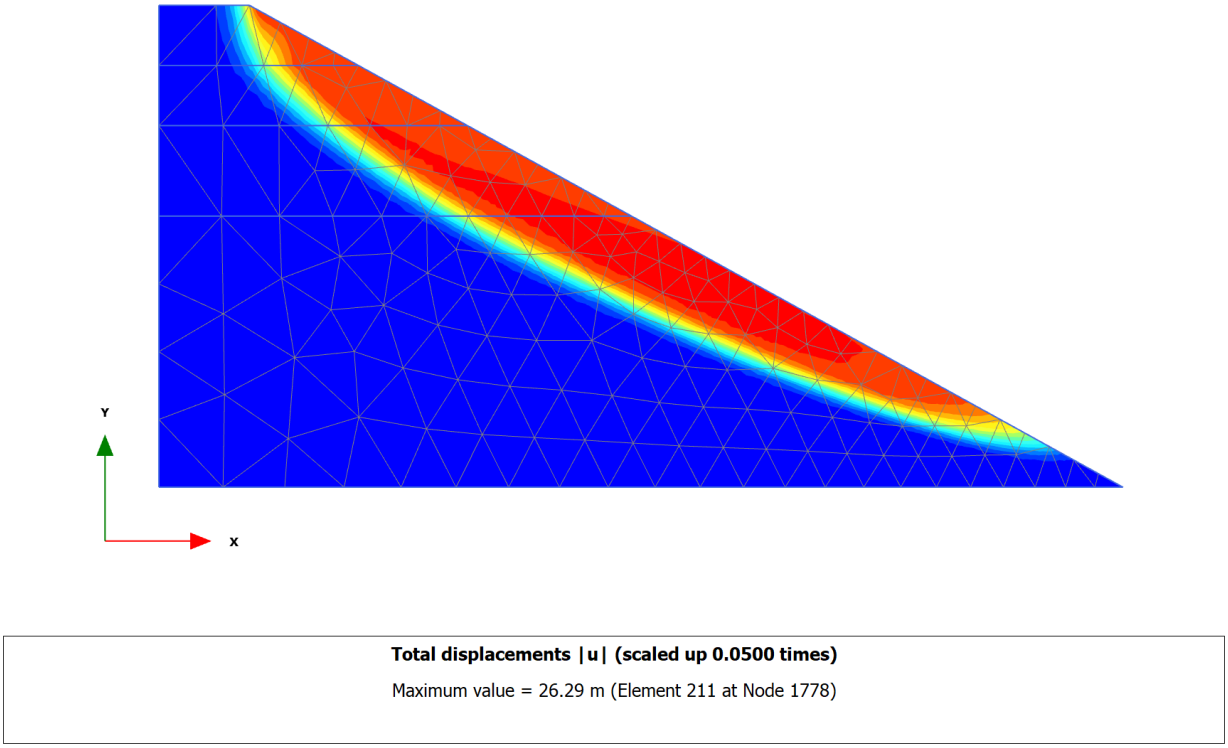

Figure 5.32 Location 01-After earthquake, Displacement-Seismic Coefficient 0.5(Phase-03)

Factor of Safety:

As before, the factor of safety remained at 1.400.

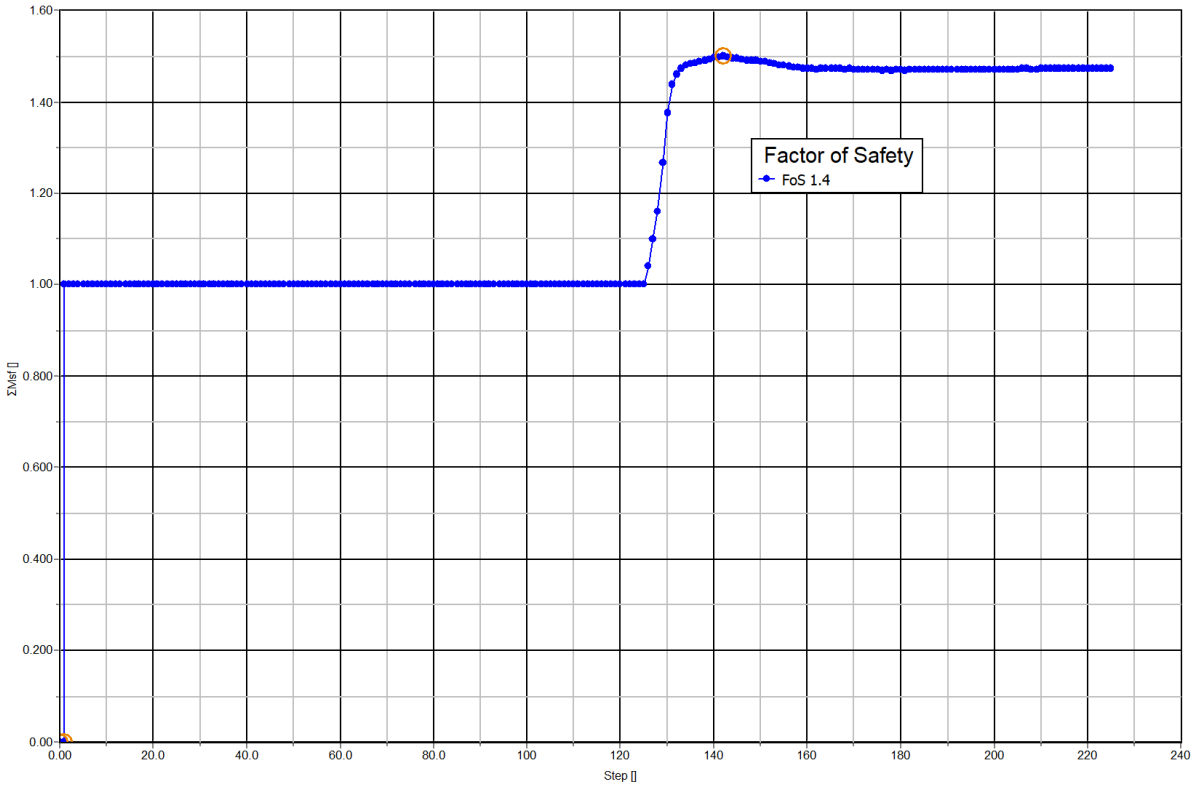

Figure 5.33 Location 01-After earthquake, Factor of Safety-Seismic Coefficient 0.5

5.2 Location 02

5.2.1 Before earthquake

Deformed Mesh:

In the before-earthquake condition at location 2, the deformed mesh displayed a maximum value of 0.02573 m at a 50.0 times scaled-up scale in phase 1. Additionally, in phase 2, at a scaled-up scale of $5.00*10^3$, the maximum deformed mesh value reached 212.0 m.

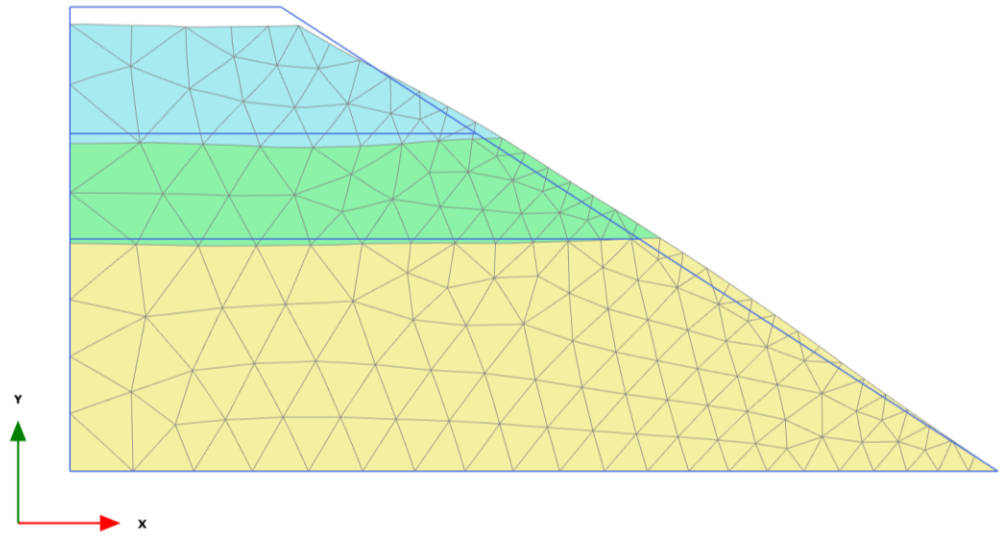

Deformed mesh |u| (scaled up 50.0 times)

Maximum value = 0.02573 m (Element 21 at Node 2080)

Figure 5.34 Location 02-Before earthquake, Deformed Mesh (Phase-01)

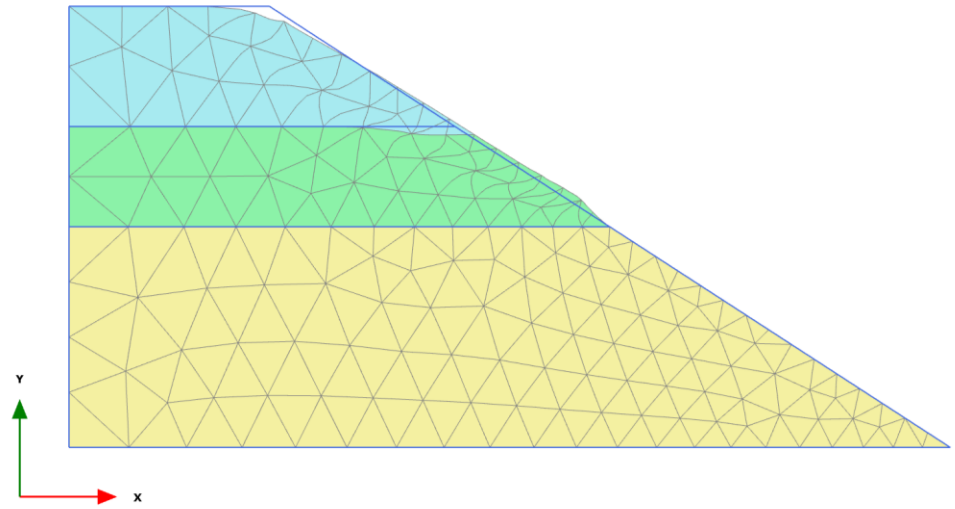

Deformed mesh |u| (scaled up 5.00*10^{-3} times)

Maximum value = 212.0 m (Element 88 at Node 1025)

Figure 5.35 Location 02-Before earthquake, Deformed Mesh (Phase-02)

Displacement:

Regarding total displacement, the highest value recorded was 0.02573 m at a 50.0 times scaled-up scale in phase 01. Furthermore, in phase 02, at a scaled-up scale of $5.00*10^{-3}$, the maximum total displacement measured 212.0 m.

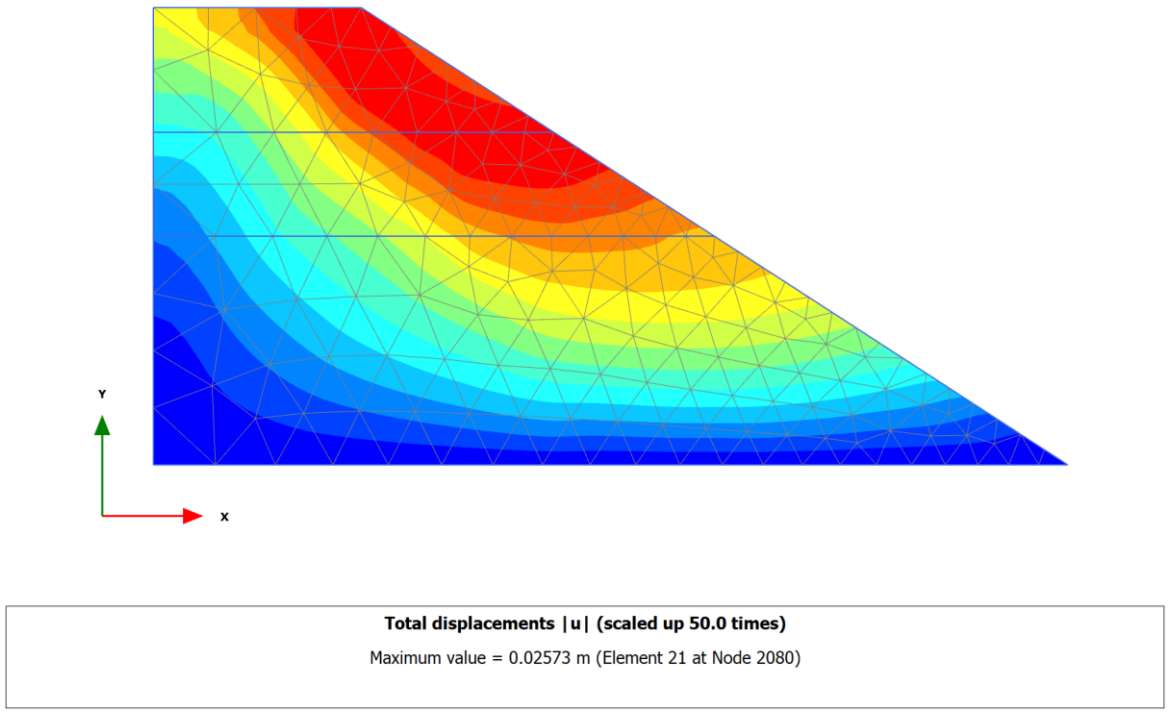

Figure 5.36 Location 02-Before earthquake, Displacement (Phase-01)

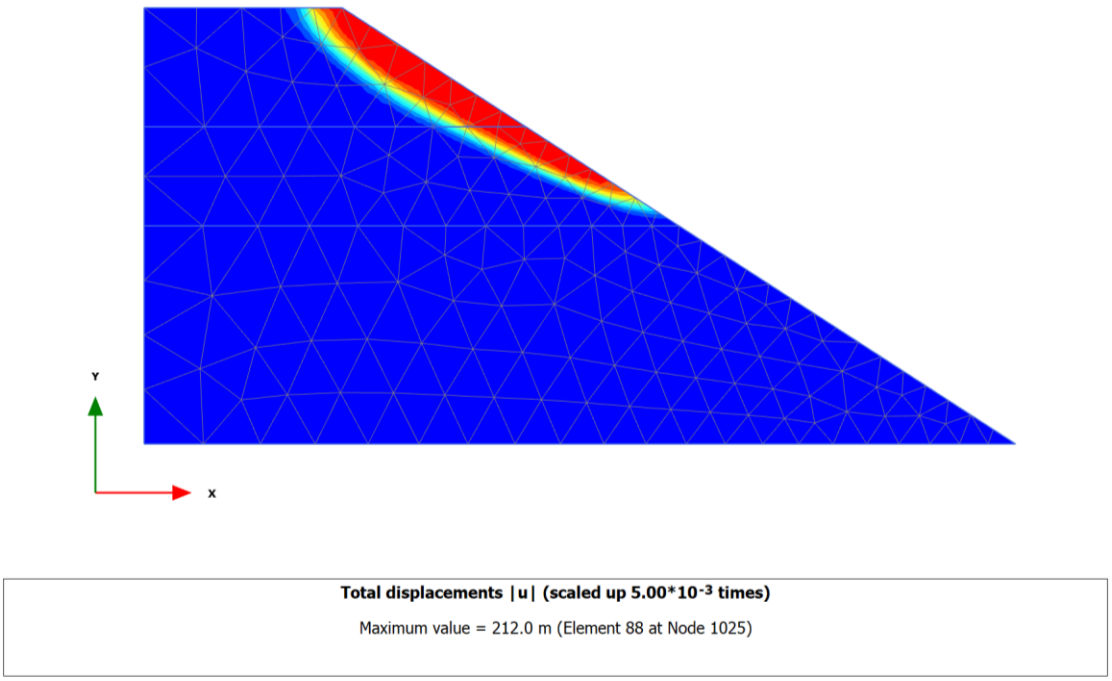

Figure 5.37 Location 02-Before earthquake, Displacement (Phase-02)

Factor of Safety:

Throughout these assessments, the factor of safety remained at 1.289.

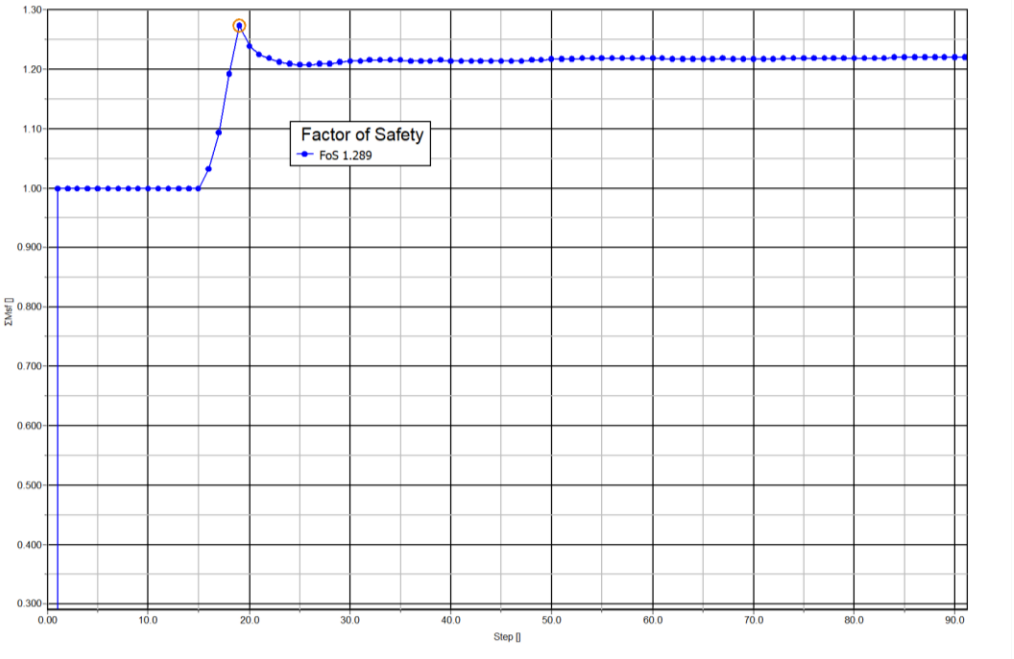

Figure 5.38 Location 02-Before earthquake, Factor of Safety

5.2.2 After Earthquake

5.2.2.1 Seismic Coefficient 0.1

Deformed Mesh:

In the after-earthquake condition of location 2, seismic coefficient 0.1 was employed to analyze the effects. At a 5.0 times scaled-up scale, the maximum deformed mesh values were determined. In phase 01, the maximum deformed mesh value recorded was 0.5659 m, while in phase 02, at a 50 times scaled-up scale, it reached 0.02573 m.

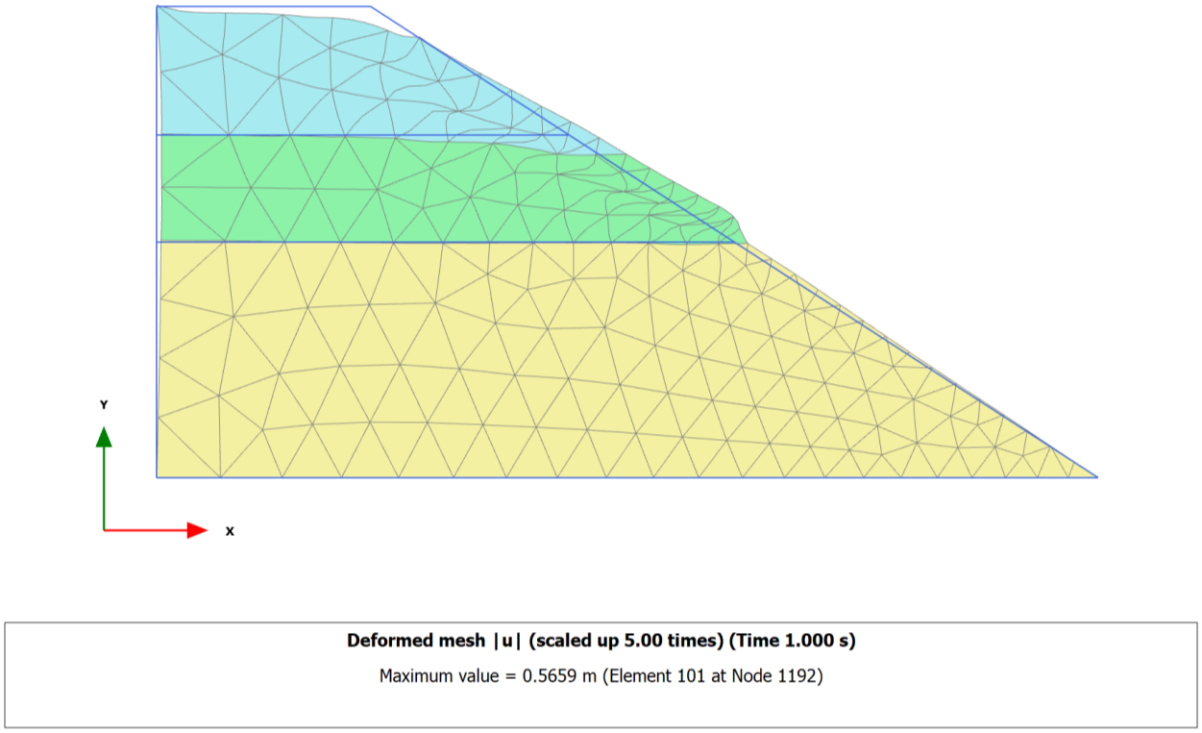

Figure 5.39 Location 02-After earthquake, Deformed Mesh-Seismic Coefficient 0.1 (Phase-01)

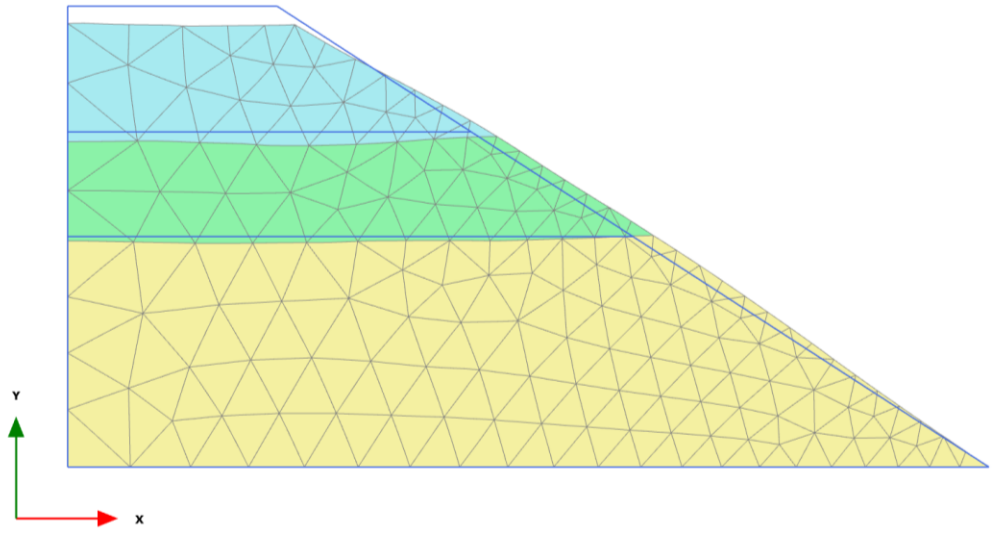

Deformed mesh |u| (scaled up 50.0 times)

Maximum value = 0.02573 m (Element 21 at Node 2080)

Figure 5.40 Location 02-After earthquake, Deformed Mesh-Seismic Coefficient 0.1 (Phase-02)

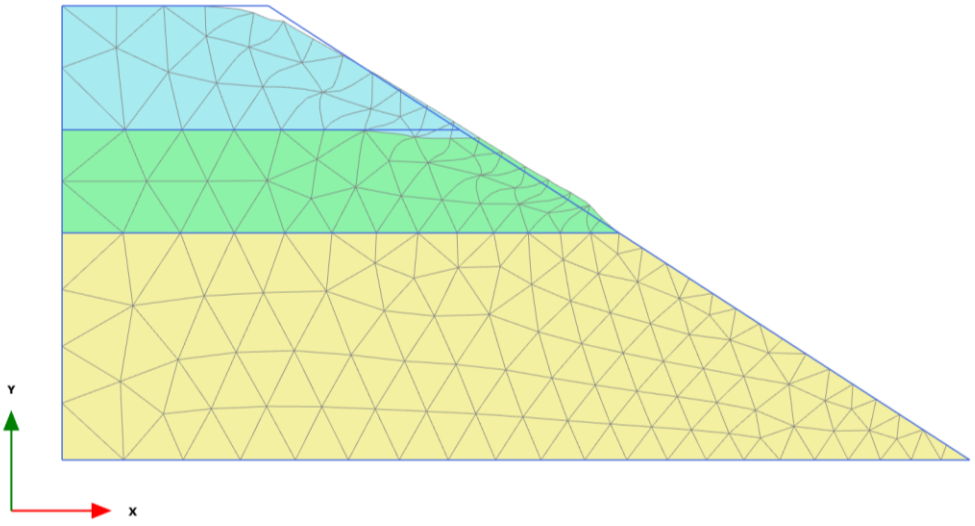

Deformed mesh |u| (scaled up 5.00*10^{-3} times)

Maximum value = 212.0 m (Element 88 at Node 1025)

Figure 5.41 Location 02-After earthquake, Deformed Mesh-Seismic Coefficient 0.1 (Phase-03)

Displacement:

Furthermore, in phase 03, at a scaled-up scale of $5.00*10^{-3}$, the maximum deformed mesh value measured 212.0 m. Considering total displacements, at a 5.0 times scaled-up scale in phase 01, the maximum value obtained was 0.5659 m. In phase 02, at a 50 times scaled-up scale, the maximum total displacement measured 0.02573 m. Similarly, in phase 03, at a scaled-up scale of $5.00*10^{-3}$, the maximum total displacement reached 212.0 m.

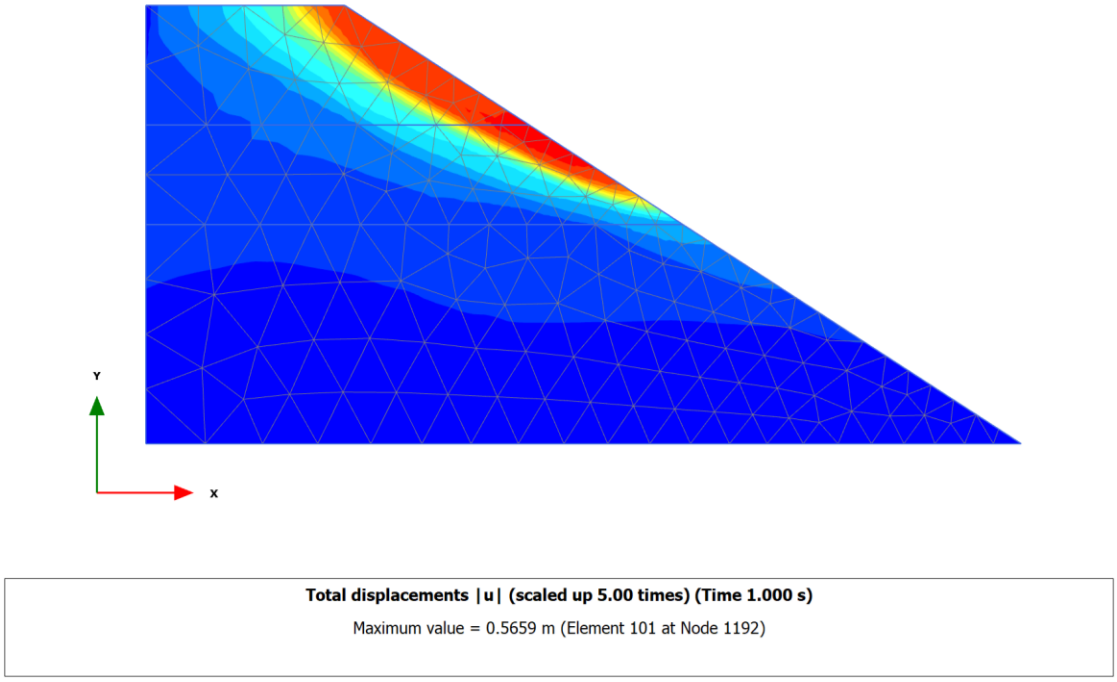

Figure 5.42 Location 02-After earthquake, Displacement-Seismic Coefficient 0.1 (Phase-01)

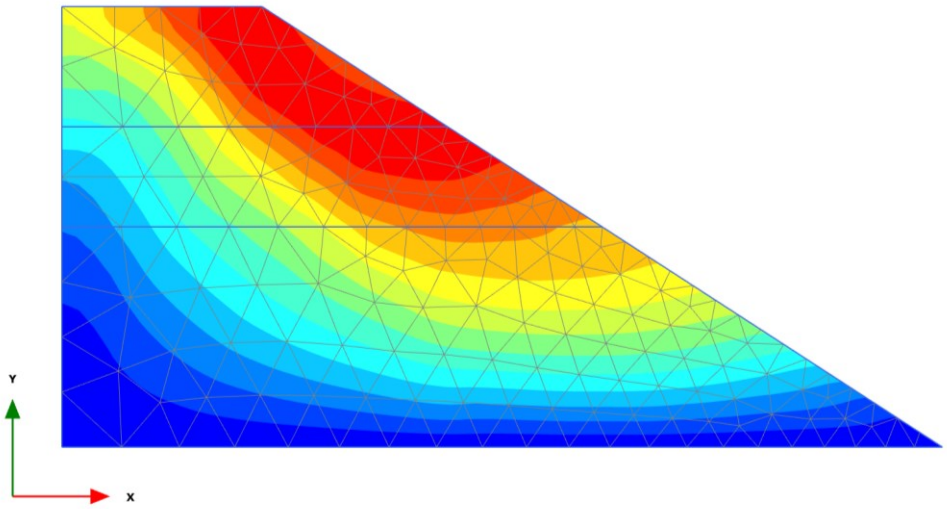

Total displacements |u| (scaled up 50.0 times)

Maximum value = 0.02573 m (Element 21 at Node 2080)

Figure 5.43 Location 02-After earthquake, Displacement-Seismic Coefficient 0.1 (Phase-02)

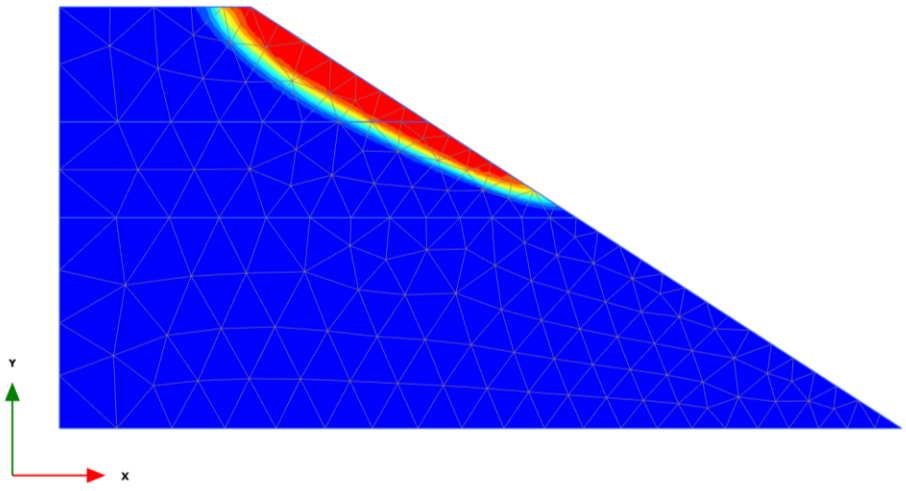

Total displacements |u| (scaled up 5.00*10^{-3} times)

Maximum value = 212.0 m (Element 88 at Node 1025)

Figure 5.44 Location 02-After earthquake, Displacement-Seismic Coefficient 0.1 (Phase-03)

Factor of Safety:

The factor of safety remained at 1.270 throughout these evaluations.

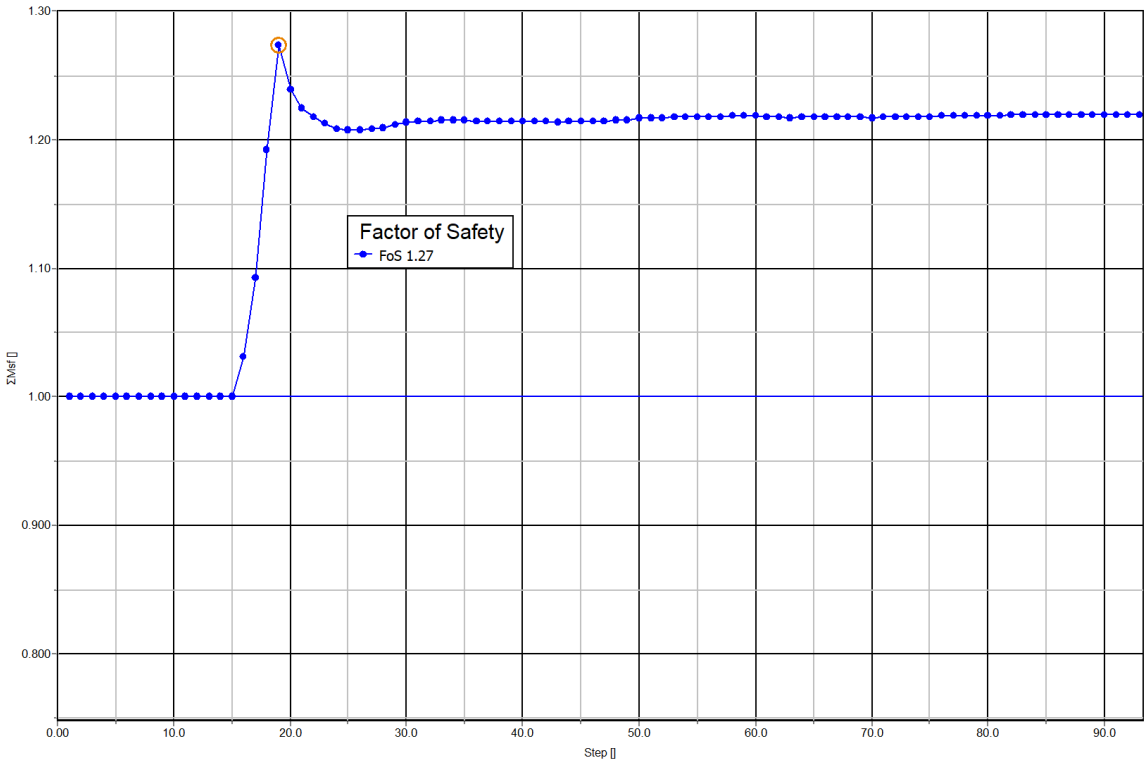

Figure 5.45Location 02-After earthquake, Factor of Safety-Coefficient 0.1

5.2.2.2 Seismic Coefficient 0.28

Deformed Mesh:

Similarly, in the after-earthquake condition of location 2, with a seismic coefficient of 0.28, the maximum deformed mesh values were assessed. At a 0.500 times scaled-up scale, the maximum deformed mesh value in phase 01 was determined as 1.482 m, while in phase 02, at a 5.0 times scaled-up scale, it reached 1.455 m. Furthermore, in phase 03, at a scaled-up scale of $5.00*10^{-3}$, the maximum deformed mesh value measured 160.7 m.

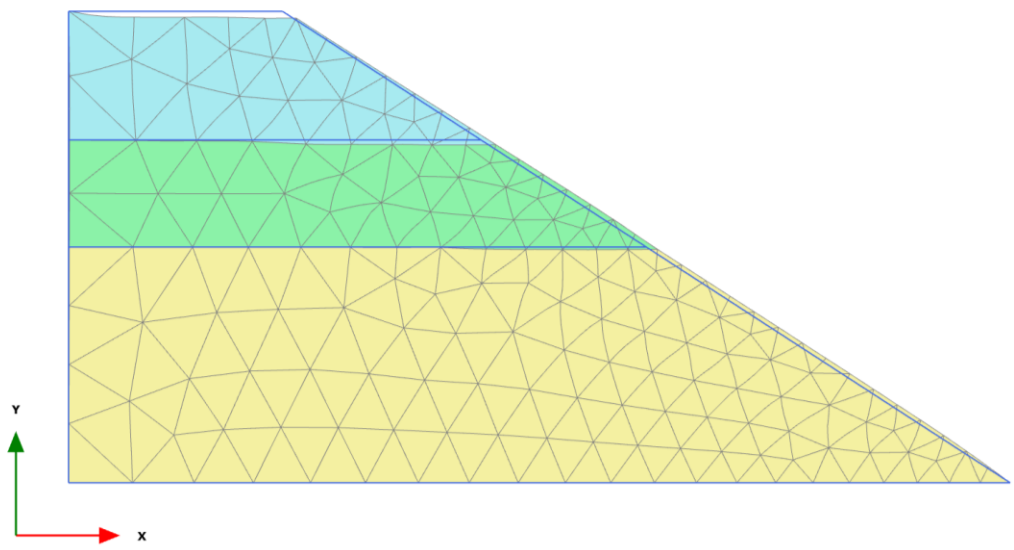

Deformed mesh |u| (scaled up 0.500 times) (Time 1.000 s)

Maximum value = 1.482 m (Element 101 at Node 1184)

Figure 5.46 Location 02-After earthquake, Deformed Mesh-Seismic Coefficient 0.28 (Phase-01)

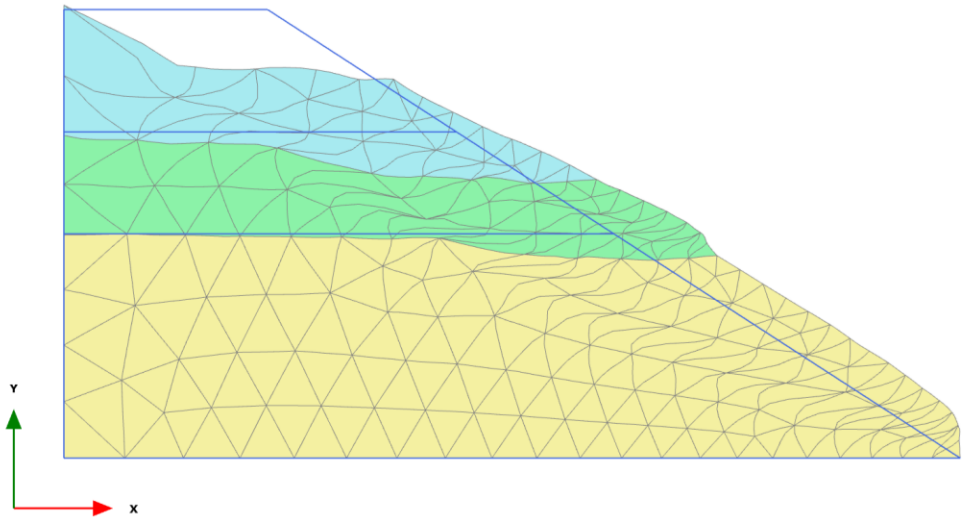

Deformed mesh |u| (scaled up 5.00 times)

Maximum value = 1.455 m (Element 86 at Node 1321)

Figure 5.47 Location 02-After earthquake, Deformed Mesh-Seismic Coefficient 0.28 (Phase-02)

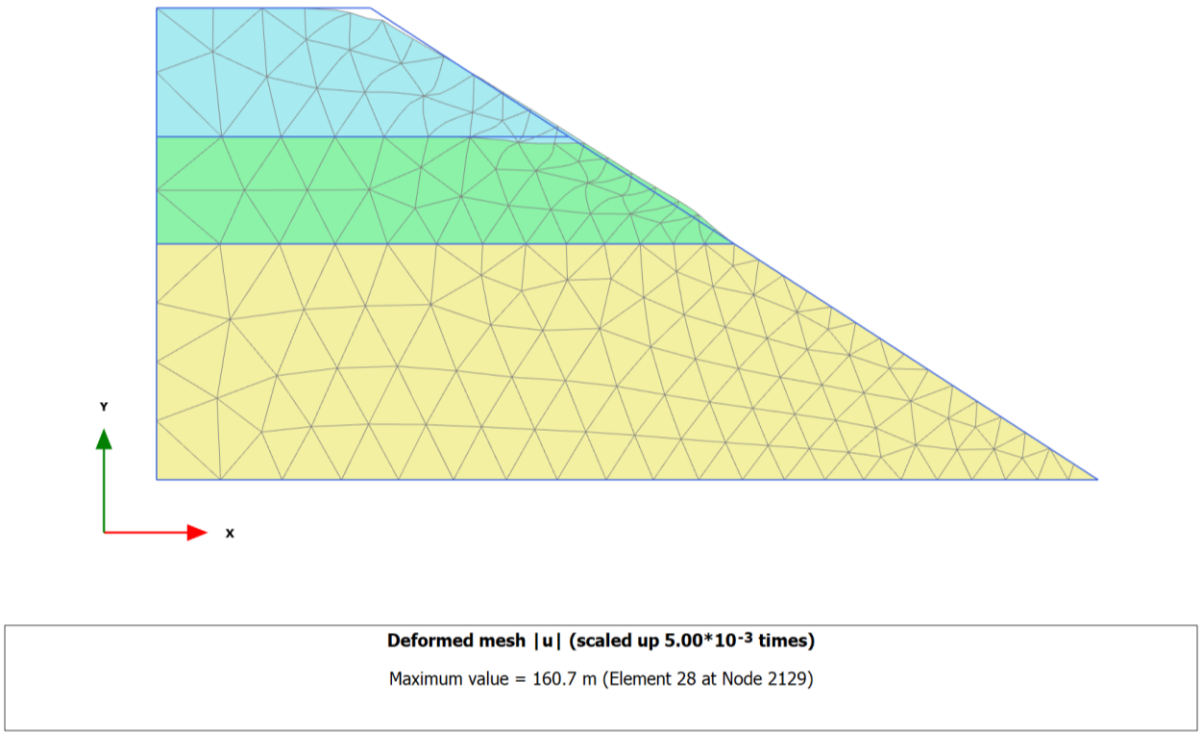

Figure 5.48 Location 02-After earthquake, Deformed Mesh-Seismic Coefficient 0.28 (Phase-03)

Displacement:

Examining the total displacements, at a 0.500 times scaled-up scale in phase 01, the maximum value obtained was 1.482 m. In phase 02, at a 5.0 times scaled-up scale, the maximum total displacement measured 1.455 m. Similarly, in phase 03, at a scaled-up scale of $5.00*10^{-3}$, the maximum total displacement reached 160.7 m.

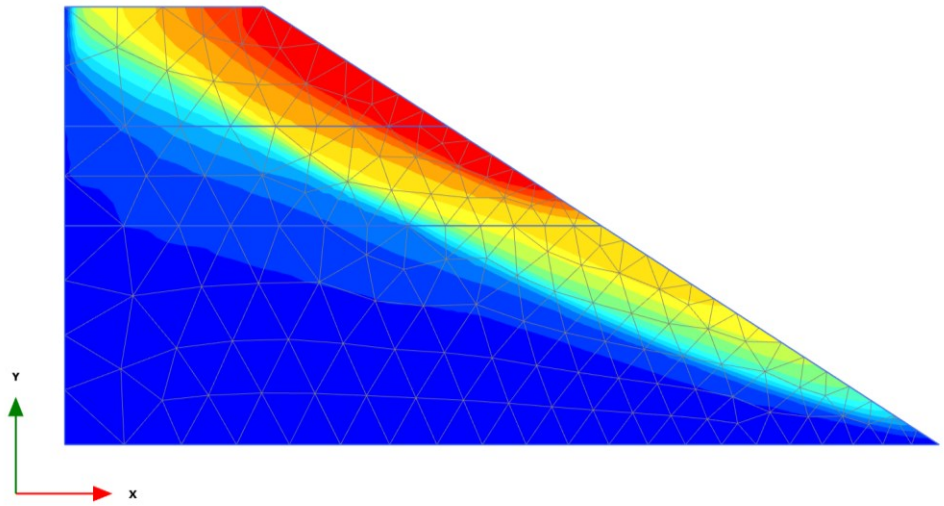

Total displacements |u| (scaled up 0.500 times) (Time 1.000 s)

Maximum value = 1.482 m (Element 101 at Node 1184)

Figure 5.49 Location 02-After earthquake, Displacement-Seismic Coefficient 0.28 (Phase-01)

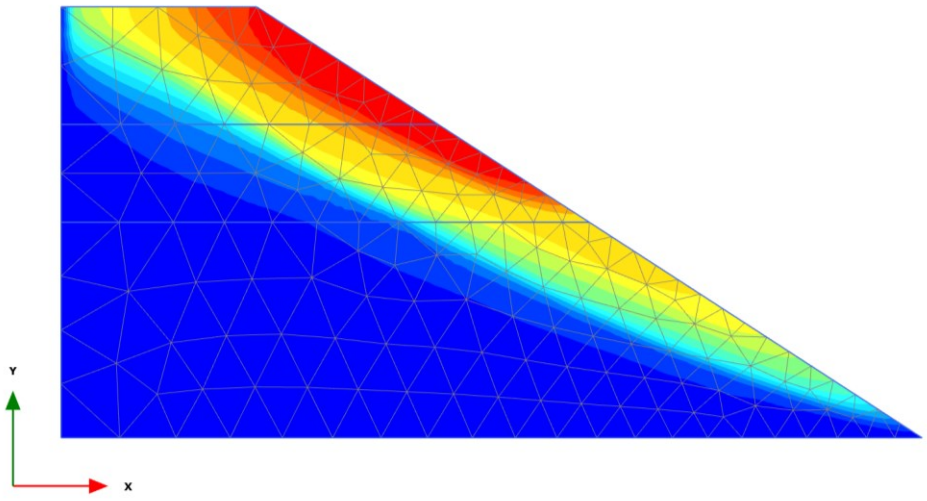

Total displacements |u| (scaled up 5.00 times)

Maximum value = 1.455 m (Element 86 at Node 1321)

Figure 5.50 Location 02-After earthquake, Displacement-Seismic Coefficient 0.28 (Phase-02)

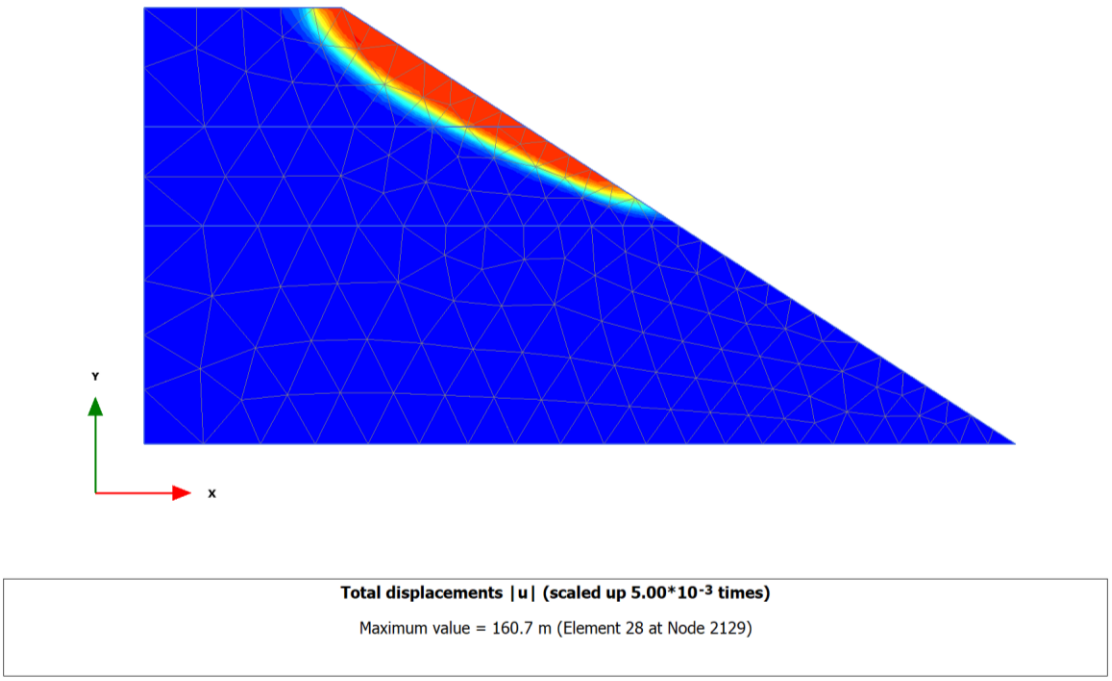

Figure 5.51 Location 02-After earthquake, Displacement-Seismic Coefficient 0.28 (Phase-03)

Factor of Safety:

The factor of safety remained at 1.261 during these analyses.

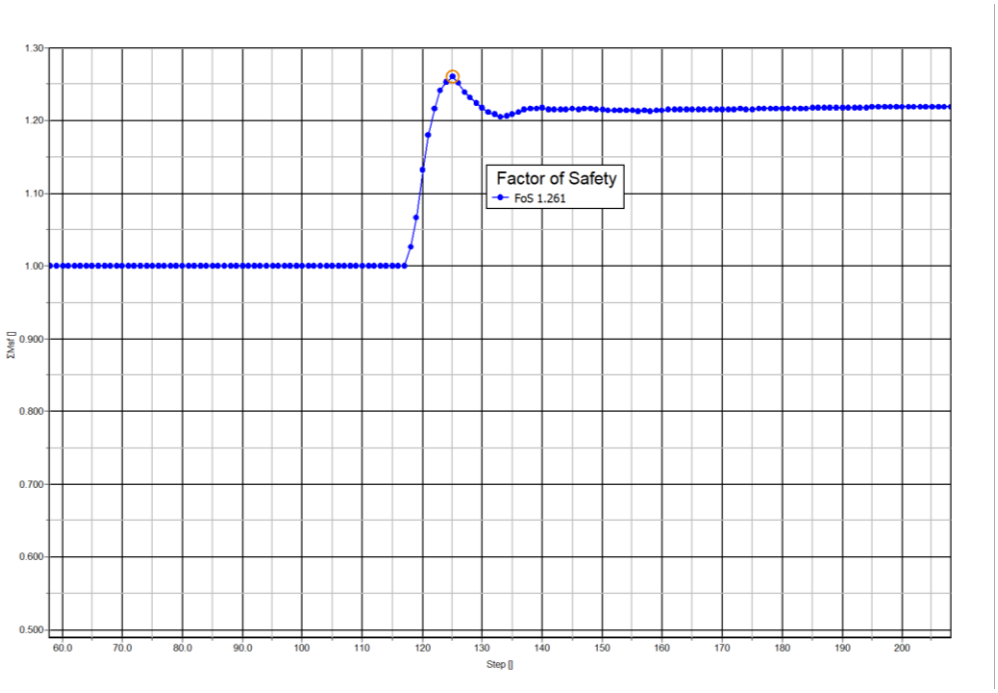

Figure 5.52 Location 02-After earthquake, Factor of Safety-Seismic Coefficient 0.28

5.2.2.3 Seismic Coefficient 0.3

Deformed Mesh:

Moreover, in the after-earthquake condition of location 2, utilizing a seismic coefficient of 0.3, the maximum deformed mesh values were examined. At a 0.500 times scaled-up scale, in phase 01, the maximum deformed mesh value measured 1.584 m. In phase 02, at a 50.0 times scaled-up scale, the maximum deformed mesh value recorded was 0.02573 m. Additionally, in phase 03, at a scaled-up scale of $5.00*10^{-3}$, the maximum deformed mesh value reached 212.0 m.

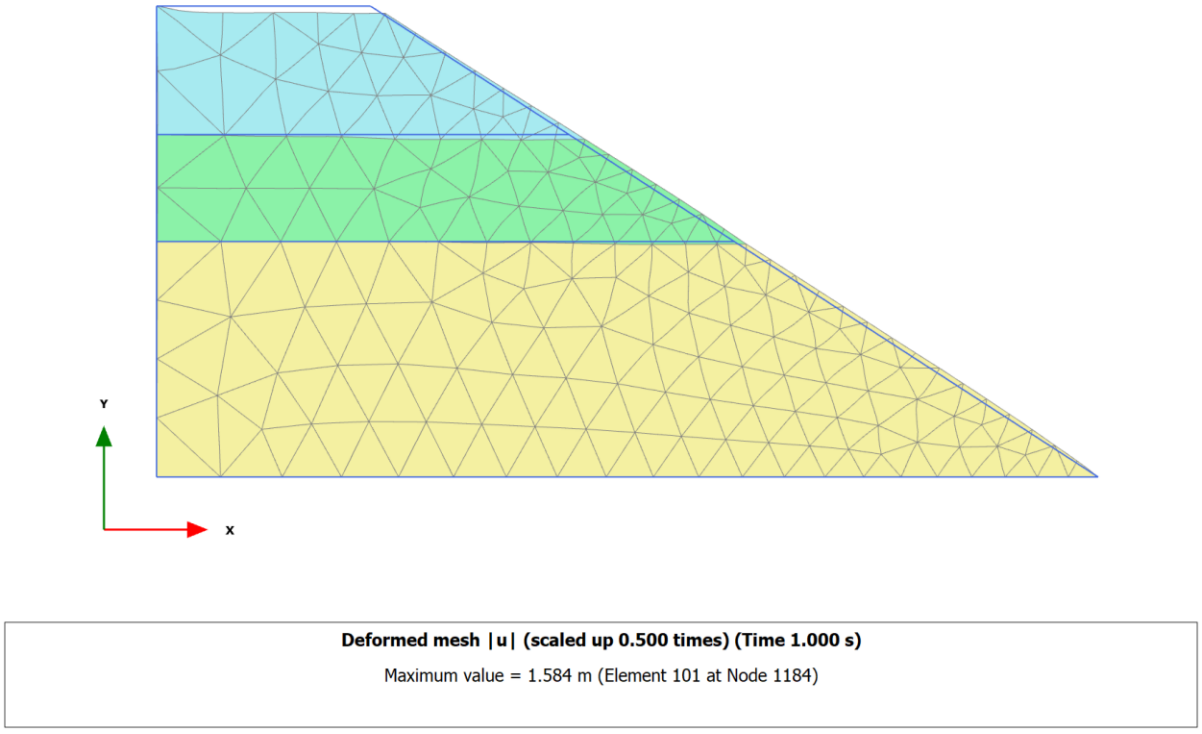

Figure 5.53 Location 02-After earthquake, Deformed Mesh-Seismic Coefficient 0.3 (Phase-01)

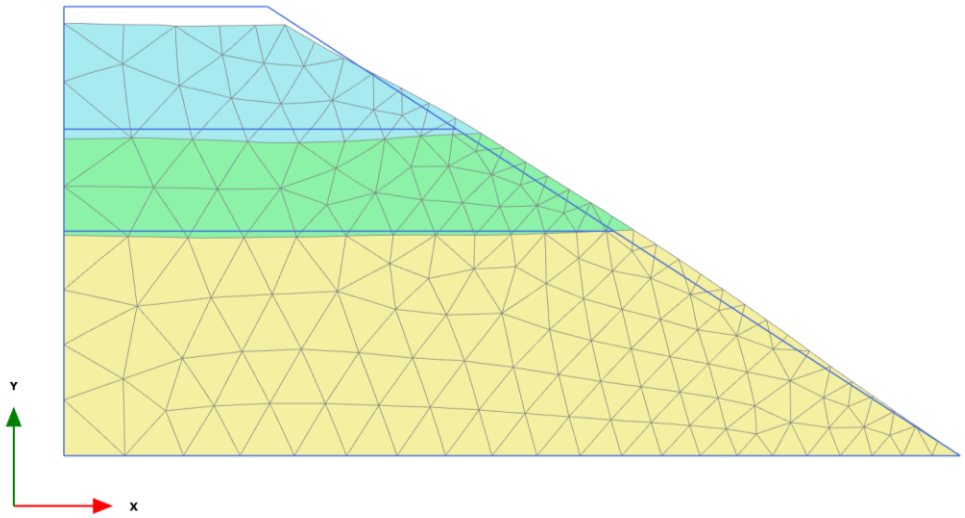

Figure 5.54 Location 02-After earthquake, Deformed Mesh-Seismic Coefficient 0.3 (Phase-02)

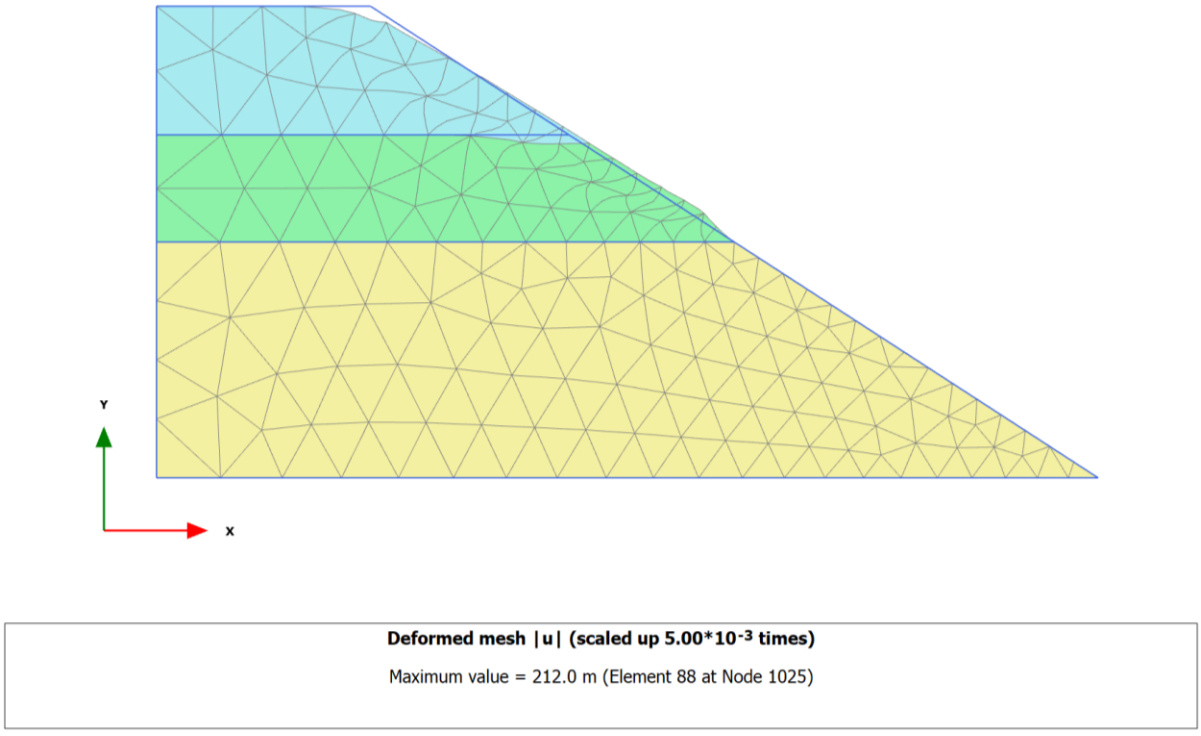

Figure 5.55 Location 02-After earthquake, Deformed Mesh-Seismic Coefficient 0.3 (Phase-03)

Displacement:

Evaluating the total displacements, in phase 01, at a 0.500 times scaled-up scale, the maximum value obtained was 1.584 m. In phase 02, at a 50.0 times scaled-up scale, the maximum total displacement measured 0.02573 m. Similarly, in phase 03, at a scaled-up scale of $5.00*10^{-3}$, the maximum total displacement reached 212.0 m.

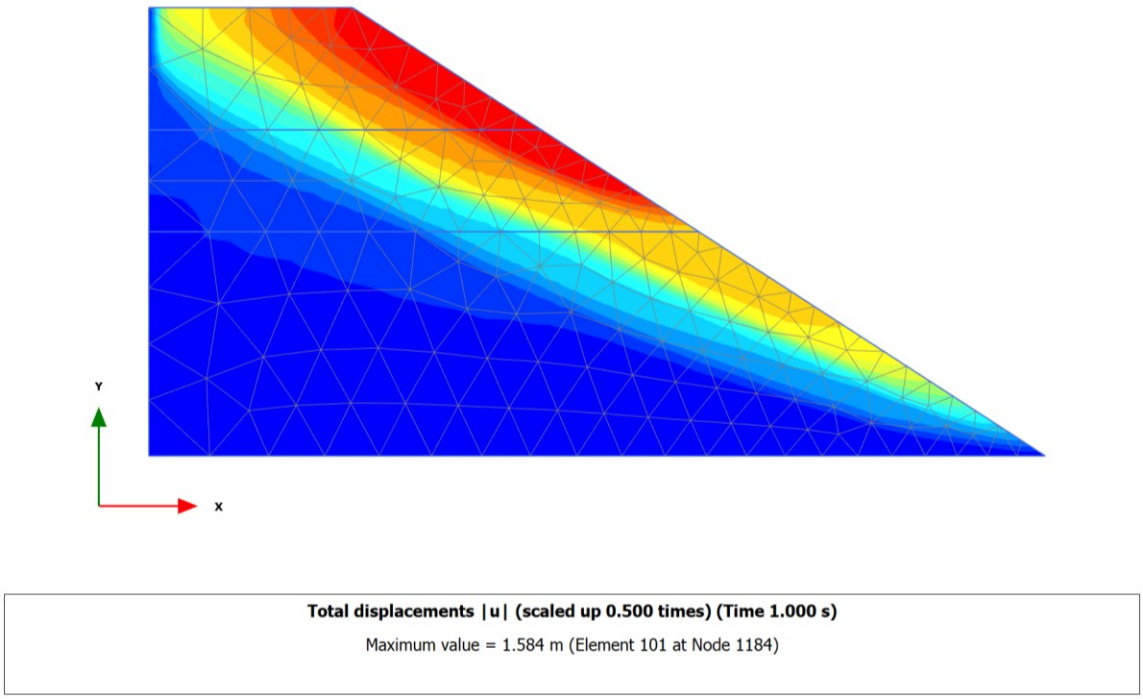

Figure 5.56 Location 02-After earthquake, Displacement-Seismic Coefficient 0.3 (Phase-01)

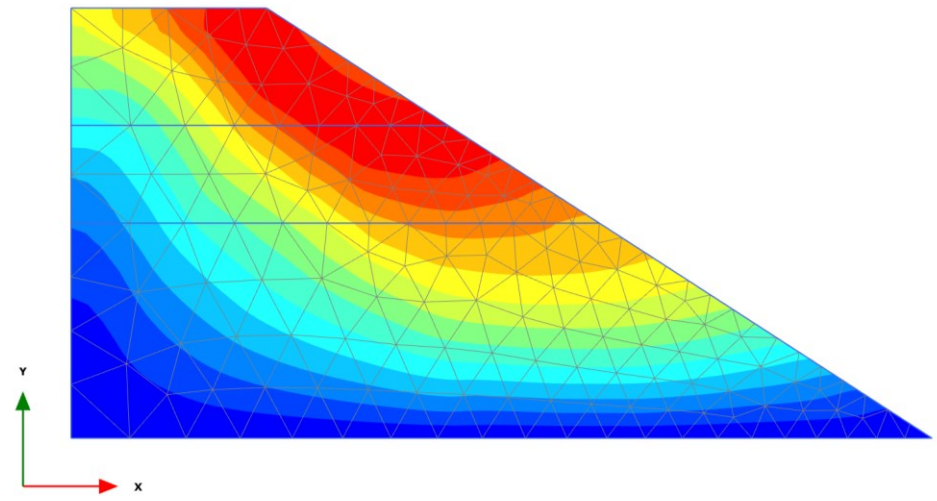

Total displacements |u| (scaled up 50.0 times)

Maximum value = 0.02573 m (Element 21 at Node 2080)

Figure 5.57 Location 02-After earthquake, Displacement-Seismic Coefficient 0.3 (Phase-02)

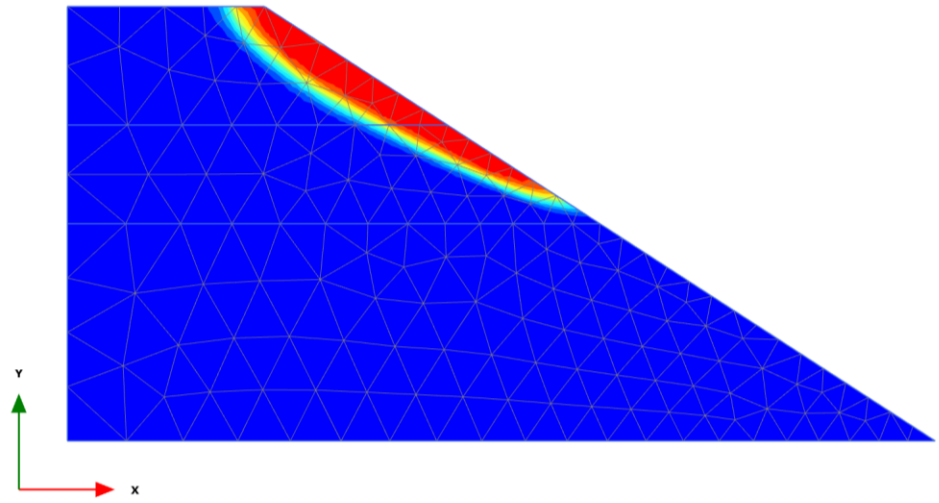

Total displacements |u| (scaled up 5.00*10^{-3} times)

Maximum value = 212.0 m (Element 88 at Node 1025)

Figure 5.58 Location 02-After earthquake, Displacement-Seismic Coefficient 0.3 (Phase-03)

Factor of Safety:

The factor of safety remained at 1.258 throughout these evaluations.

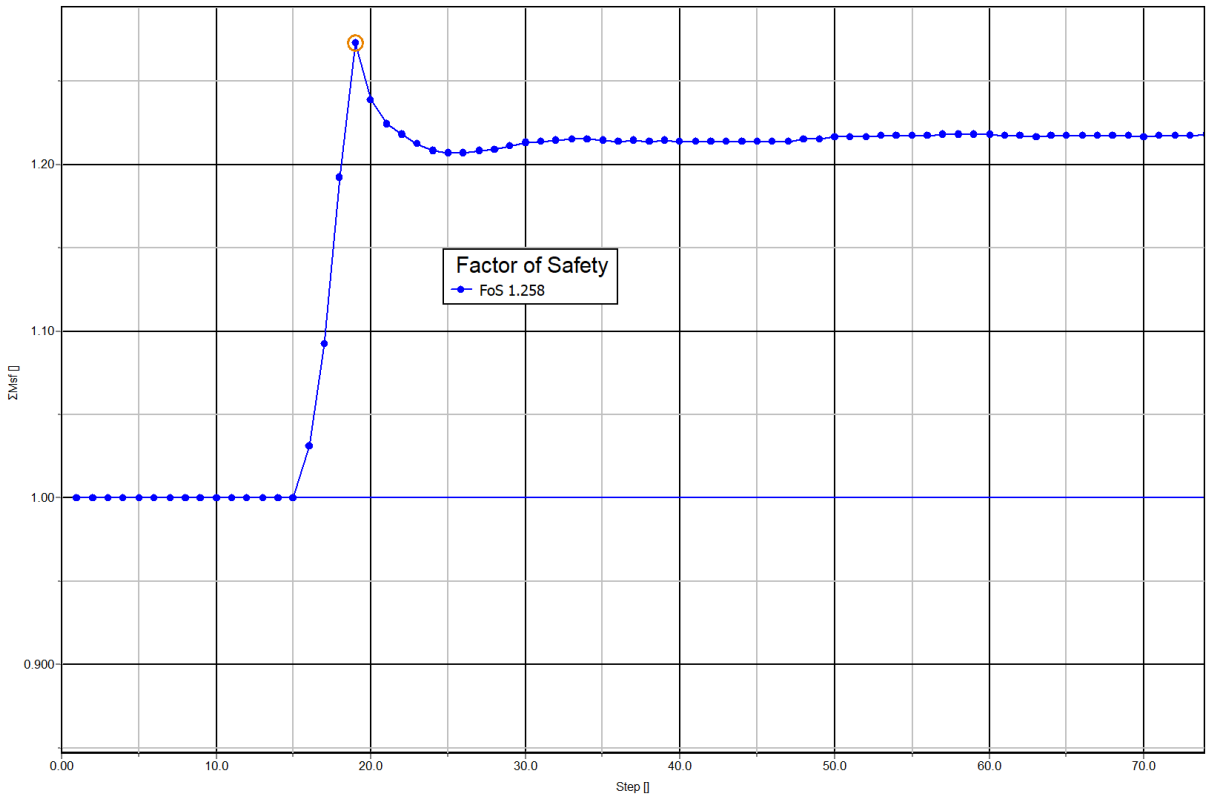

Figure 5.59 Location 02-After earthquake, Factor of Safety-Seismic Coefficient 0.3

5.2.2.4 Seismic Coefficient 0.5

Deformed Mesh:

Lastly, in the after-earthquake condition of location 2, with a seismic coefficient of 0.5, the maximum deformed mesh values were determined. At a 0.500 times scaled-up scale, in phase 01, the maximum deformed mesh value measured 2.708 m. In phase 02, at a 50.0 times scaled-up scale, the maximum deformed mesh value reached 0.02573 m. Additionally, in phase 03, at a scaled-up scale of $5.00*10^{-3}$, the maximum deformed mesh value recorded was 212.0 m.

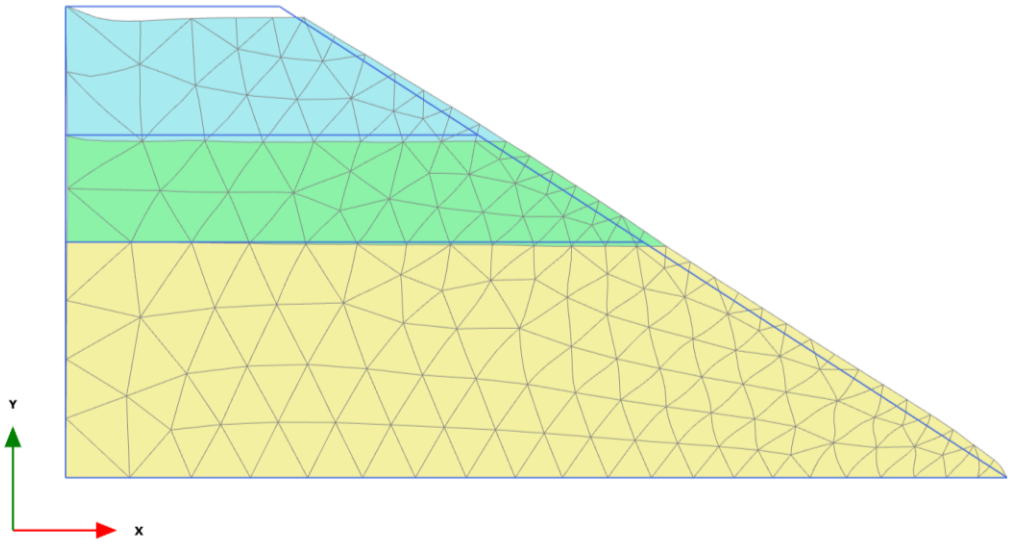

Deformed mesh |u| (scaled up 0.500 times) (Time 1.000 s)

Maximum value = 2.708 m (Element 98 at Node 1183)

Figure 5.60 Location 02-After earthquake, Deformed Mesh-Seismic Coefficient 0.5 (Phase-01)

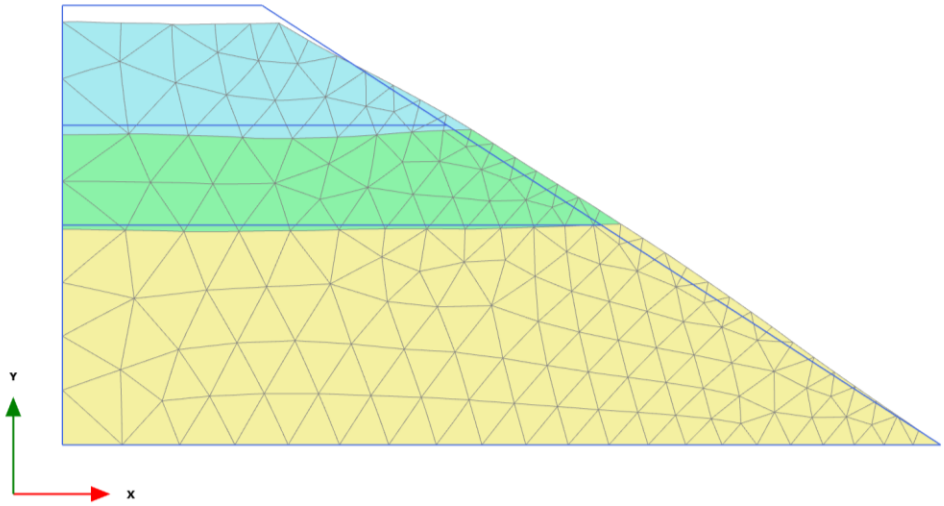

Deformed mesh |u| (scaled up 50.0 times)

Maximum value = 0.02573 m (Element 21 at Node 2080)

Figure 5.61 Location 02-After earthquake, Deformed Mesh-Seismic Coefficient 0.5 (Phase-02)

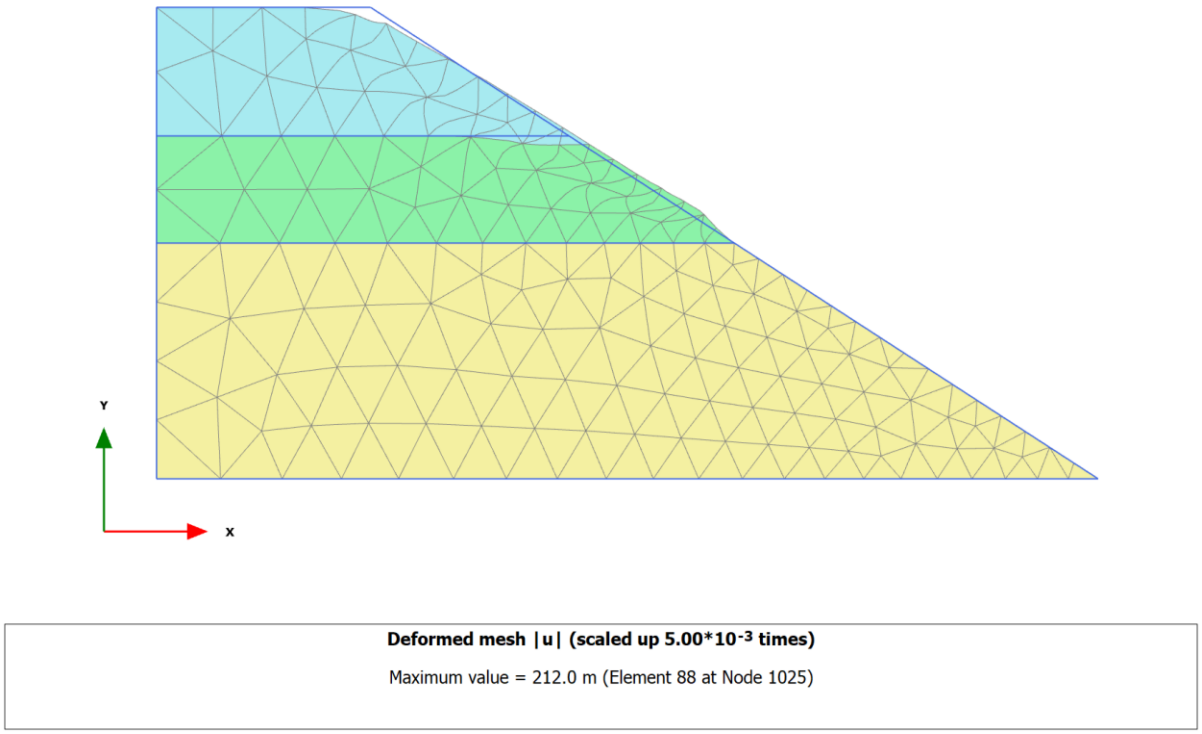

Figure 5.62 Location 02-After earthquake, Deformed Mesh-Seismic Coefficient 0.5 (Phase-03)

Displacement:

Assessing the total displacements, in phase 01, at a 0.500 times scaled-up scale, the maximum value obtained was 2.708 m. In phase 02, at a 50.0 times scaled-up scale, the maximum total displacement measured 0.02573 m. Similarly, in phase 03, at a scaled-up scale of $5.00*10^{-3}$, the maximum total displacement reached 212.0 m.

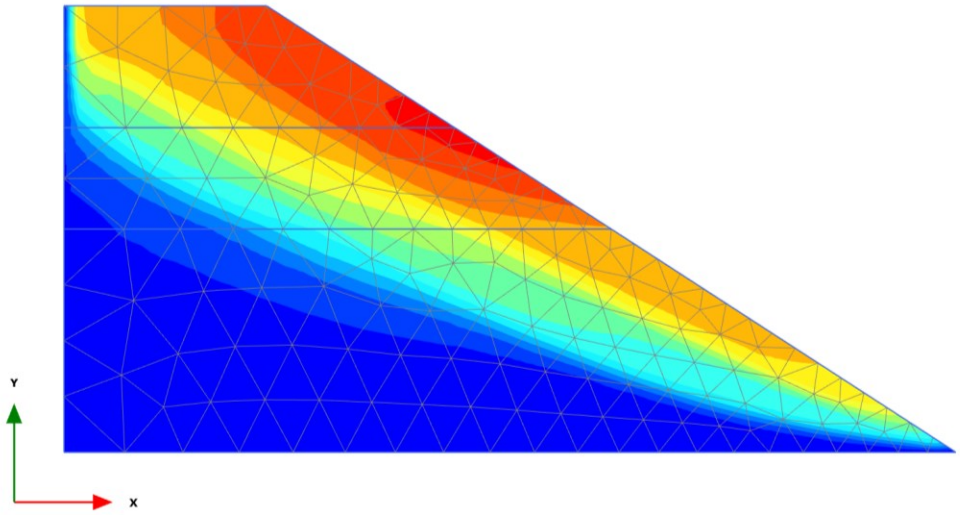

Total displacements |u| (scaled up 0.500 times) (Time 1.000 s)

Maximum value = 2.708 m (Element 98 at Node 1183)

Figure 5.63 Location 02-After earthquake, Displacement-Seismic Coefficient 0.5 (Phase-01)

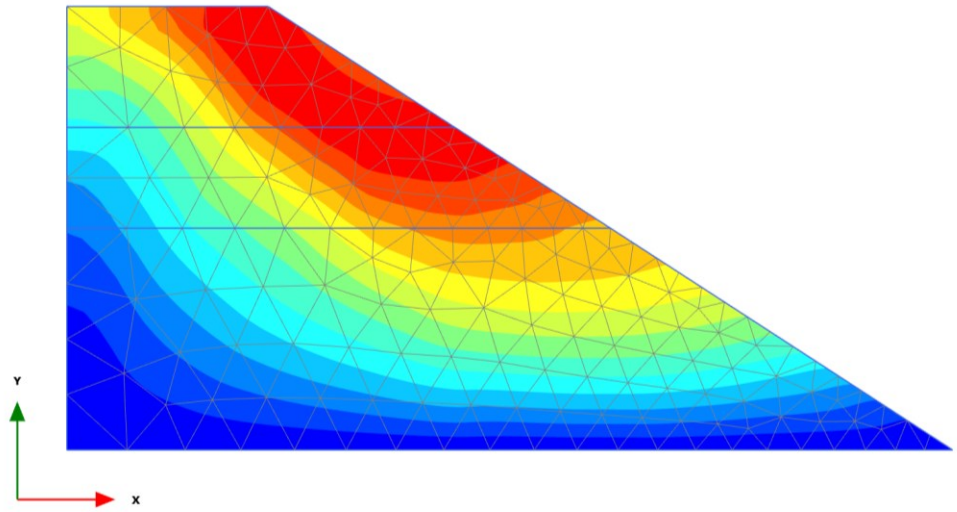

Total displacements |u| (scaled up 50.0 times)

Maximum value = 0.02573 m (Element 21 at Node 2080)

Figure 5.64 Location 02-After earthquake, Displacement-Seismic Coefficient 0.5 (Phase-02)

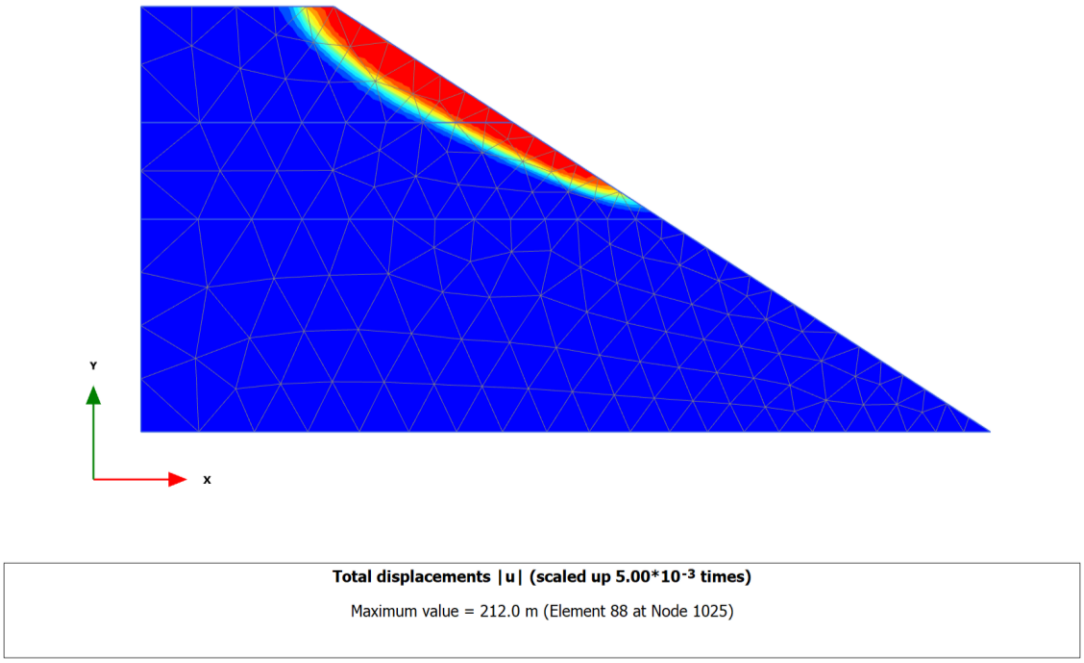

Figure 5.65 Location 02-After earthquake, Displacement-Seismic Coefficient 0.5 (Phase-03)

Factor of Safety:

The factor of safety remained at 1.242 throughout these analyses.

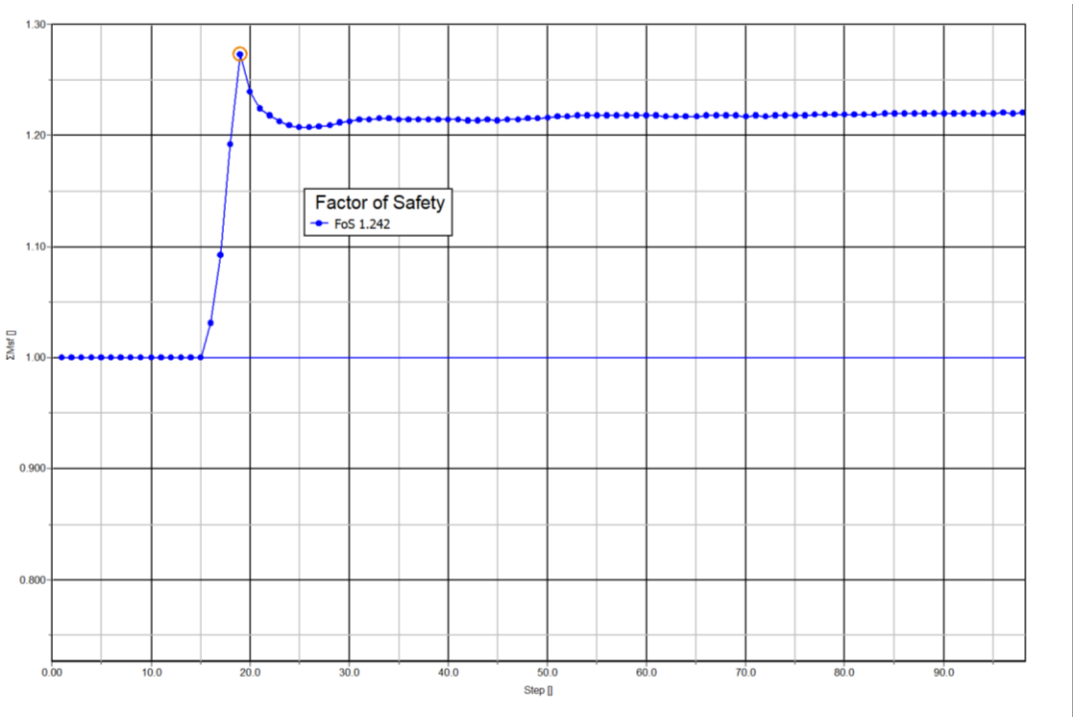

Figure 5.66 Location 02-After earthquake, Factor of Safety-Seismic Coefficient 0.5

5.3 Location 03

5.3.1 Before earthquake

Deformed Mesh:

In the before-earthquake condition at location 3, the deformed mesh analysis resulted in a maximum value of 0.01064 m at a 50.0 times scaled-up scale during phase 1. Additionally, in phase 2, at a scaled-up scale of 0.0200, the maximum deformed mesh value measured 57.50 m.

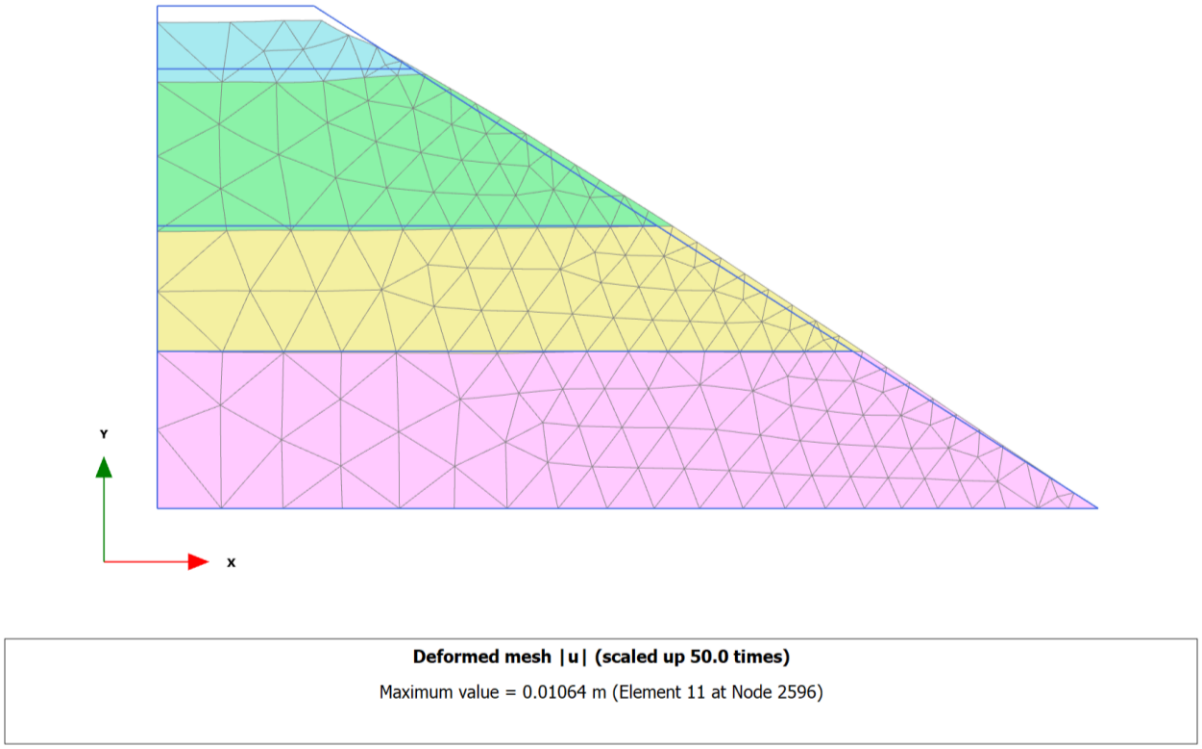

Figure 5.67 Location 03-Before earthquake, Deformed Mesh (Phase-01)

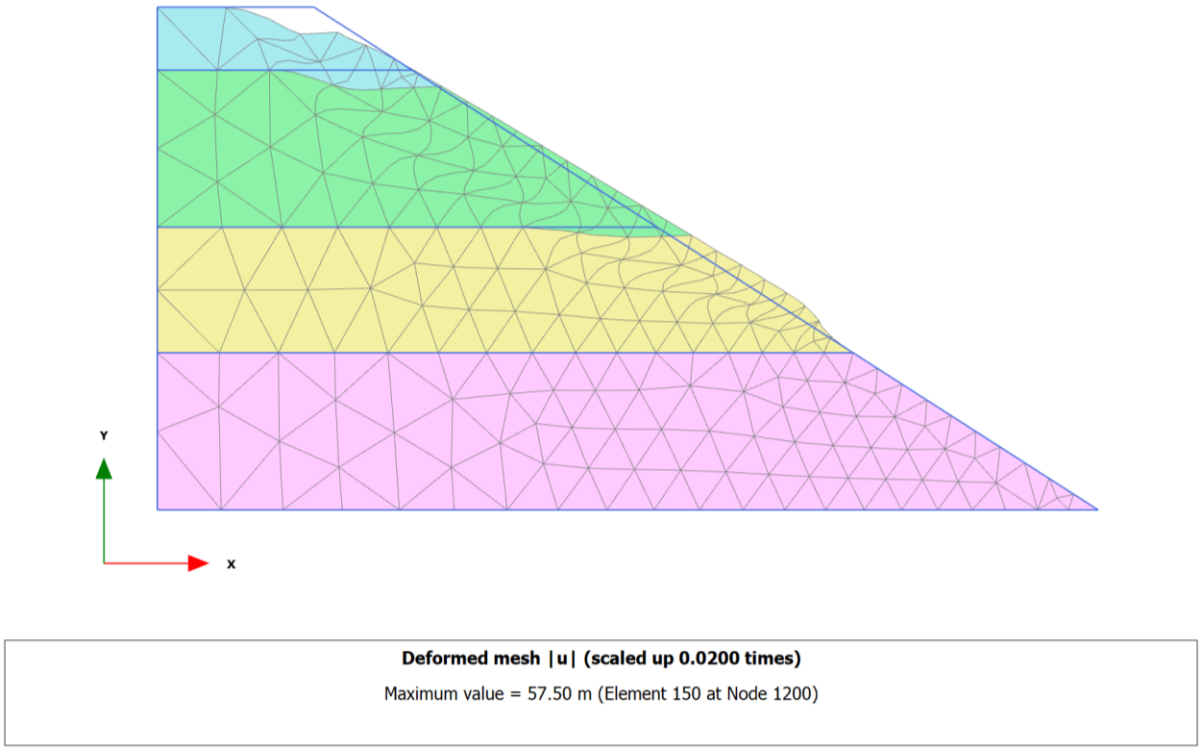

Figure 5.68 Location 03-Before earthquake, Deformed Mesh (Phase-02)

Displacement:

Assessing the total displacements, the maximum value obtained was 0.01064 m at a 50.0 times scaled-up scale in phase 01. Furthermore, in phase 02, at a scaled-up scale of 0.0200, the maximum total displacement reached 57.50 m.

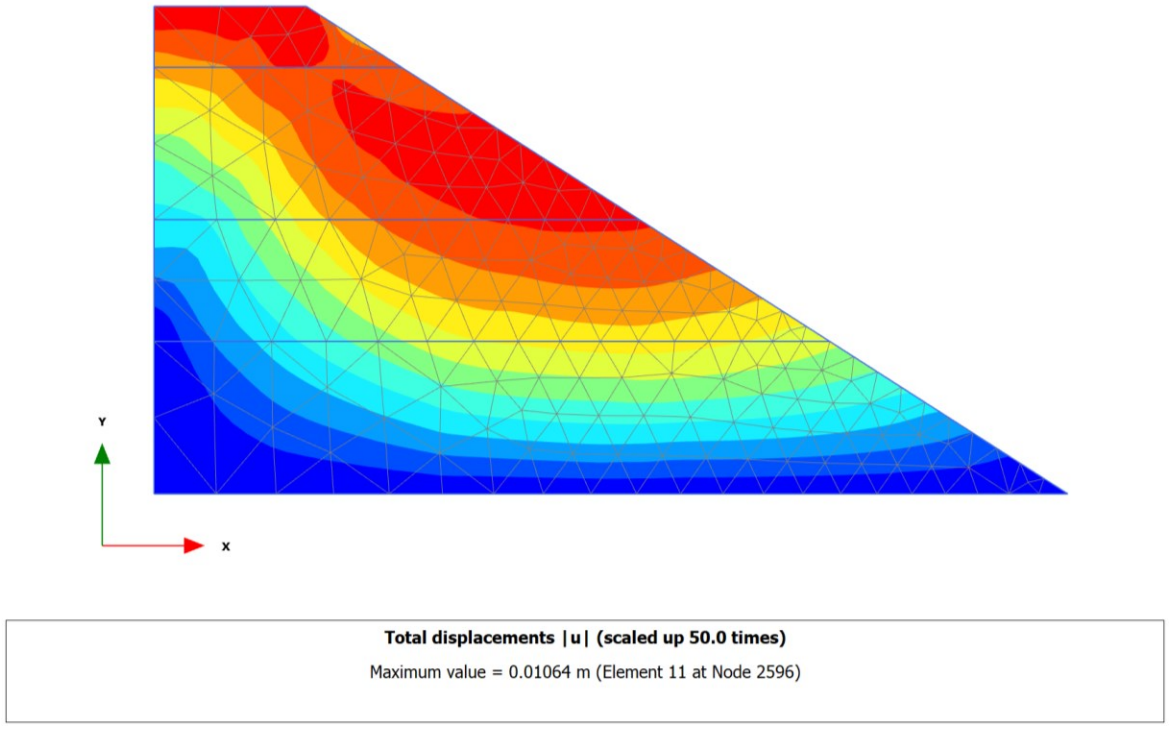

Figure 5.69 Location 03-Before earthquake, Displacement (Phase-01)

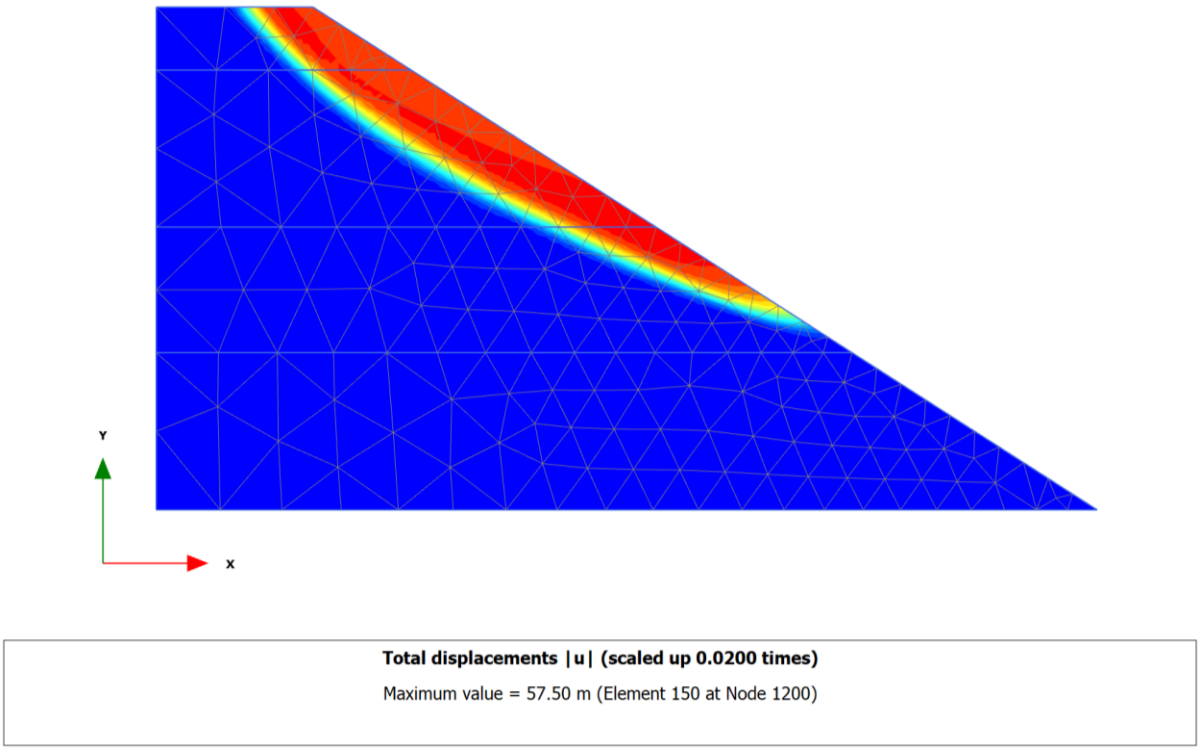

Figure 5.70 Location 03-Before earthquake, Displacement (Phase-02)

Factor of Safety:

The factor of safety remained at 1.488 throughout these evaluations.

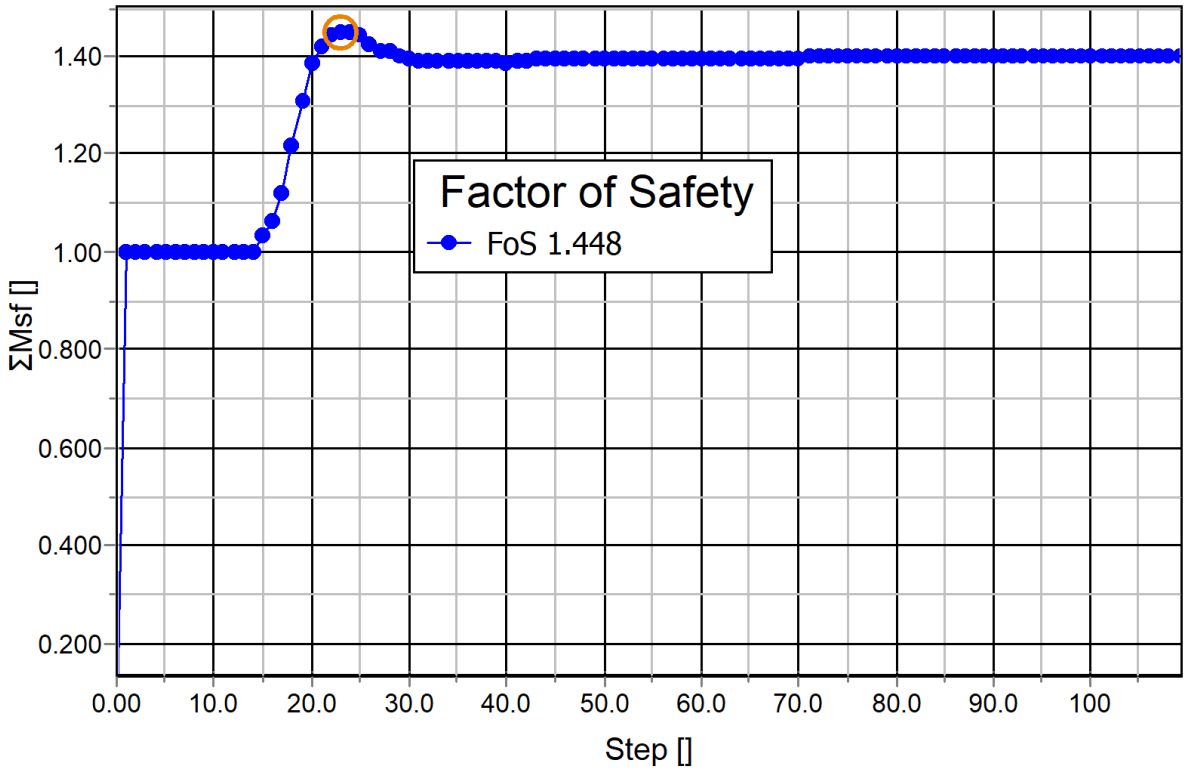

Figure 5.71 Location 03-Before earthquake, Factor of Safety

5.3.2 After Earthquake

5.3.2.1 Seismic Coefficient 0.1

Deformed Mesh:

In the after-earthquake condition of location 3, utilizing a seismic coefficient of 0.1, the analysis was performed at various scaled-up scales. At a 50.0 times scaled-up scale, in phase 01, the maximum deformed mesh value measured 0.02525 m. In phase 02, at a 50.0 times scaled-up scale, the maximum deformed mesh value reached 0.02753 m. Additionally, in phase 03, at a scaled-up scale of 5.0, the maximum deformed mesh value recorded was 0.1843 m.

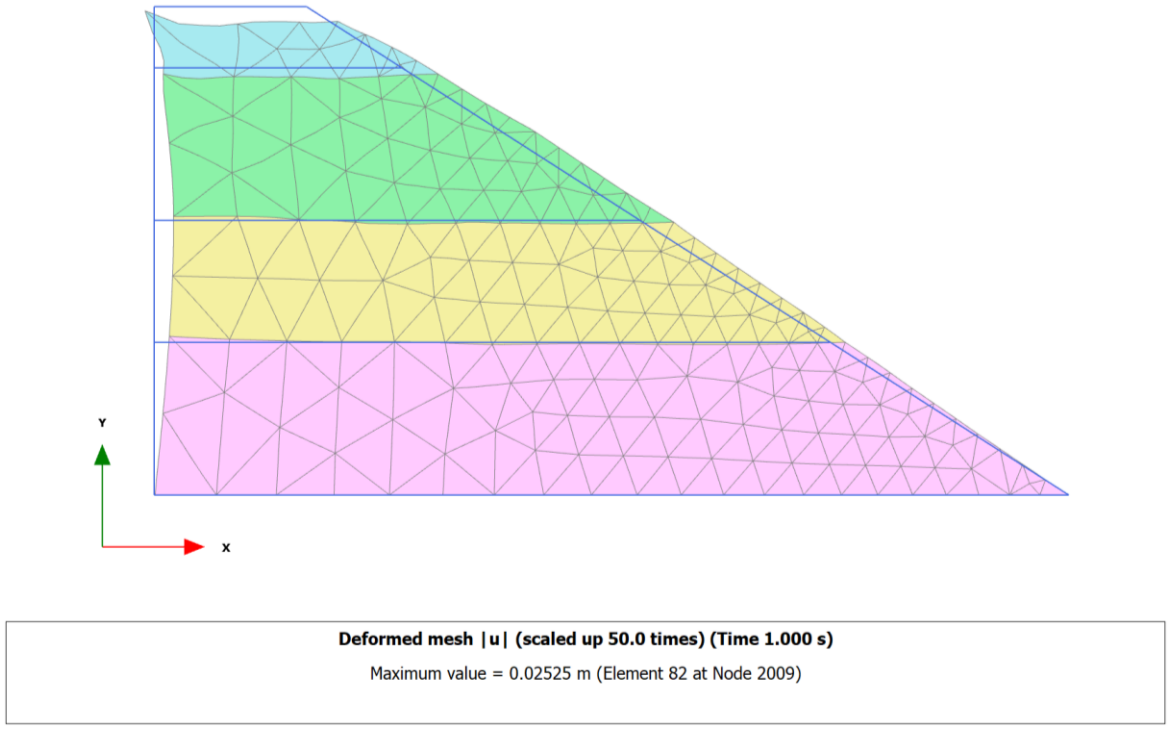

Figure 5.72 Location 03-After earthquake, Deformed Mesh-Seismic Coefficient 0.1 (Phase-01)

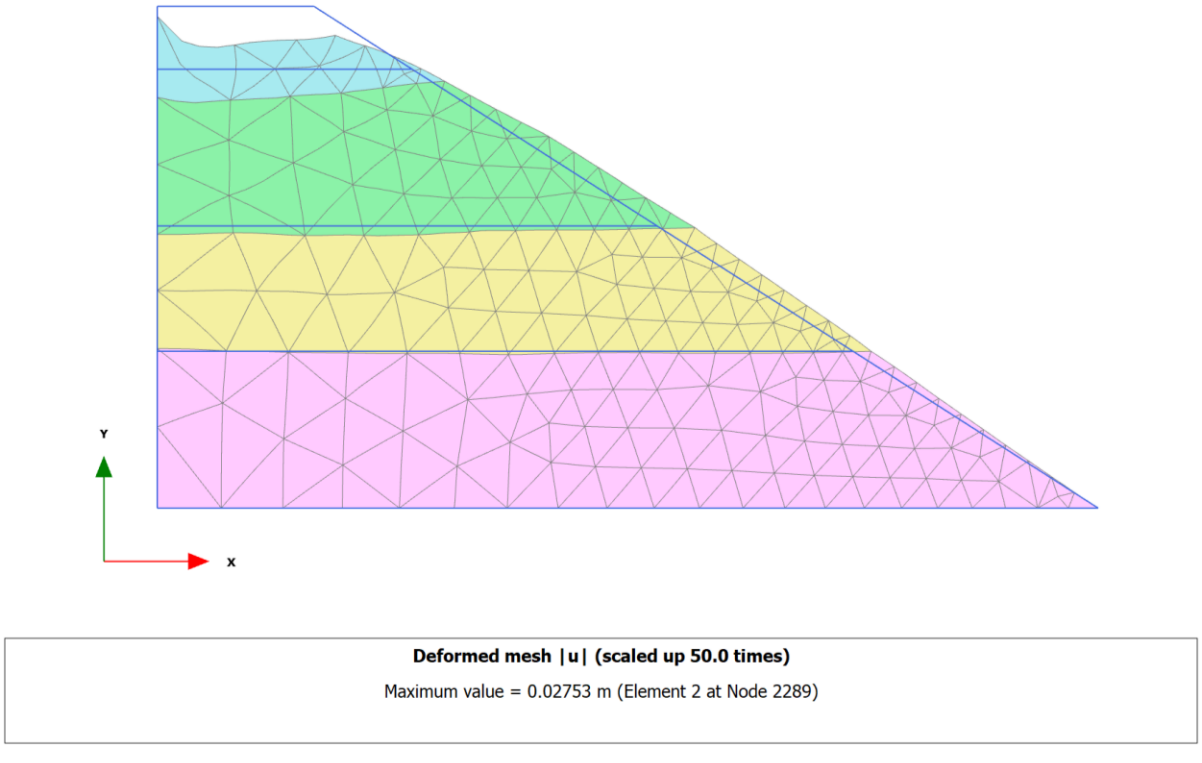

Figure 5.73 Location 03-After earthquake, Deformed Mesh-Seismic Coefficient 0.1 (Phase-02)

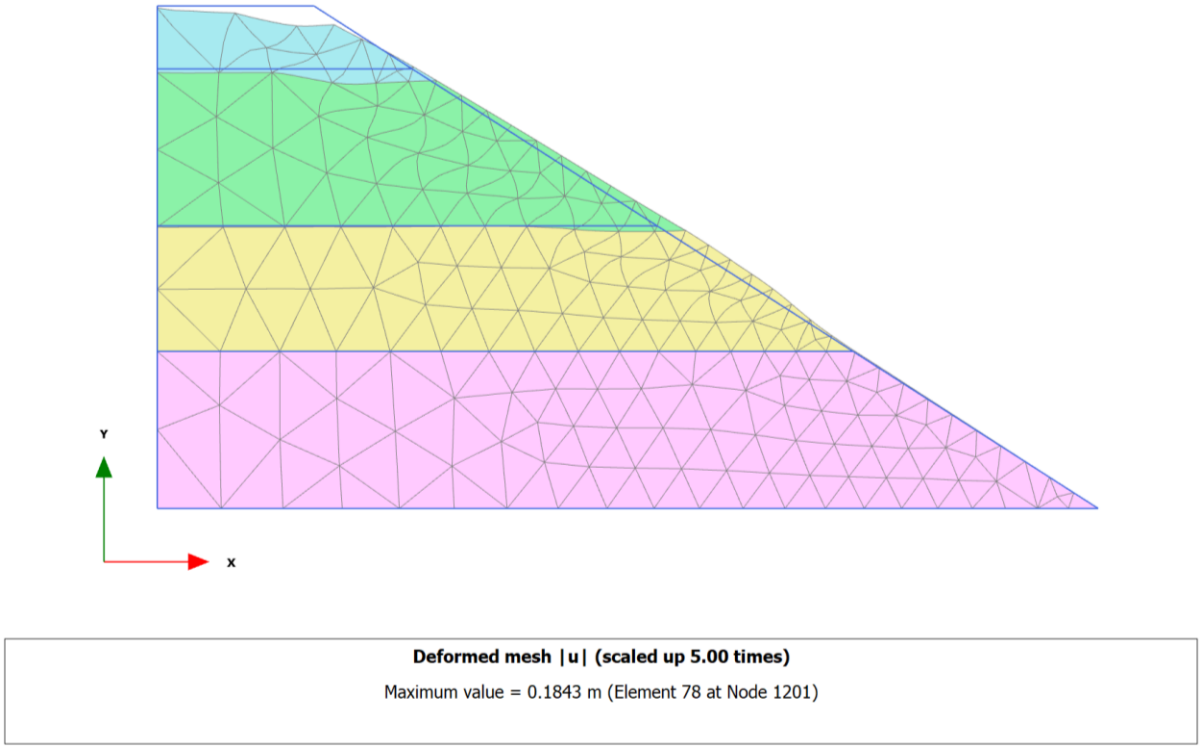

Figure 5.74 Location 03-After earthquake, Deformed Mesh-Seismic Coefficient 0.1 (Phase-03)

Displacement:

Evaluating the total displacements, at a 50.0 times scaled-up scale in phase 01, the maximum value obtained was 0.02525 m. In phase 02, at a 50.0 times scaled-up scale, the maximum total displacement measured 0.02753 m. Similarly, in phase 03, at a scaled-up scale of 5.0 , the maximum total displacement reached 0.1843 m.

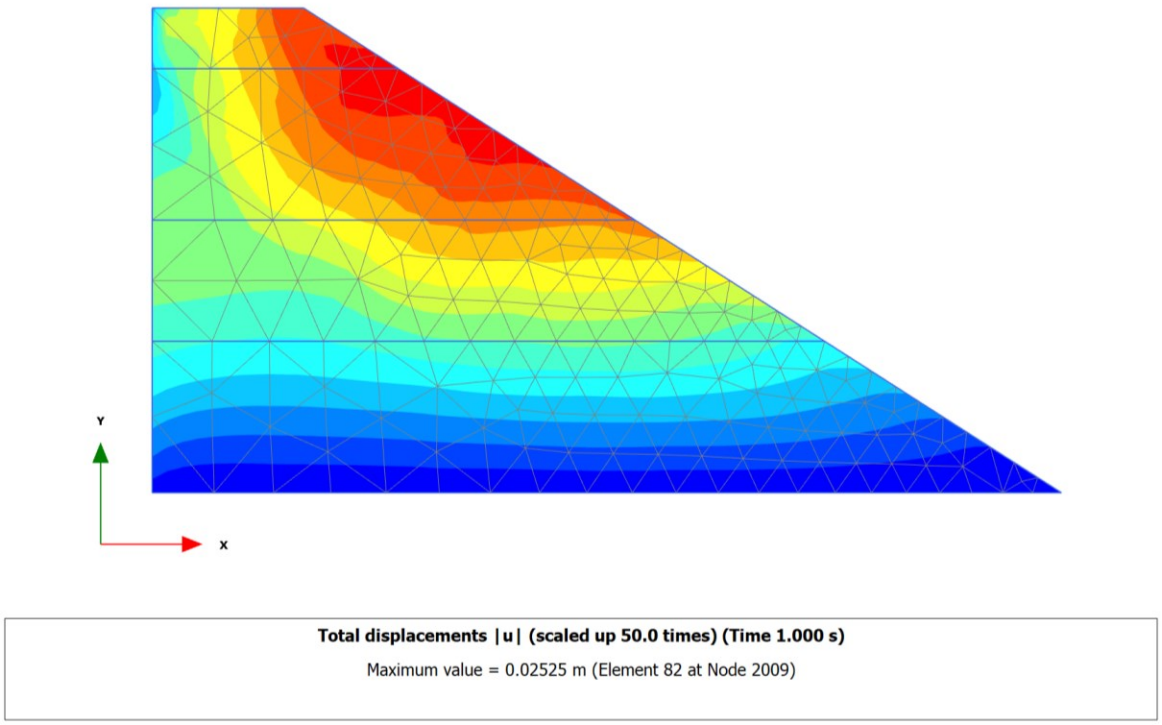

Figure 5.75 Location 03-After earthquake, Displacement-Seismic Coefficient 0.1 (Phase-01)

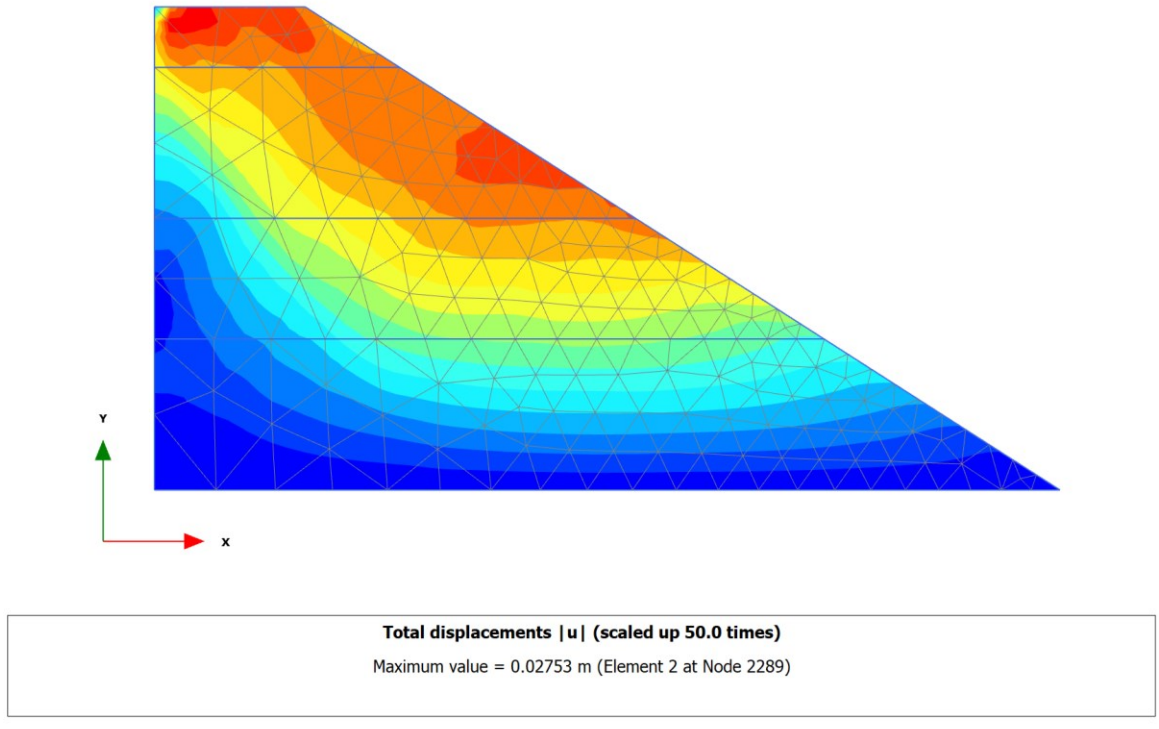

Figure 5.76 Location 03-After earthquake, Displacement -Seismic Coefficient 0.1 (Phase-02)

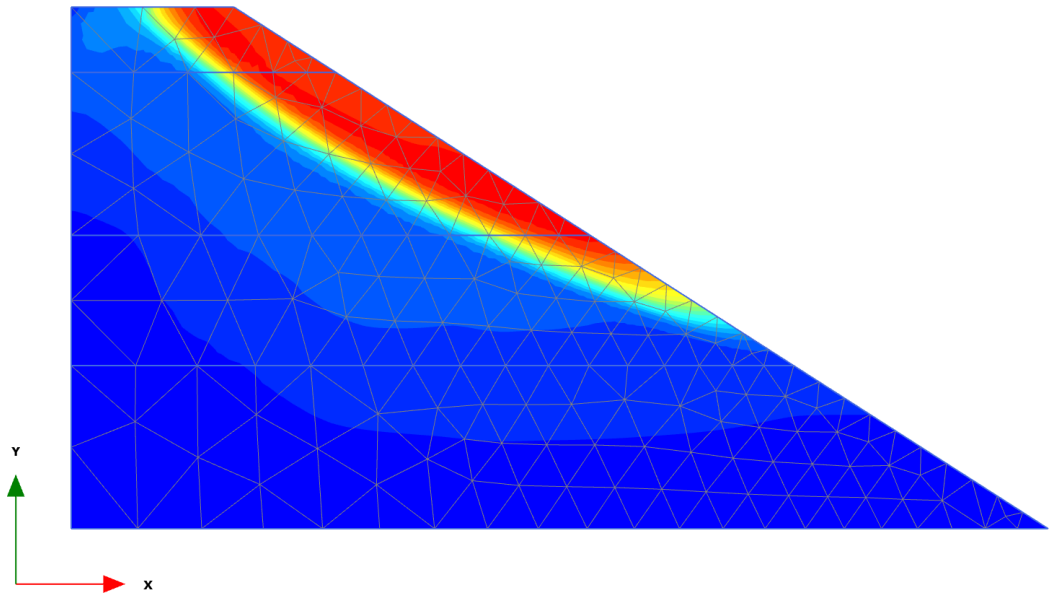

Total displacements |u| (scaled up 5.00 times)

Maximum value = 0.1843 m (Element 78 at Node 1201)

Figure 5.77 Location 03-After earthquake, Displacement-Seismic Coefficient 0.1 (Phase-03)

Factor of Safety:

The factor of safety remained at 1.422 during these analyses.

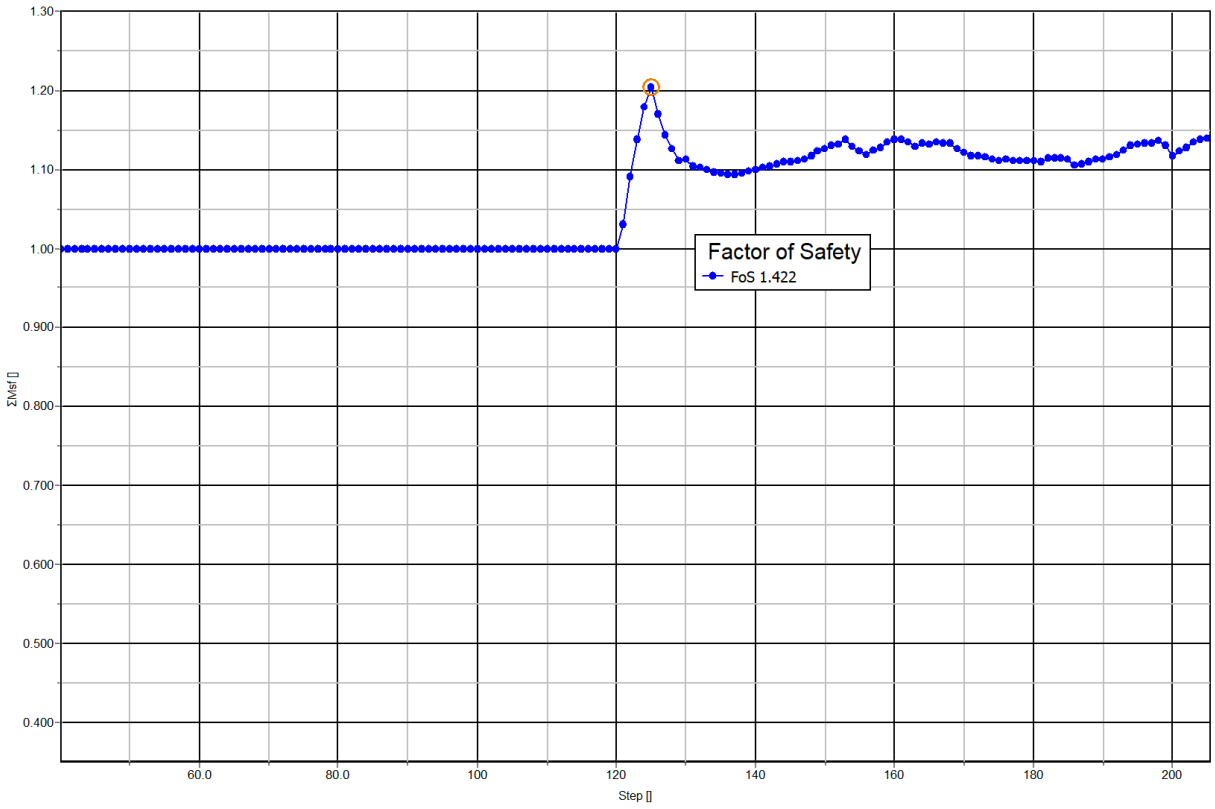

Figure 5.78 Location 03-After earthquake, Factor of Safety-Seismic Coefficient 0.1

5.3.2.2 Seismic Coefficient 0.28

Deformed Mesh:

Similarly, in the after-earthquake condition of location 3, with a seismic coefficient of 0.28, the maximum deformed mesh values were examined. At a 50.0 times scaled-up scale in phase 01, the maximum deformed mesh value measured 0.02525 m. In phase 02, the maximum deformed mesh value recorded was 0.02753 m. Additionally, in phase 03, at a scaled-up scale of 5.0, the maximum deformed mesh value reached 0.1843 m.

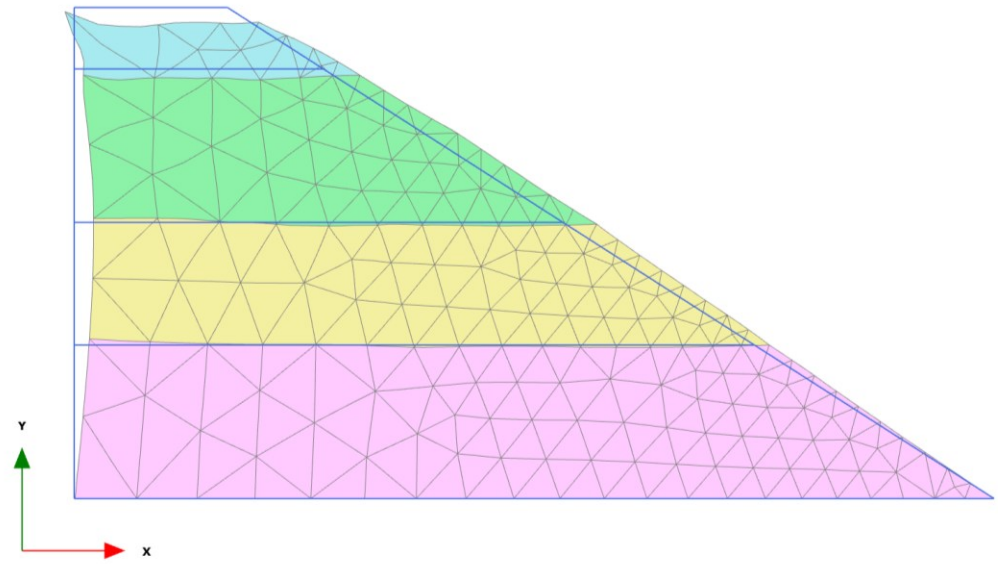

Deformed mesh |u| (scaled up 50.0 times) (Time 1.000 s)

Maximum value = 0.02525 m (Element 82 at Node 2009)

Figure 5.79 Location 03-After earthquake, Deformed Mesh-Seismic Coefficient 0.28 (Phase-01)

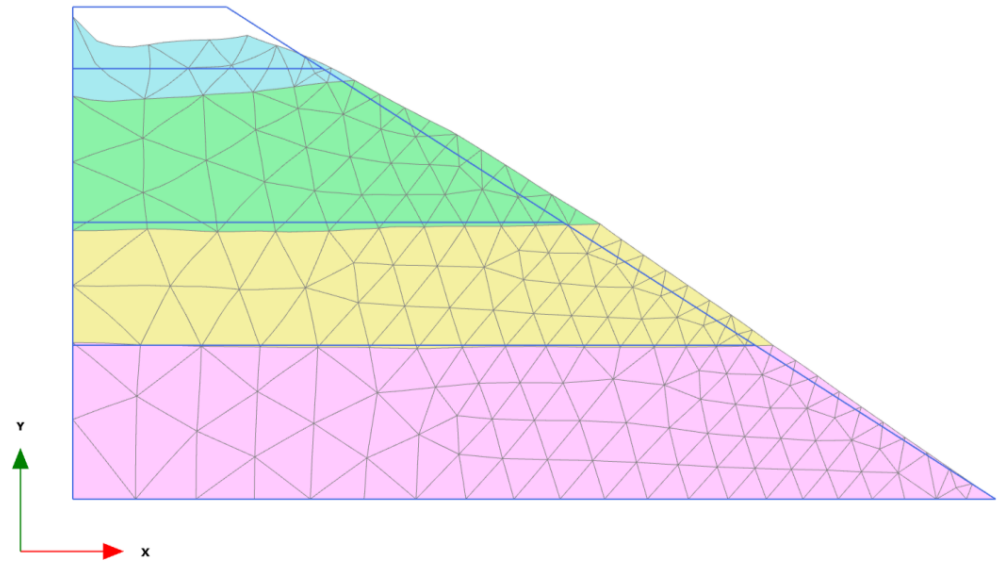

Deformed mesh |u| (scaled up 50.0 times)

Maximum value = 0.02753 m (Element 2 at Node 2289)

Figure 5.80 Location 03-After earthquake, Deformed Mesh-Seismic Coefficient 0.28 (Phase-02)

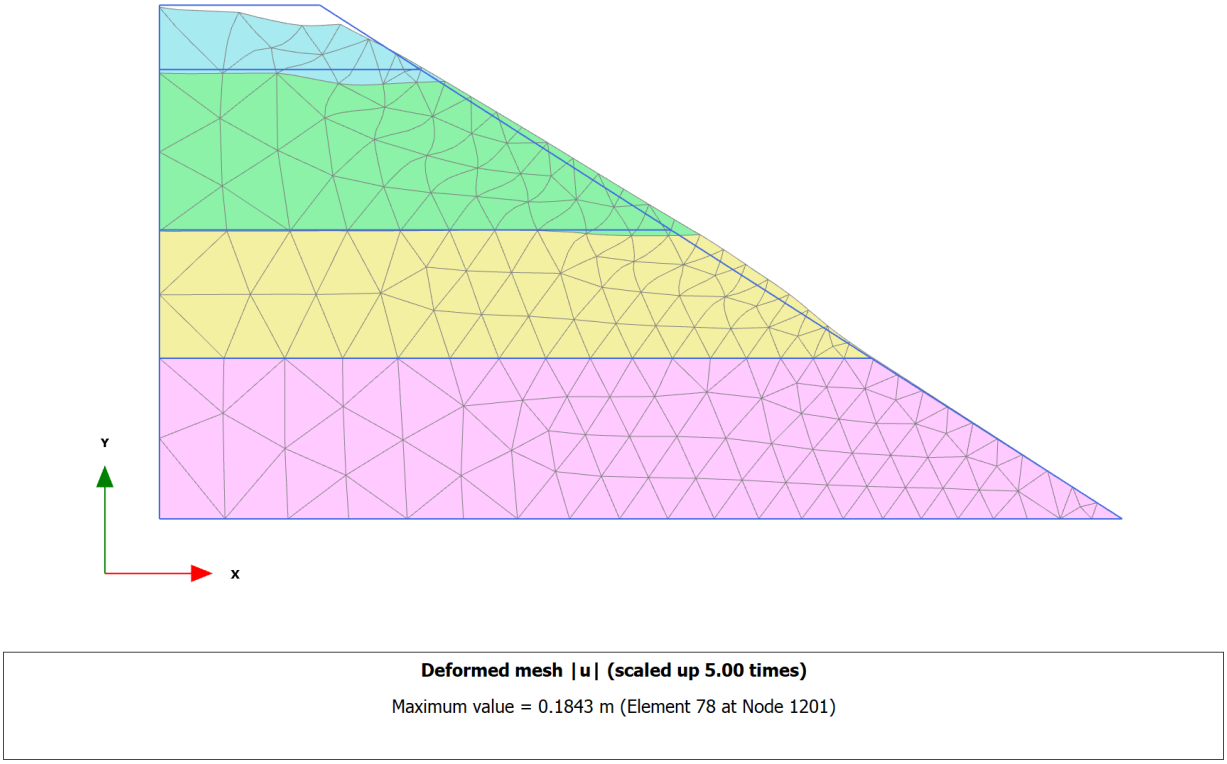

Figure 5.81 Location 03-After earthquake, Deformed Mesh-Seismic Coefficient 0.28 (Phase-03)

Displacement:

Assessing the total displacements, at a 50.0 times scaled-up scale in phase 01, the maximum value obtained was 0.02525 m. In phase 02, the maximum total displacement measured 0.02753 m. Similarly, in phase 03, at a scaled-up scale of 0.0200, the maximum total displacement reached 0.1843 m.

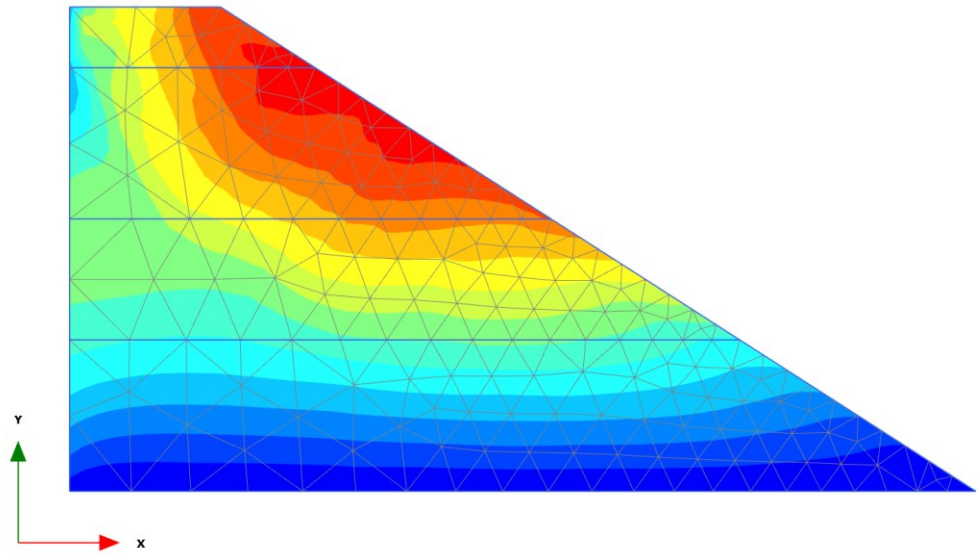

Total displacements |u| (scaled up 50.0 times) (Time 1.000 s)

Maximum value = 0.02525 m (Element 82 at Node 2009)

Figure 5.82 Location 03-After earthquake, Displacement-Seismic Coefficient 0.28 (Phase-01)

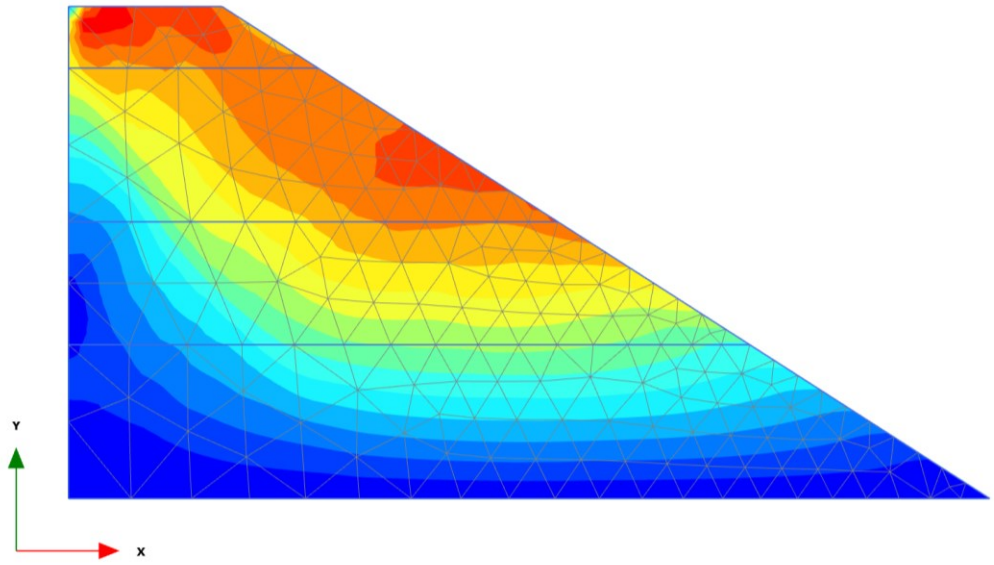

Total displacements |u| (scaled up 50.0 times)

Maximum value = 0.02753 m (Element 2 at Node 2289)

Figure 5.83 Location 03-After earthquake, Displacement-Seismic Coefficient 0.28 (Phase-02)

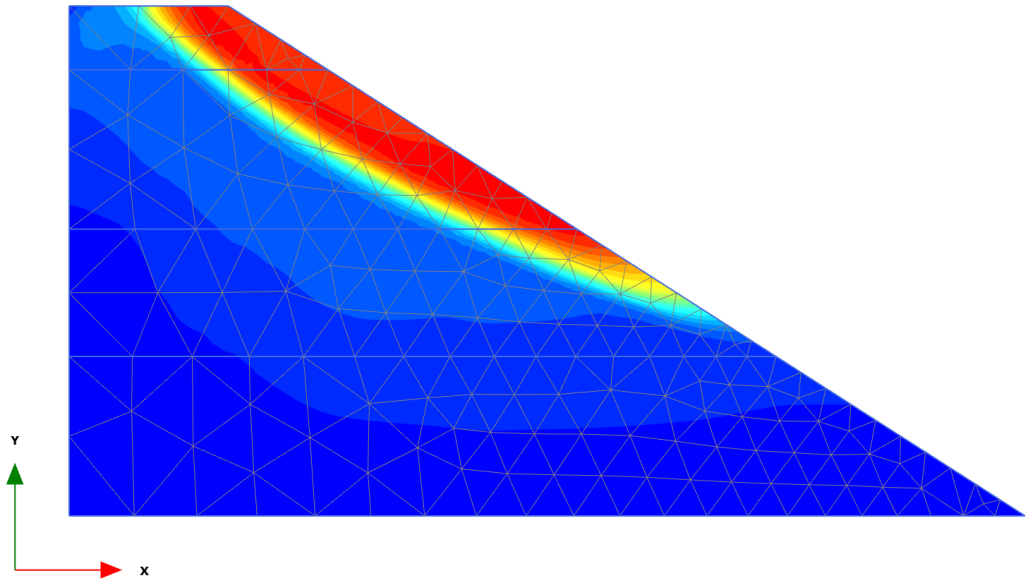

Total displacements |u| (scaled up 5.00 times)

Maximum value = 0.1843 m (Element 78 at Node 1201)

Figure 5.84 Location 03-After earthquake, Displacement-Seismic Coefficient 0.28 (Phase-03)

Factor of Safety:

The factor of safety remained at 1.418 throughout these evaluations.

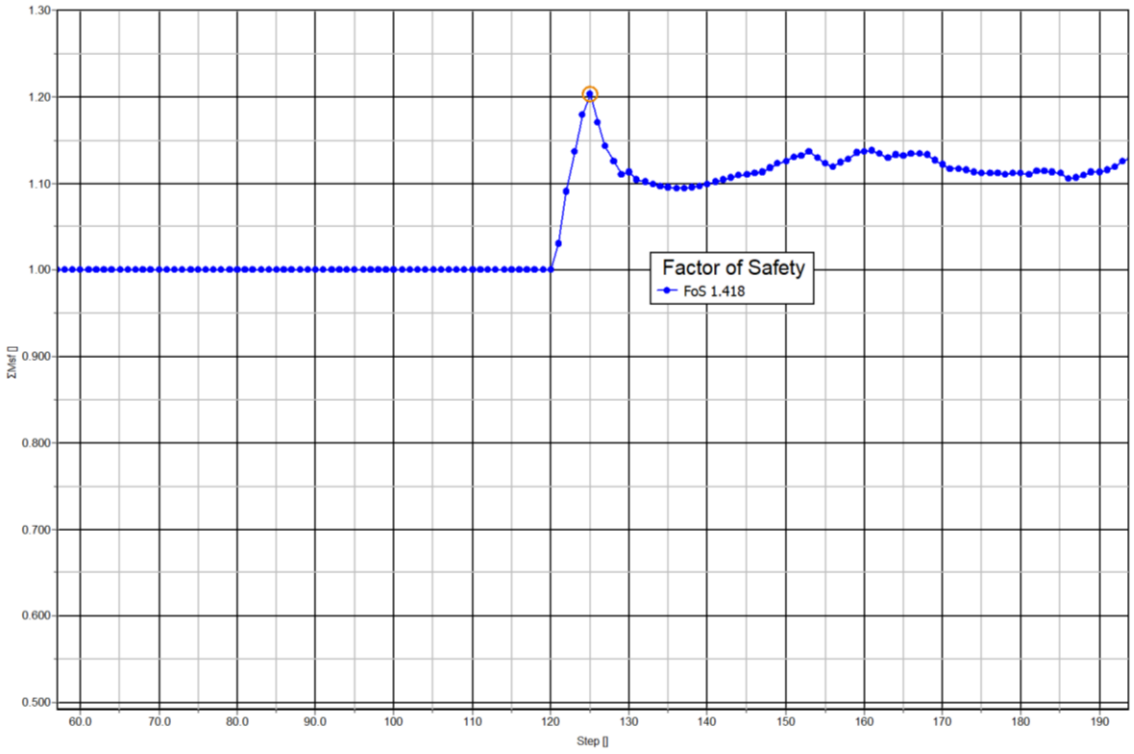

Figure 5.85 Location 03-After earthquake, Factor of Safety-Seismic Coefficient 0.28

5.3.2.3 Seismic Coefficient 0.3

Deformed Mesh:

Furthermore, in the after-earthquake condition of location 3, utilizing a seismic coefficient of 0.3, the maximum deformed mesh values were analyzed. At a 50.0 times scaled-up scale in phase 01, the maximum deformed mesh value measured 0.02525 m, while in phase 02, it reached 0.02753 m. Additionally, in phase 03, at a scaled-up scale of 0.0200, the maximum deformed mesh value recorded was 0.1843 m.

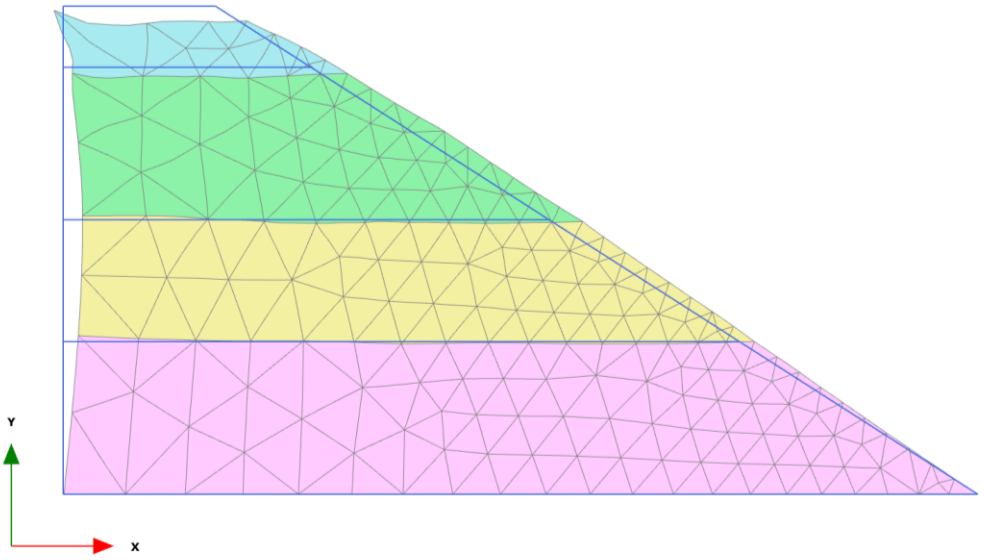

Deformed mesh |u| (scaled up 50.0 times) (Time 1.000 s)

Maximum value = 0.02525 m (Element 82 at Node 2009)

Figure 5.86 Location 03-After earthquake, Deformed Mesh-Seismic Coefficient 0.3 (Phase-01)

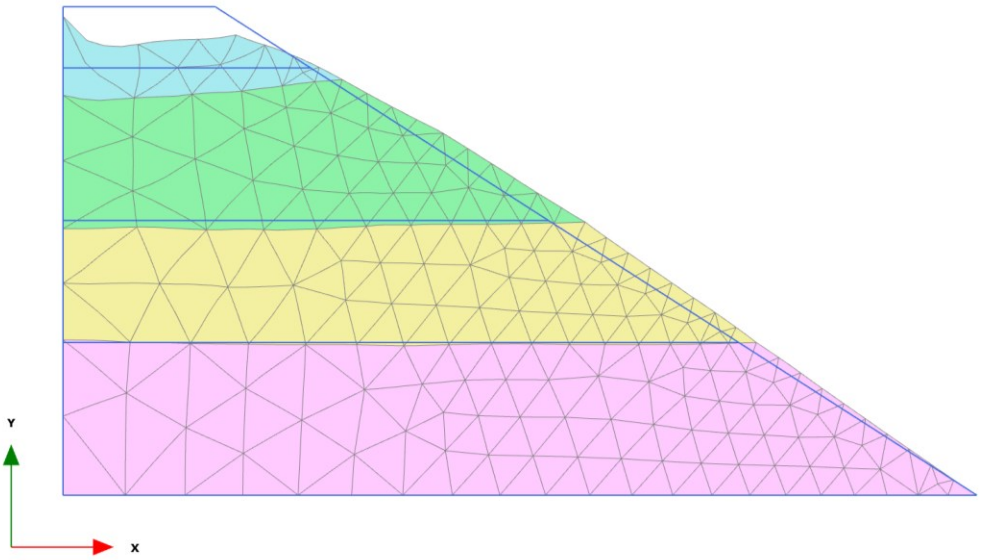

Deformed mesh |u| (scaled up 50.0 times)

Maximum value = 0.02753 m (Element 2 at Node 2289)

Figure 5.87 Location 03-After earthquake, Deformed Mesh-Seismic Coefficient 0.3 (Phase-02)

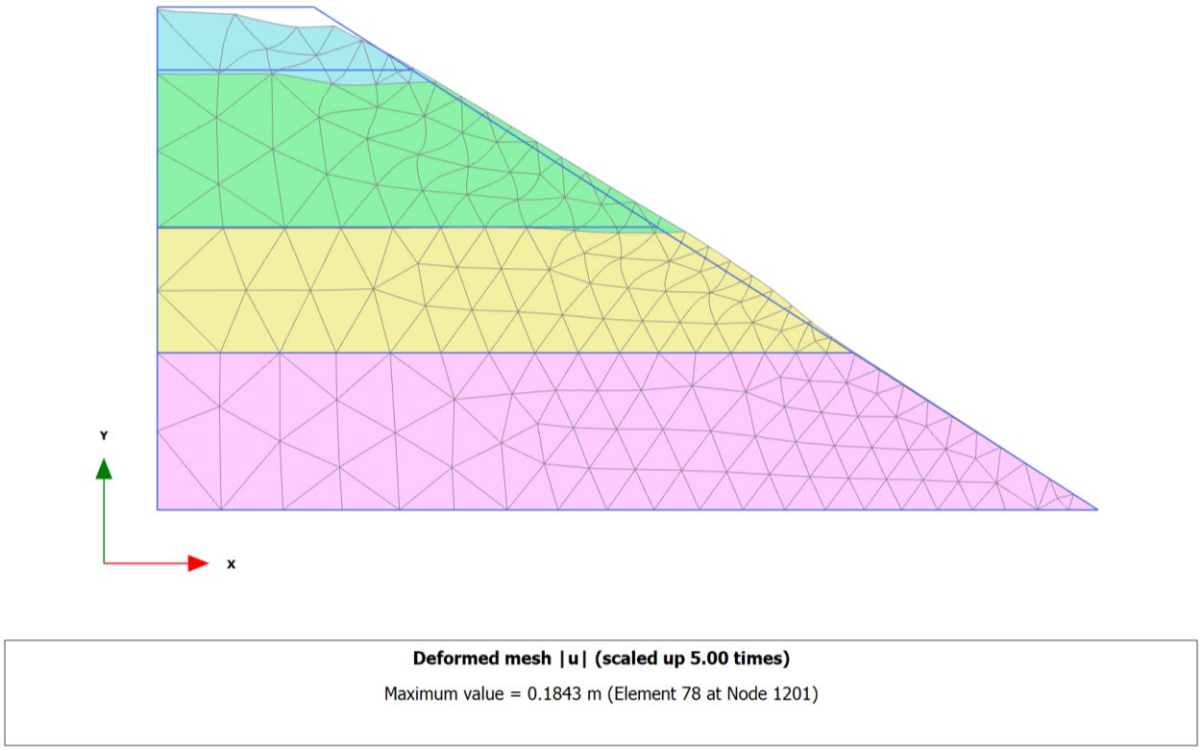

Figure 5.88 Location 03-After earthquake, Deformed Mesh-Seismic Coefficient 0.3 (Phase-03)

Displacement:

Examining the total displacements, at a 50.0 times scaled-up scale in phase 01, the maximum value obtained was 0.02525 m. In phase 02, the maximum total displacement measured 0.02753 m. Similarly, in phase 03, at a scaled-up scale of 5.0, the maximum total displacement reached 0.1843 m.

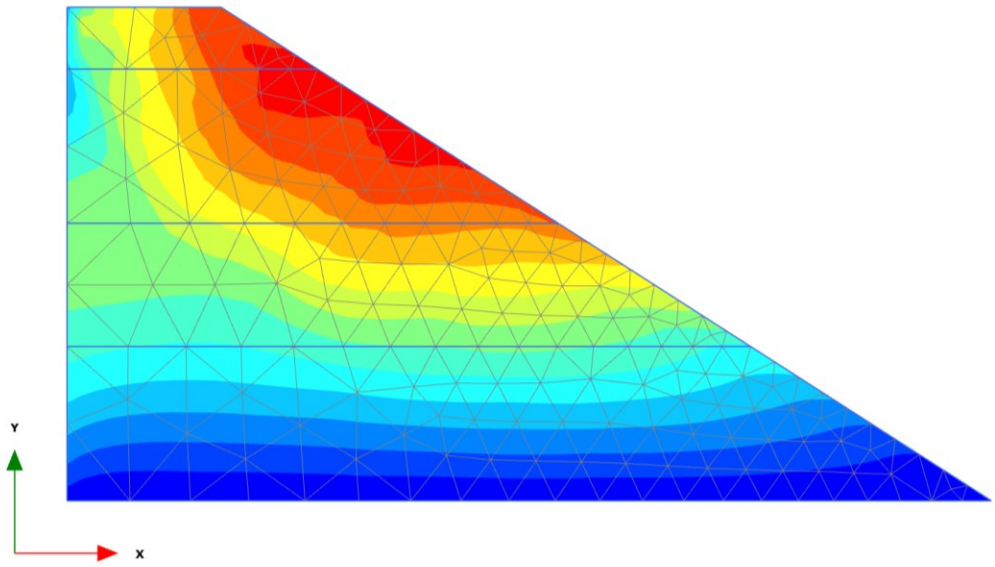

Total displacements |u| (scaled up 50.0 times) (Time 1.000 s)

Maximum value = 0.02525 m (Element 82 at Node 2009)

Figure 5.89 Location 03-After earthquake, Displacement-Seismic Coefficient 0.3 (Phase-01)

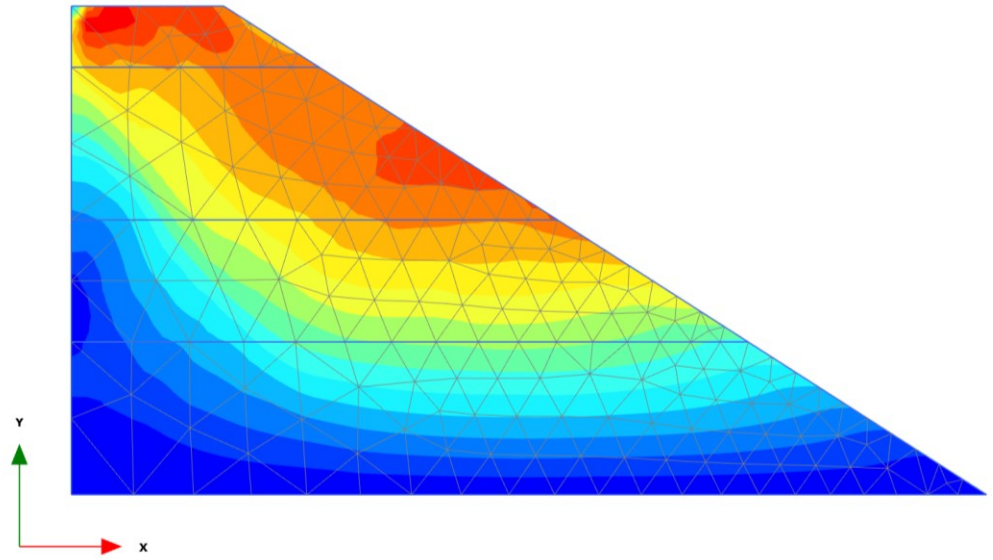

Total displacements |u| (scaled up 50.0 times)

Maximum value = 0.02753 m (Element 2 at Node 2289)

Figure 5.90 Location 03-After earthquake, Displacement-Seismic Coefficient 0.3 (Phase-02)

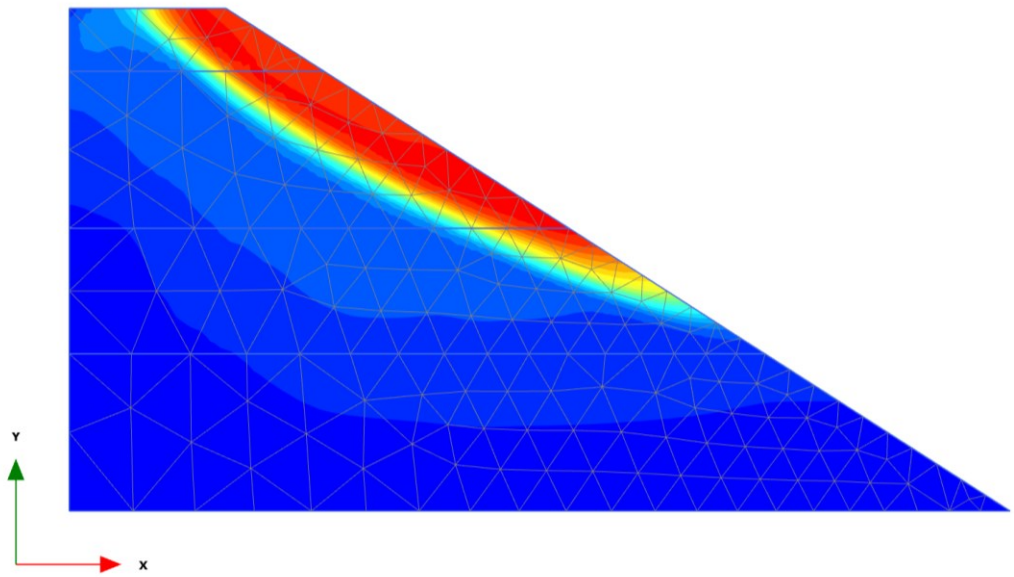

Total displacements |u| (scaled up 5.00 times)

Maximum value = 0.1843 m (Element 78 at Node 1201)

Figure 5.91 Location 03-After earthquake, Displacement-Seismic Coefficient 0.3 (Phase-03)

Factor of Safety:

The factor of safety remained at 1.403 during these analyses.

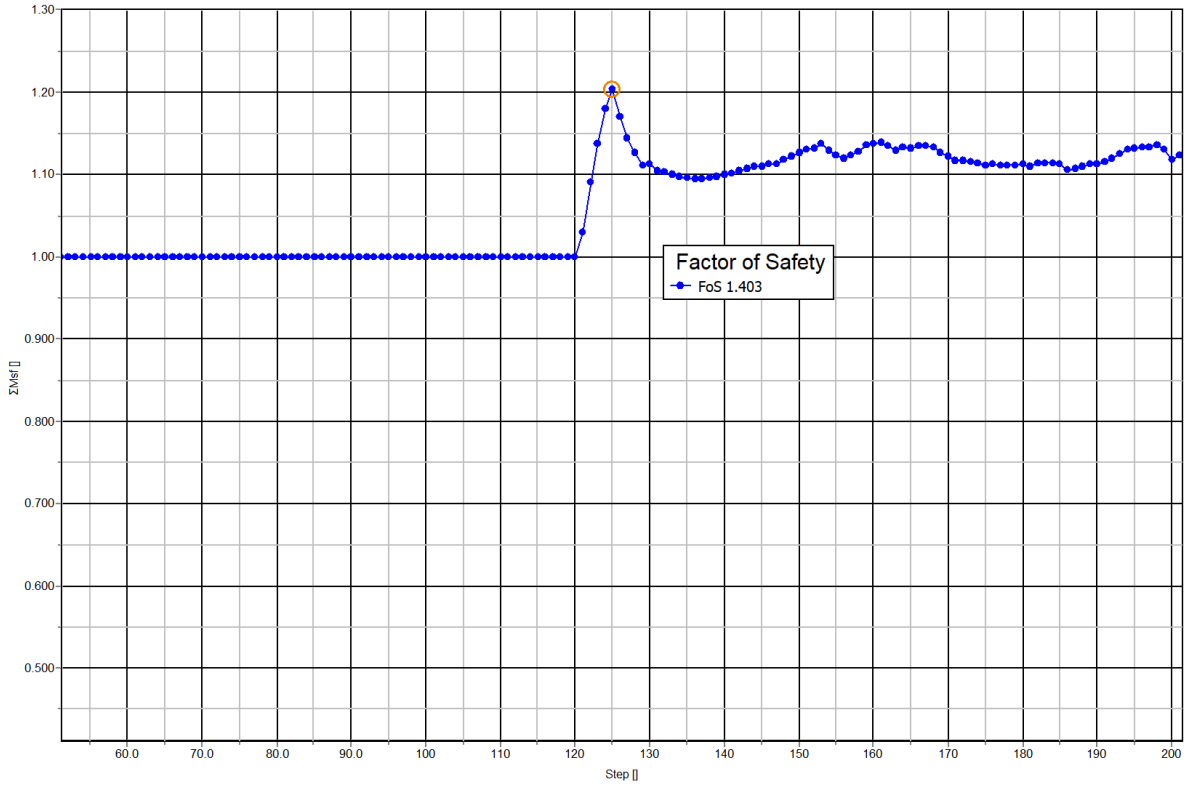

Figure 5.92 Location 03-After earthquake, Factor of Safety-Seismic Coefficient 0.3

5.3.2.4 Seismic Coefficient 0.5

Deformed Mesh:

Lastly, in the after-earthquake condition of location 3, with a seismic coefficient of 0.5, the maximum deformed mesh values were evaluated. At a 0.500 times scaled-up scale in phase 01, the maximum deformed mesh value measured 2.139 m. In phase 02, the maximum deformed mesh value recorded was 0.027523m. Additionally, in phase 03, at a scaled-up scale of 0.0200, the maximum deformed mesh value reached 0.1843 m.

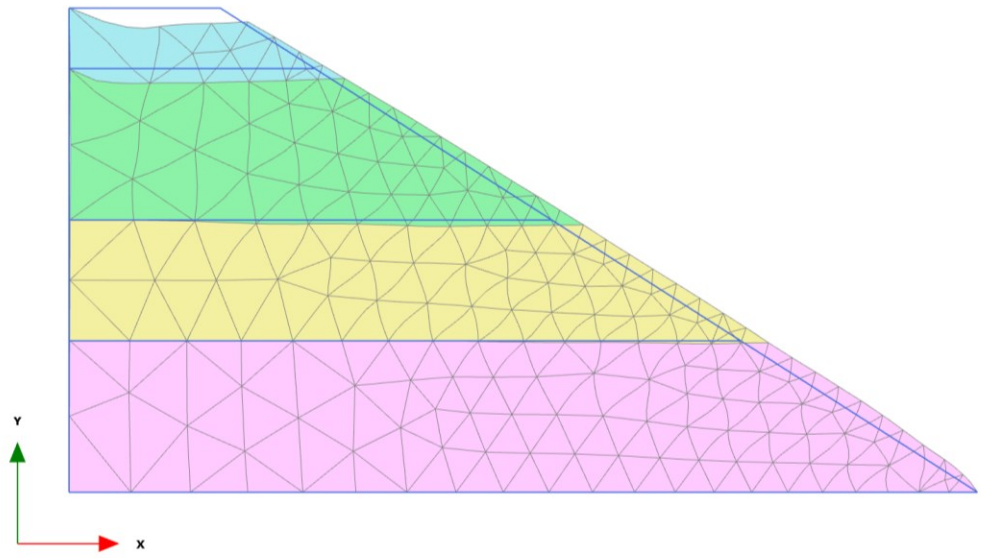

Deformed mesh |u| (scaled up 0.500 times) (Time 1.000 s)

Maximum value = 2.139 m (Element 65 at Node 1681)

Figure 5.93 Location 03-After earthquake, Deformed Mesh-Seismic Coefficient 0.5 (Phase-01)

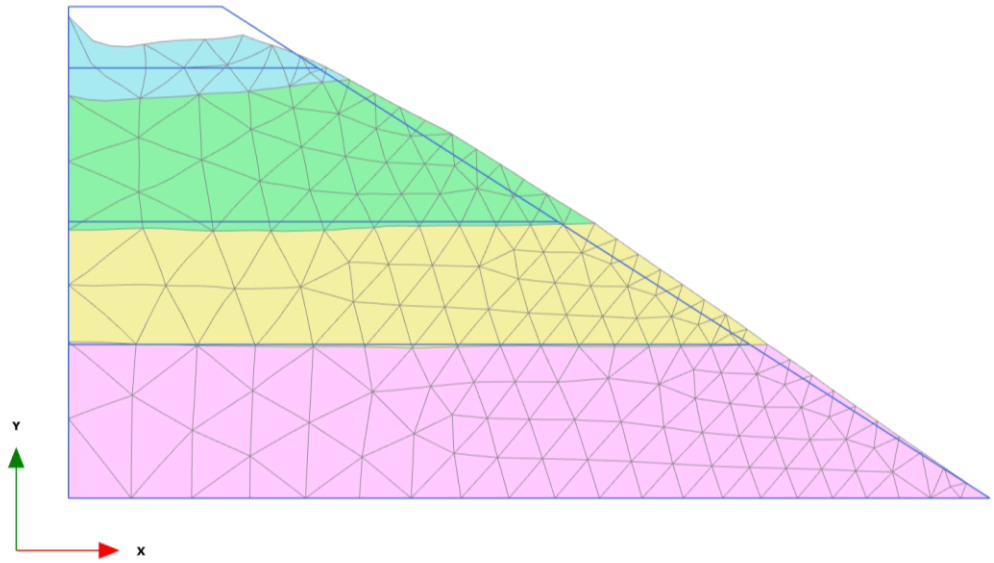

Deformed mesh |u| (scaled up 50.0 times)

Maximum value = 0.02753 m (Element 2 at Node 2289)

Figure 5.94 Location 03-After earthquake, Deformed Mesh-Seismic Coefficient 0.5 (Phase-02)

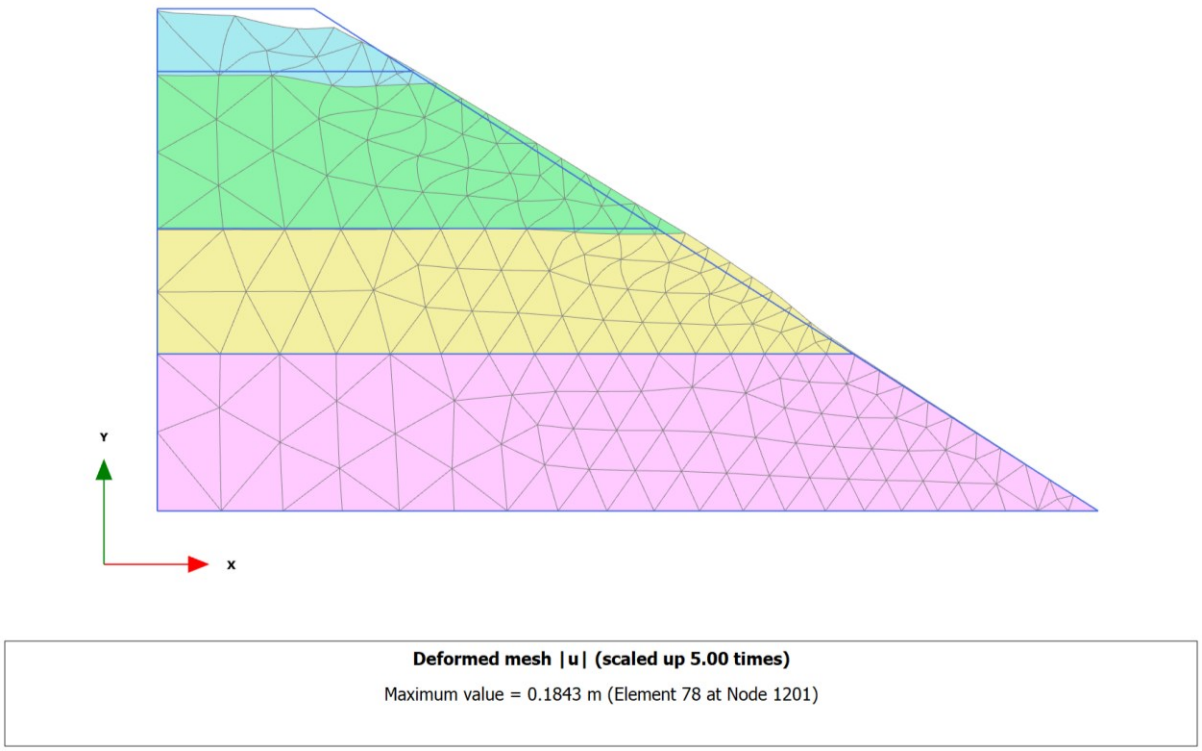

Figure 5.95 Location 03-After earthquake, Deformed Mesh-Seismic Coefficient 0.5 (Phase-03)

Displacement:

Analyzing the total displacements, at a 0.500 times scaled-up scale in phase 01, the maximum value obtained was 2.139 m. In phase 02, the maximum total displacement measured 0.02753 m. Similarly, in phase 03, at a scaled-up scale of 5.0, the maximum total displacement reached 0.1843m.

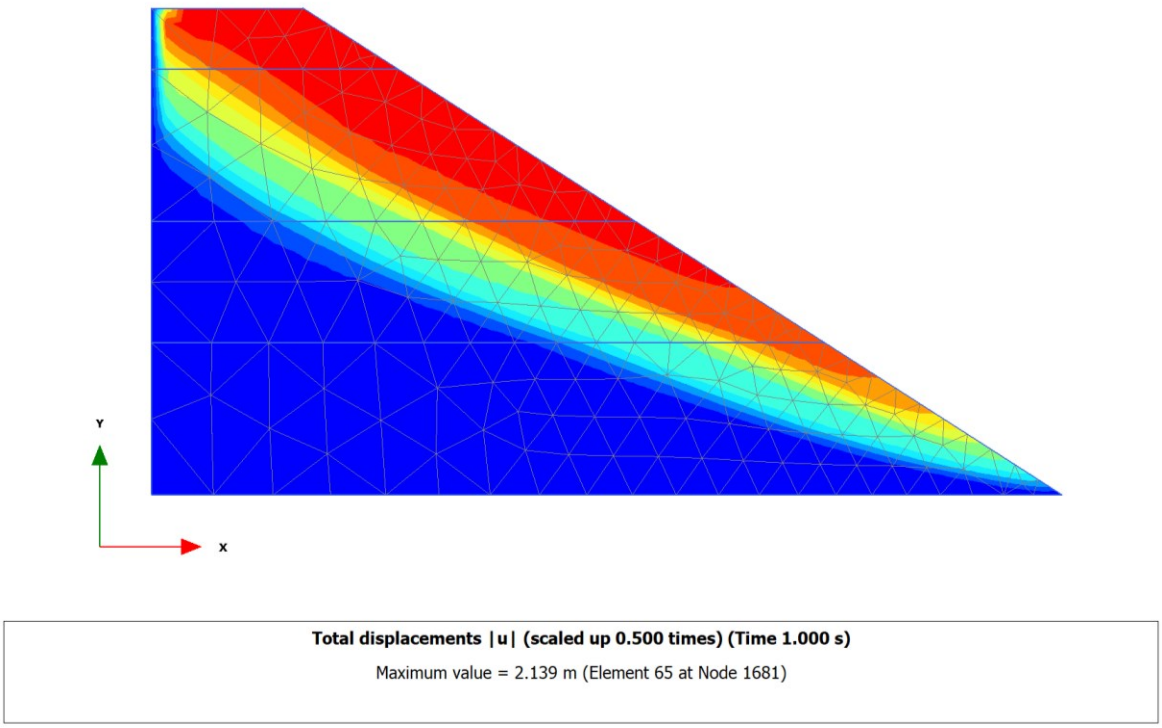

Figure 5.96 Location 03-After earthquake, Displacement-Seismic Coefficient 0.5 (Phase-01)

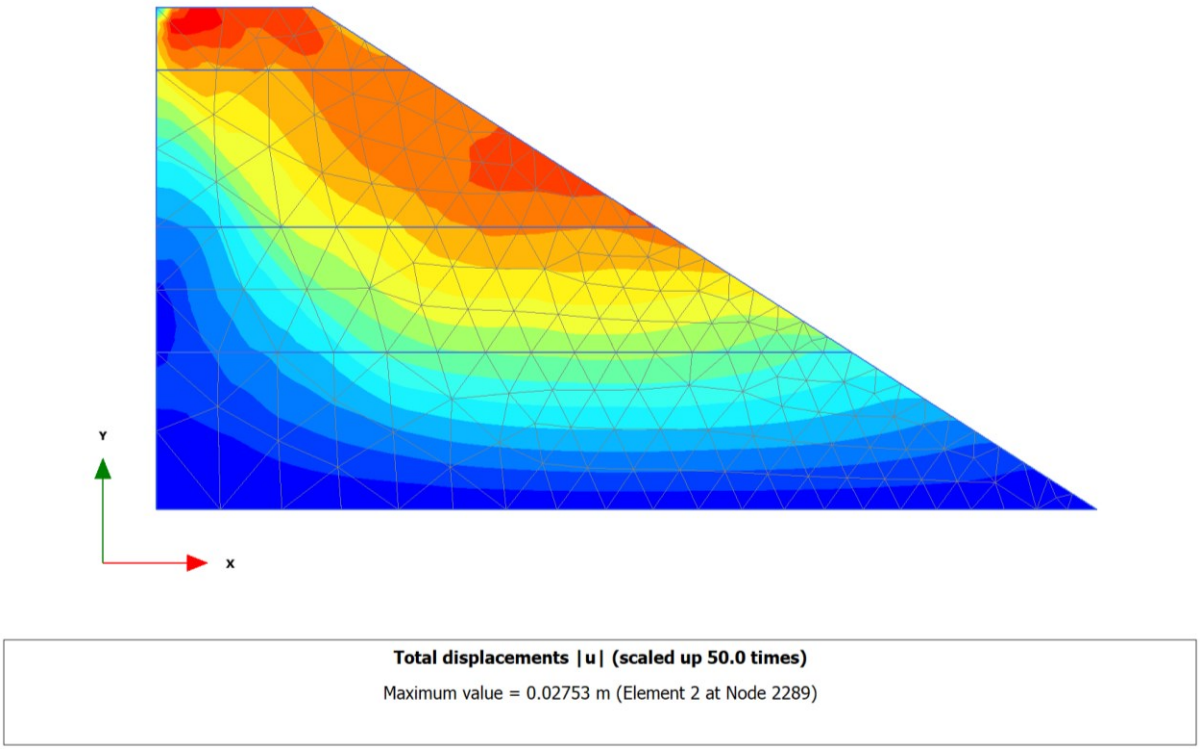

Figure 5.97 Location 03-After earthquake, Displacement-Seismic Coefficient 0.5 (Phase-02)

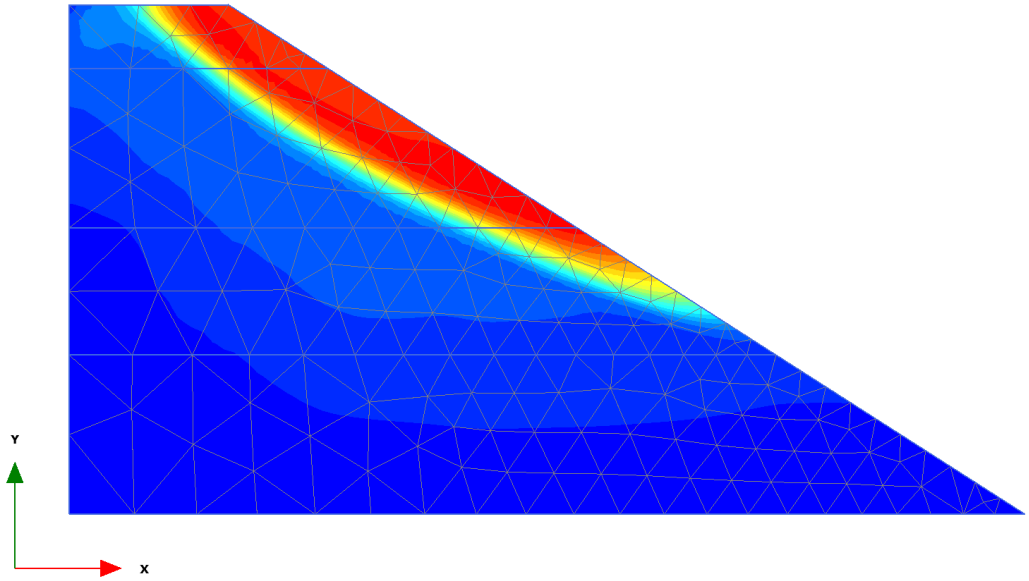

Total displacements |u| (scaled up 5.00 times)

Maximum value = 0.1843 m (Element 78 at Node 1201)

Figure 5.98 Location 03-After earthquake, Displacement-Seismic Coefficient 0.5 (Phase-03)

Factor of Safety:

The factor of safety remained at 1.308 throughout these assessments.

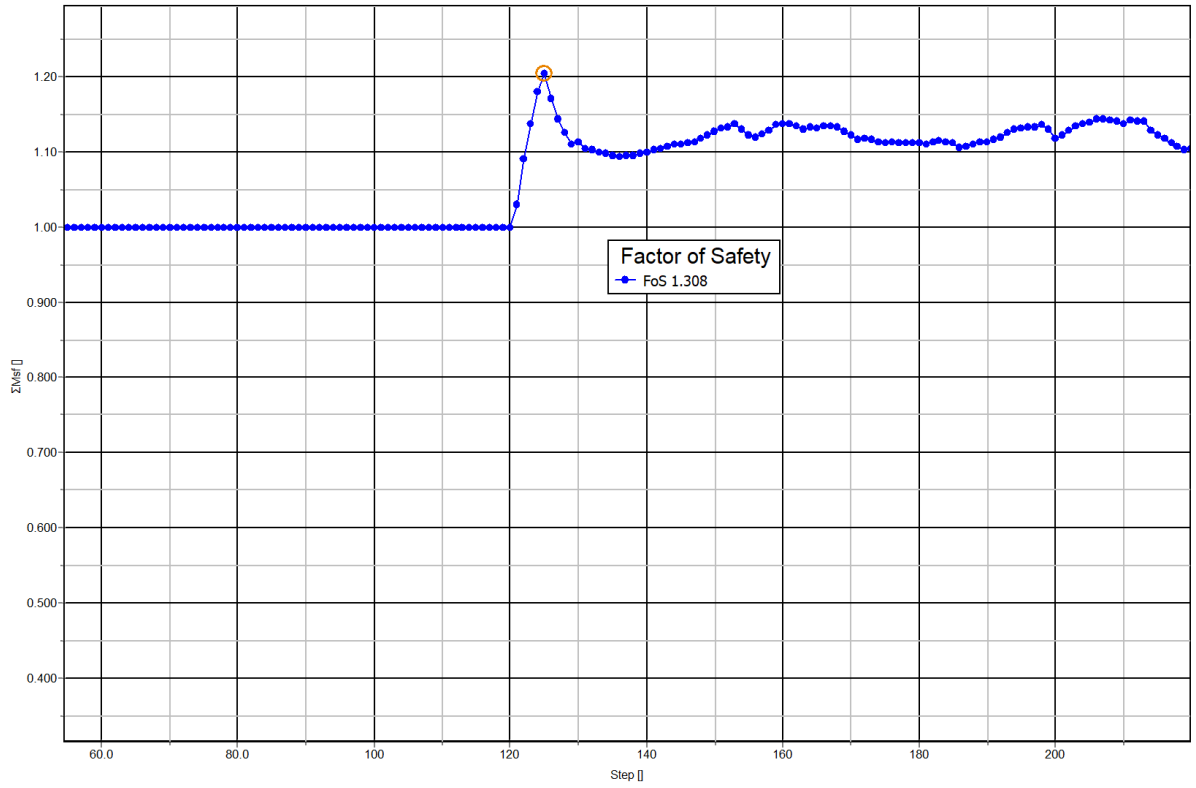

Figure 5.99 Location 03-After earthquake, Factor of Safety-Seismic Coefficient 0.5

5.4 Discussion

5.4.1 Comparison between Seismic Coefficients

Based on our study, it is evident that the deformation of slopes is directly related to the seismic coefficient. The seismic coefficient represents the ground acceleration experienced during an earthquake, with higher values indicating stronger ground shaking.

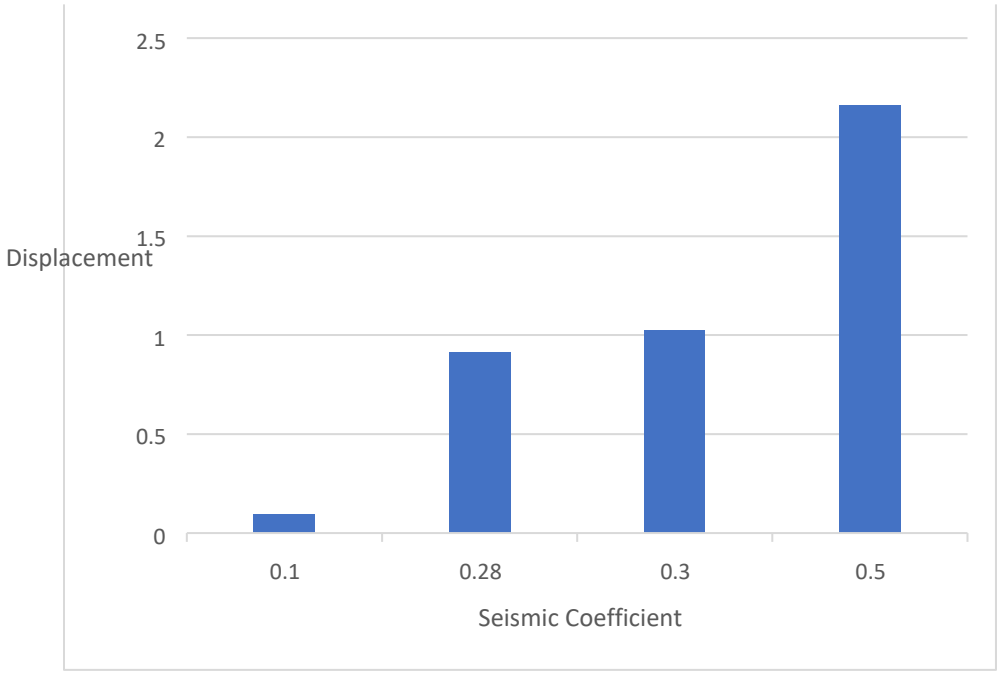

Graph 1 Seismic Coefficient Vs Displacement for Location 01

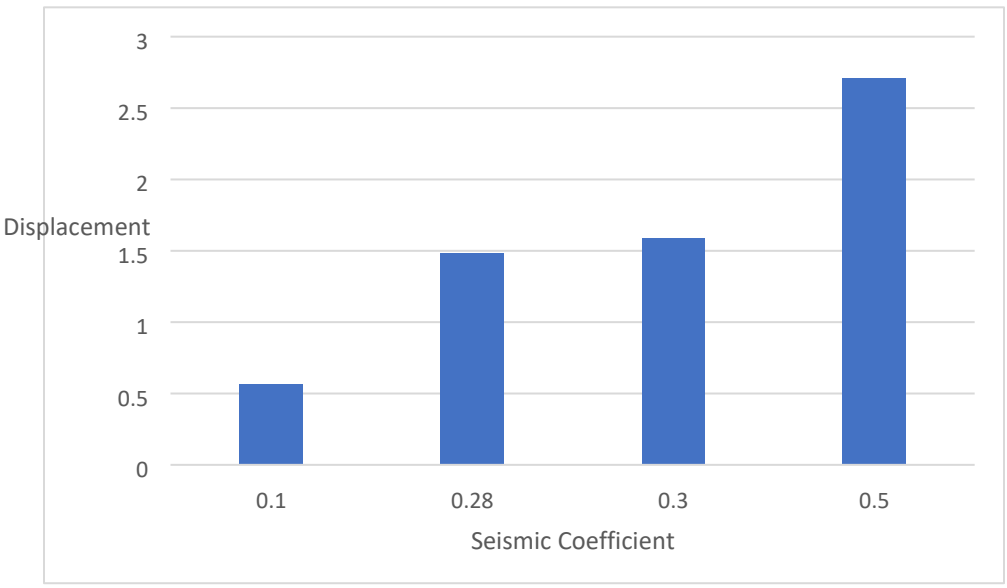

Graph 2 Seismic Coefficient Vs Displacement for Location 02

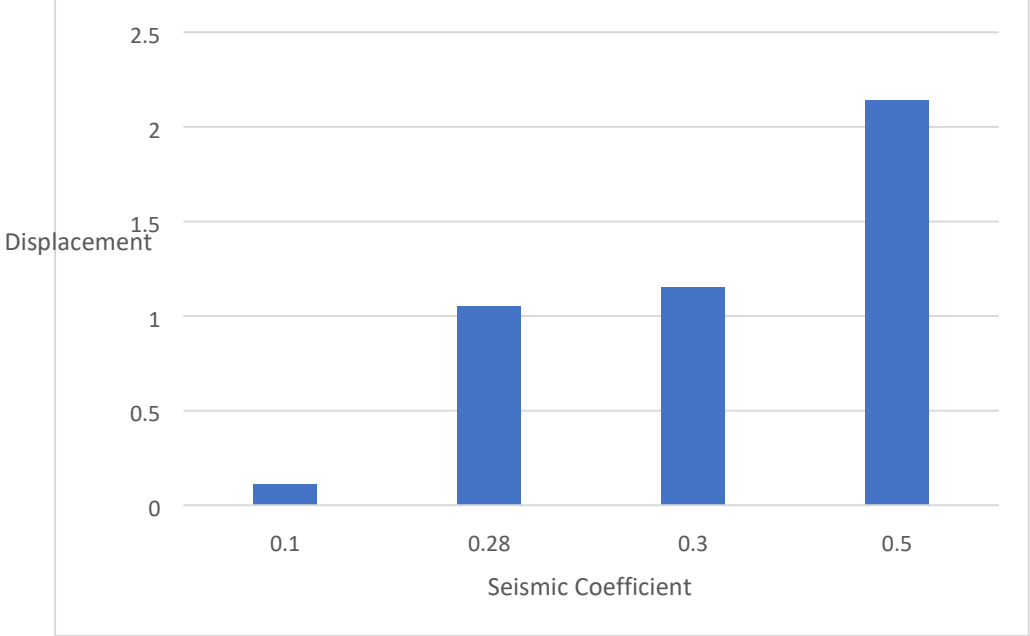

Graph 3 Seismic Coefficient Vs Displacement for Location 03

The slope deforms by 84-93% as the seismic coefficient rises from 0.1 to 0.28. This suggests that increased ground shaking will have a substantial effect on the slope's stability. The precise amount of deformation will depend on the slope's unique properties and the local geology, but the general trend points to a noticeable rise in distortion.

Furthermore, the deformation increases by 9-11% as the seismic coefficient rises from 0.28 to 0.3. Even while this increase is somewhat less than the prior range, it nevertheless shows that seismic activity is still having an impact on the slope.

The dramatic increase in deformation that occurs when the seismic coefficient increases from 0.3 to 0.5 is the most striking observation, though. Comparatively, the distortion almost doubles. This suggests that the analyzed sites may sustain significant damage from a seismic event with a coefficient of 0.5g. The slope is more likely to collapse or fail in these circumstances, according to the significant rise in deformation.

It's vital to keep in mind that the precise threshold for serious damage may vary depending on a number of variables, including the slope's geological properties, its stability, and the design standards for nearby structures or infrastructure. The precise implications and potential effects of a seismic event with a coefficient of 0.5g require site-specific evaluations and engineering skills.

5.4.2 Comparison between Study Areas

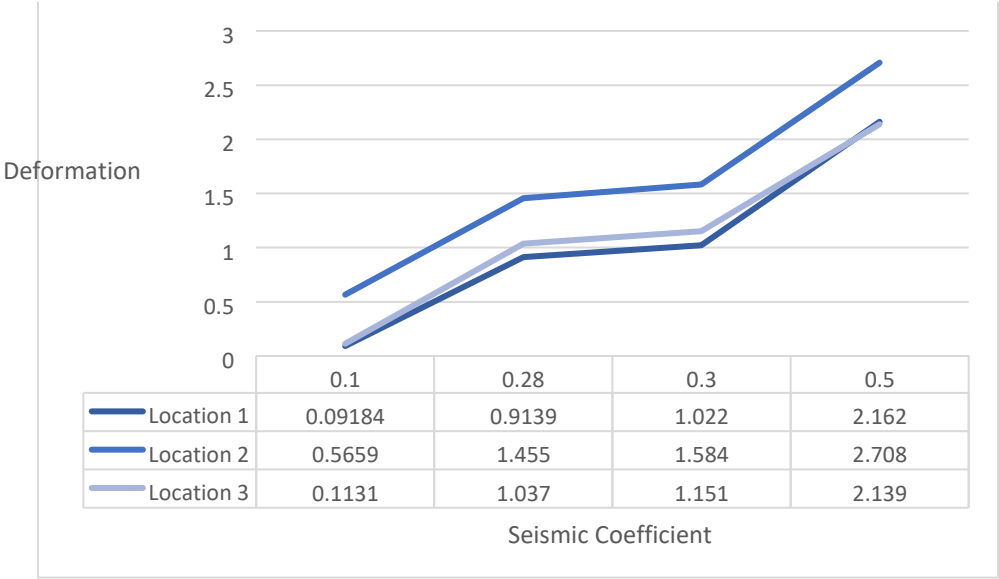

	0.1	0.28	0.3	0.5
Location 1	0.09184	0.9139	1.022	2.162
Location 2	0.5659	1.455	1.584	2.708
Location 3	0.1131	1.037	1.151	2.139

Graph 4 Deformation Vs Seismic Coefficient (All Locations)

The graph represents the deformation of all locations in case of all seismic coefficients. It is noticeable that location 2 has dealt with a larger impact than other locations. Due to the soil properties and surrounding infrastructure location 2 is more vulnerable to earthquake than location 1 and 3.

5.4.3 Factor of Safety

The factor of safety is a quantity used to assess the stability of slopes or structures. It contrasts the pushing forces acting on the slope with the resisting factors, such as soil strength. In contrast, a lower factor of safety represents a larger danger of slope instability. A higher factor of safety denotes a more stable state.

It is evident from the study that when the seismic coefficient rises, the safety factor falls. This suggests that seismic activity has a major impact on the slope's stability, especially as the ground shaking intensifies.

With a seismic coefficient of 0.1g, a reduction of 2-8% is seen when the factor of safety is compared with and without any earthquake stress. This implies that slope stability may be significantly impacted by even a very mild seismic event, jeopardizing the factor of safety.

Furthermore, the factor of safety decreases by 0.4–1% for a seismic value of 0.28g. The slope's stability under more intense ground shaking circumstances has decreased, despite the fact that this decrease is relatively modest.

At a seismic coefficient of 0.5g, the factor of safety changes most significantly. In this situation, the safety factor is decreased by 5–11%. This suggests that when the slope is subjected to an earthquake of this size, it becomes more susceptible to instability. Due to such severe ground shaking occurrences, there may be a greater danger of slope failure or collapse, according to the larger drop in the factor of safety.

Chapter 6 Conclusions & Further Studies

6.1 Conclusions

The analysis of slopes using PLAXIS 2D software gave an insight into the variation of deformation and factor of safety with the variation in slope angles, cohesion strength, frictional angle, and accelerations of earthquakes. The following findings have been reached:

1. Location 2 exhibits a higher vulnerability to earthquake-induced damage compared to locations 1 and 3. This shows that the elements at site 2 have comparatively inferior structural integrity and resilience, leaving them more vulnerable to seismic activity.

2. As the seismic coefficient increases, the factor of safety decreases. It's crucial to remember, though, that variations in soil qualities and the surroundings could lead to some deviations. To effectively quantify the influence of earthquakes in such situations, it becomes important to use sophisticated modeling tools. These cutting-edge techniques provide a more accurate analysis by taking into account additional parameters that affect the behavior of the soil and structure under seismic loading.

6.2 Further Studies

In this research work only the effects of various magnitudes of earthquake were displayed. In future studies we can propose solutions to mitigate the effects. Here is an outline of further study scopes of this study:

1. Analyzing the effectiveness of various methods, such as soil nailing, geotextiles, geo-grids, and ground anchors, in reducing the effects of earthquakes can be done in-depth. Analyzing case studies, consecutively numerical models, and taking into account difficulties in actual implementation are all possible parts of this research. Finding the best methods for strengthening the stability and safety of slopes and structures under seismic circumstances can be aided by evaluating the performance, cost-effectiveness, and feasibility of various solutions.

2. It is possible to evaluate the effects of earthquakes under various scenarios by taking into account numerous slope ratios as well as differences in cohesion and friction angles. Researchers can examine how different geological conditions affect slope stability and factor of safety by modifying these parameters in numerical models or laboratory studies. This analysis assists in determining how sensitive slopes are to seismic forces and helps to develop effective mitigation tactics for certain slope designs.

3. The accuracy of determining how earthquakes may affect a region can be enhanced by using more sophisticated modeling approaches. Advanced modeling techniques like finite element analysis and numerical simulations with Plaxis or Abaqus software can give a further accurate picture of the interaction amid soil and structure and the dynamic response to seismic incidences. These techniques provide a more accurate estimation of deformation and factor of safety by taking into account variables including nonlinearity, soil liquefaction, and wave propagation. Improved forecasts and a better comprehension of the behavior of geotechnical systems under seismic loads can result from incorporating cutting-edge modeling approaches.

4. The pseudo-static approach, which is frequently used to estimate earthquake consequences, cannot give a perfect evaluation. This suggests that the analysis carried out using the pseudo-static method might not fully account for all the complexity and nuanced aspects of earthquake behavior. Alternative and more advanced analysis techniques should be taken into consideration in order to get a more systematic understanding of earthquake consequences. These cutting-edge methods provide a more accurate picture of the earthquake impact by taking into account dynamic aspects including soil-structure interaction and seismic wave propagation.

Reference

1. Matasovic, N. (1991). Selection of method for seismic slope stability analysis.
2. Melo, C., & Sharma, S. (2004, August). Seismic coefficients for pseudostatic slope analysis. In *13th World conference on earthquake engineering* (Vol. 369, p. 15).
3. Albataineh, N. (2006). *Slope stability analysis using 2D and 3D methods* (Doctoral dissertation, University of Akron).
4. Seshu, P. (2006). *Textbook of Finite Element Analysis* (10th ed.). PHI Learning Pvt. Ltd. https://doi.org/10.1007/978-3-319-40358-8
5. Anisuzzaman Masud, M. (2007). Earthquake risk analysis for Chittagong city.
6. Sarwar, G. M. (2008, November). Landslide tragedy of Bangladesh. In *The first world landslide forum* (Vol. 11).
7. Shirdel, M., Ghanbari, A., & Davoudi, M. (2012). Evaluation of geometric effect on the pseudo-static seismic coefficient in embankment dams. *Gazi University Journal of Science*, *25*(3), 707-719.
8. Islam, M. S., Hosain, M., Islam, M. S., Ahmed, A. D., Hoque, F., Karim, S. U., & Islam, A. (2015). Disaster due to slope failure in the Pahartoli area of the Chittagong city, Bangladesh. *International Journal of Scientific and Engineering Research*, *6*(3), 246-251.
9. Carlton, B., Kaynia, A. M., & Nadim, F. (2016). Some important considerations in analysis of earthquake-induced landslides. Geoenvironmental Disasters, 3(1). https://doi.org/10.1186/s40677-016-0045-x
10. Islam, R., Islam, M. N., & Islam, M. N. (2016). Earthquake risks in Bangladesh: causes, vulnerability, preparedness and strategies for mitigation. *Arpn J Earth Sci*, *5*(2), 75-90.
11. Zardari, M. A., Mattsson, H., Knutsson, S., Khalid, M. S., Ask, M. V. S., & Lund, B. (2017). Numerical analyses of earthquake-induced liquefaction and deformation behaviour of an upstream tailings dam. Advances in Materials Science and Engineering, 2017. https://doi.org/10.1155/2017/5389308
12. Jia, J. (2018). *Soil Dynamics and Foundation Modeling* (1st ed.). Springer Cham.
13. Toha, M. T., Setiabudidaya, D., Ghadafi, M. A., Adiwarman, M., & Irvan, M. (2019, September). Pseudo-static slope stability analysis around the landslide at railway tunnel, South Sumatera, Indonesia. In *IOP Conference Series: Materials Science and Engineering* (Vol. 620, No. 1, p. 012129). IOP Publishing.
14. Özmen, B. O. (2019). Modelling the variability in seismically induced slope displacements due to ground motion selection (Master's thesis, Middle East Technical University).
15. Ramkrishnan, R., Karthik, V., Sruthy, M. R., & Sharma, A. (2019). Soil reinforcement and slope stabilization using natural jute fibres. In *New Solutions for Challenges in Applications of New Materials and Geotechnical Issues: Proceedings of the 5th GeoChina International Conference 2018–Civil Infrastructures Confronting Severe Weathers and Climate Changes: From Failure to Sustainability, held on July 23 to 25, 2018 in HangZhou, China* (pp. 130-143). Springer International Publishing.
16. Copana, J., Rodriguez-Marek, A., & Mauldon, M. (2020). Seismic Slope Stability: A Comparison Study of Empirical Predictive Methods with the Finite Element Method.

17. Sultana, N. (2020). Analysis of landslide-induced fatalities and injuries in Bangladesh: 2000-2018. *Cogent Social Sciences*, *6*(1), 1737402.
18. Ghosh, B. (n.d.). Seismic response analysis of Earth Dam using PLAXIS.
19. Siby Jacob, A., & Venkataramana, K. (n.d.). Slope Stability Analysis Under Earthquake Load Using Plaxis Software.
20. Ancheli Siby Jacob, & Katta Venkataramana. (2021). Slope Stability Analysis Under Earthquake Load Using Plaxis Software.
21. Sabur, M. A., & Rana, M. S. (2021). Knowledge Level of Urban Residents on Disaster Response: A Case Study on Earthquake Response of Chandrima Residential Area Residents, Chandgaon, Chattogram.
22. Ali, M. J. (2021). Causes of Landslide and its Socio-economic Effects: a study on Chattogram City and Surrounding Areas, Bangladesh. *Ilomata International Journal of Social Science*, *2*(4), 275-286.
23. Noël, W. N., Adolphe, K., Harmel, O. O., Gampio, M. U., Lacaba, R. G., Gonçalves, A. O., & Florent, B. (2022). Earthquake Effects on Slope Stability by Using Finite Element Method. Case Study: Brazzaville City, Republic of Congo. International Journal of Environment and Climate Change, 12(12), 798-804.
24. Kallimath, S. S., & Malagihal, R. Stability Analysis of Earth Slopes using Plaxis Software.
25. Islam, M. S., Islam, M. S., Ahmed, A. S. D., Karim, S. U., Hosain, M., & Hoque, F. Seismic Induced Landslide Vulnerability in the Chittagong City, Bangladesh.
26. Hossain, A., Sadman, M. A. A., & Rashid, M. M. SEISMIC STABILITY OF SLOPES IN LAYERED COHESIVE SOILS.
27. https://doi.org/10.1007/978-3-319-40358-8
28. https://www.google.com/search?q=Earthquake+Contingency+Plan+for+Ward+6%2C+Rangamati+Municipality%3A+Volume+2&oq=Earthquake+Contingency+Plan+for+Ward+6%2C+Rangamati++Municipality%3A+Volume+2&aqs=chrome..69i57j69i60.3182108310j0j15&sourceid=chrome&ie=UTF-8